Chemical Reduction at Solid-Liquid Interface: Growth and Electrical Conductance of Thin Films of Cu/Ag-TCNQ and Cu-Hexacyanoferrate

A Thesis

Submitted in Partial Fulfillment of the Requirements

for the Degree of

Doctor of Philosophy

by

Shammi Rana

ID: 20143304

INDIAN INSTITUTE OF SCIENCE EDUCATION AND RESEARCH, PUNE

2019

Dedicated

to my parents and all the mentors in life

भारतीय विज्ञान शिक्षा एवं अनुसंधान संस्थान, पुणे
INDIAN INSTITUTE OF SCIENCE EDUCATION AND RESEARCH (IISER), PUNE
(An Autonomous Institution, Ministry of Human Resource Development, Govt. of India)

Dr. NIRMALYA BALLAV
Associate Professor (Chemistry)
E-mail: nballav@iiserpune.ac.in
Web: http://www.iiserpune.ac.in/~nballav/

Dr. Homi Bhabha Road, Pashan
Pune 411 008, INDIA
Tel: +91 20 2590 8215
Fax: +91 20 2586 5315

CERTIFICATE

Certified that the work incorporated in the thesis entitled ***"Chemical Reduction at Solid-Liquid Interface: Growth and Electrical Conductance of Thin Films of Cu/Ag-TCNQ and Cu-Hexacyanoferrate"*** submitted by ***Mr. Shammi Rana*** was carried out by the candidate, under my supervision. The work presented here or any part of it has not been included in any other thesis submitted previously for the award of any degree or diploma from any other university or institution.

Date: 15th February, 2019

Dr. Nirmalya Ballav
(Research Supervisor)

भारतीय विज्ञान शिक्षा एवं अनुसंधान संस्थान, पुणे
INDIAN INSTITUTE OF SCIENCE EDUCATION AND RESEARCH (IISER), PUNE
(An Autonomous Institution, Ministry of Human Resource Development, Govt. of India)

Declaration

I ***Mr. Shammi Rana*** declare that, this written submission represents my ideas in my own words and where others' ideas have been included; I have adequately cited and referenced the original sources. I also declare that I have adhered to all principles of academic honesty and integrity and have not misrepresented or fabricated or falsified any idea/data/fact/source in my submission. I understand that violation of the above will be cause for disciplinary action by the Institute and can also evoke penal action from the sources which have thus not been properly cited or from whom proper permission has not been taken when needed.

The work reported in this thesis is the original work done by me under the guidance of ***Dr. Nirmalya Ballav.***

Date: 15th Feb, 2018

Mr. Shammi Rana
(ID: 20143304)

nballav@iiserpune.ac.in Tel: +91 (020) 2590 8215 www.iiserpune.ac.in

Acknowledgements

First and foremost, I would like to express my sincere gratitude and appreciation to my thesis supervisor Dr.Nirmalya Ballav for giving me an opportunity to work in his lab and for his invaluable mentorship throughout my PhD tenure. His relevant suggestions, constant encouragement, timely advice and guidance have been a constant source of motivation and support during my PhD. His immense faith in my abilities has helped me to work enthusiastically and also grow as a researcher in the process. He has helped me to broaden and widen my research aptitude due to continuous and intense scientific discussions from time to time.

Further, I would like to extend my appreciation to my Research Advisory Committee (RAC) members Dr. Shouvik Datta and Dr. Pramod Pillai for their continuous support, guidance, valuable time and suggestion throughout my PhD tenure. In particular, I am indebted to Dr. Shouvik Datta, for permitting me to independently handle FESEM, and Sputtering instruments which have been important part of my thesis. I am further thankful to my first collaborator Dr. Pinaki Talukdar and his students Sharad and Sopan. I would also like to thank my other collaborators Dr. Sudipta Roy Barman (XPS), and Dr. Vasant Sathe (Raman) from IUC Indore. In addition, I am very much thankful to our former and present director as well as all the faculty members of IISER Pune. I am very grateful to all the staff members of IISER Pune especially Anil Prathamshetti, T.S. Yatish, Nilesh Dumbre, Praveen Nasa, Mayuresh Kulkarni, Megha Paygude, Mahesh Jadhav, Ganesh Dimbre, Sanjay Meena, Tushar Kurulkar, Sandeep Kanade.

It has been a great privilege and delight to be a member of Interfacial Material Chemistry (IMC) team, due to the presence of such amazing and fun loving bunch of people. I would like to first thank my seniors Dr. Barun Dhara, Dr. Ranguwar Rajendra, and Dr. Plawan K. Jha for their guidance, help and scientific teaching. I am also grateful to all other members of IMC team; Kriti, Debashree, Pooja, Vikash, Anupam, Ashwini, Jainendra, Gopi, Pranay, Ishan, Anita, Manish, Satyam, Utkarsh, Dr. Syed Zahid Hassan, and Dr. Sujit Bhand for their friendly demeanor and co-operation throughout my PhD journey.

I would like to take this opportunity to express my sincere gratitude to Madam (Dr. Tanushree Bhattacharjee) and Tani for their constant encouragement and support.

I convey my deepest sense of gratitude to all my school teachers especially, Mrs. Raksha Sharma, Mr. Vijay Pal Dhiman, Mr. Kuldeep Singh, and Mr. Sanjay Kumar for their invaluable teachings. I am also thankful to all my college teachers especially Dr. Anushree Chadha, Dr. Sanjeev Raj, Dr. Ranjeet Thakur, Dr. Usha Sharma, Dr. Naresh Sharma, Dr. V. K. Vats, Dr. B. K. Vermani, Dr.Sonu, Dr. Reshma Mahrotra, and Dr. Jyotsna for their guidance.

I am extremely grateful to all my friends at IISER Pune without whom life would not have been so amusing and delightful at IISER-Pune, Amit, Mahesh, Dinesh, Avinash, Harshad, Dheeraj, Rakesh, Sachin, Nilesh, Debu, Anil, Saleem, Wasim, Jagdeesh, Sagar, Bhibhishan, Vijaykant, Ashok, Shyama, Ajay, and Chetan. I owe it to my best friends outside the IISER, Pawanpreet, Sandeep, Nitish, Arun, Jaideep, Kamal, Anil, Anu, Sakshi, Gunjan, Ambika, Chanchal, Rekha, Sumeet, Jyoti, Manisha and Gaurav for their consistent love, support and encouragement.

I am also thankful to IISER-Pune, MHRD, SERB, Infosys and DST Nano Mission for the financial support. I would like to thank American Chemical Society (ACS), John-Wiley & Sons (Wiley-VCH), and Elsevier for publishing a number of my research articles.

In the end, I would like to profess my deepest gratitude to my parents, elder brother and his wife for their unconditional faith, support and encouragement. I am greatly indebted to them for their eternal love and support during all my educational ventures. Their undying belief and faith in my abilities have made all this possible. Without their help, I would not have been able to complete much of what I have done and become who I am.

Shammi Rana

Table of Contents

Synopsis

The thesis entitled *"Chemical Reduction at Solid-Liquid Interface: Growth and Electrical Conductance of Thin Films of Cu/Ag-TCNQ and Cu-Hexacyanoferrate"* include 4 chapters.

An interface is a boundary between two spatial regions either occupied by different matters or by a matter in different physical states, for example, solid-solid, solid-liquid and liquid-liquid interfaces. Notable interfacial phenomena are two-dimensional electron-gas, spinterface, and heterogeneous catalysis. Various chemical reactions involving oxidation and reduction processes at interfaces may vary from those in conventional liquid-phase reactions and could thus influence the overall outcome. The present thesis primarily focuses on studying the metal-ligand coordination at solid-liquid interface.

Chapter 1. *Introduction*

This chapter comprises of general introduction for the surface and interfacial phenomenon, various techniques to fabricate thin films, Layer-by-Layer (LbL) approach, self-assembled monolayers (SAMs), M-TCNQ complexes and Copper-hexacyanoferrate (Cu-HCF). Additionally, objective of this thesis is also briefly discussed.

Chapter 2. *Thin Films by Interfacial Chemical Reaction*

In this chapter, we have studied the chemical reactions at solid-liquid interface and growth of Cu-TCNQ and Ag-TCNQ on functionalized Au substrate through Layer-by-Layer (LbL) approach. This chapter has been divided into two subsections.

Section 2A. *Growth of Cu-TCNQ*

In this section, MUDA/Au SAM was alternatively dipped into $Cu(OAc)_2$ and TCNQ solutions. Upon dipping the Cu(II) decorated MUDA/Au SAM into TCNQ solution, spontaneous reduction of Cu(II) to Cu(I) was observed at solid-liquid interface. Similar reduction was absent in liquid-phase reaction of Cu(II) and TCNQ. This interfacial reduction leads to the formation Cu-TCNQ complex on top of functionalized Au substrate. Repeating the alternate dipping procedure up to fifty consecutive cycles of LbL growth, thin film of Cu-TCNQ was fabricated.

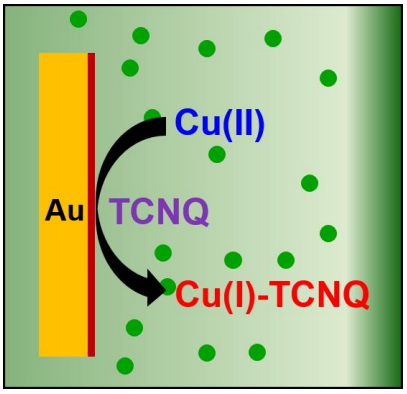

Scheme 1: *Schematic illustration of interfacial reduction of Cu(II) to Cu(I) at solid-liquid interface which lead to the growth of Cu-TCNQ complex on functionalized Au substrate.*

Publication from this chapter

1. Interfacial Reduction of Cu(II) to Cu(I)
   S. Rana, P. Sindhu, and N. Ballav.
   2019 (submitted)

Section 2B. *Growth of Ag-TCNQ*

In this section, we have employed liquid-phase heteroepitaxy (LPH) approach to grow thin film of Ag-TCNQ by using Cu-TCNQ thin film as a sacrificial template. The on-surface transformation of Cu-TCNQ to Ag-TCNQ was observed and it was realized to be sacrificial growth rather than typical ion exchange process.

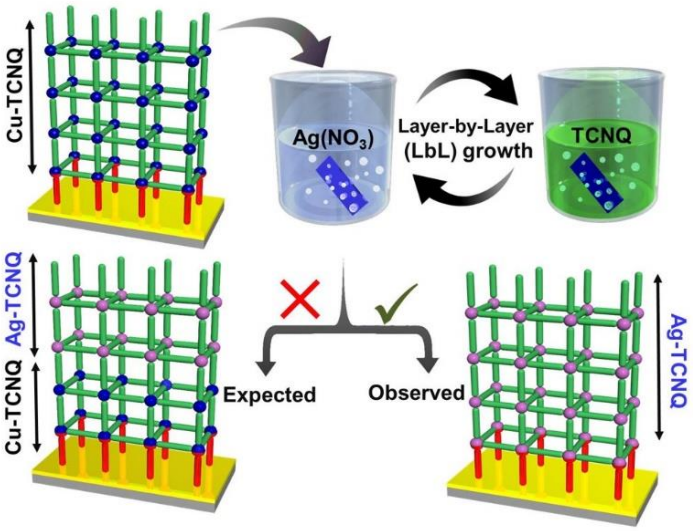

Scheme 2: *Schematic illustration of sacrificial growth of Ag-TCNQ.*

Publication from this chapter

1. Thermally Driven Resistive Switching in Solution-Processable Thin Films of Coordination Polymers .

   S. Rana, A. Prasoon, P. K. Jha, A. Prathamshetti, and N. Ballav.

   J. Phys. Chem. Lett., **2017**, *8*, 5008–5014.

Chapter 3. *Electrical Conductance in Thin Films of Cu/Ag-TCNQ*

In this chapter, we have studied the effect of external stimuli on electrical conductance of Cu-TCNQ and Ag-TCNQ. This chapter is subdivided into two subsections.

Section 3A. *Chemical Effect*

In this section, Cu-TCNQ thin film devices were fabricated by employing electron beam lithography (EBL) on functionalized Au and FTO substrate. Cu-TCNQ thin film devices showed non-ohmic current-voltage (*I-V*) characteristics. After exposing iodine (I_2) vapors to Cu-TCNQ, electrical rectification was observed. This interesting behaviour was attributed to the formation of heterostructure i.e. CuI/Cu-TCNQ. While I_2 dosing to Ag-TCNQ system lead to the formation of AgI thin film alone rather than a heterostructure.

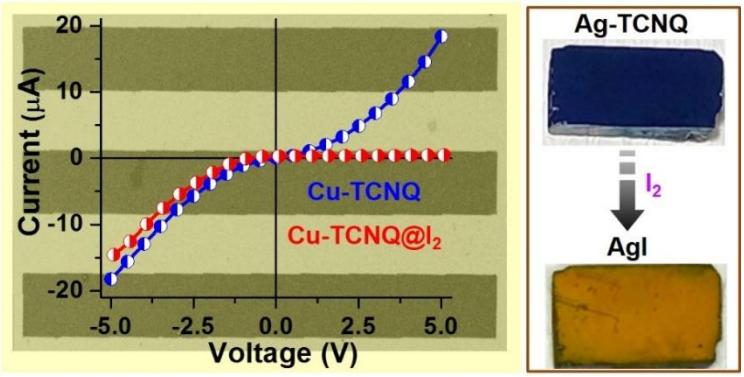

Scheme 3: *Current-Voltage (I-V) characteristics of Cu-TCNQ thin film device before and after iodine dosing (left). Optical image of Ag-TCNQ thin film before and after iodine dosing (right).*

Publications from this chapter

1. Highly Hydrophobic and Chemically Rectifiable Surface-Anchored Metal-Organic Framework Thin-Film Devices

   S. Rana, R. Rajendra, B. Dhara, P. K. Jha, and N. Ballav.

   Adv. Mater. Interfaces, **2016,** 3, 1500738-1500748.

2. On-Surface Transformation of Ag-TCNQ to AgI

   S. Rana, A. Prasoon, S. Bhand, and N. Ballav.

   2019 (submitted)

Section 3B. *Thermal Effect*

Both Cu-TCNQ and Ag-TCNQ are semiconducting coordination polymers and well known for their resistive switching behaviour. In this section, we have successfully demonstrated thermally driven reversible resistive switching in thin films of Ag-TCNQ and Cu-TCNQ. This was due to alternation of the Schottky barrier at the metal–semiconductor interfaces induced by the thermal energy. A remarkable enhancement factor in the electrical conductance with an excellent switching durability is observed.

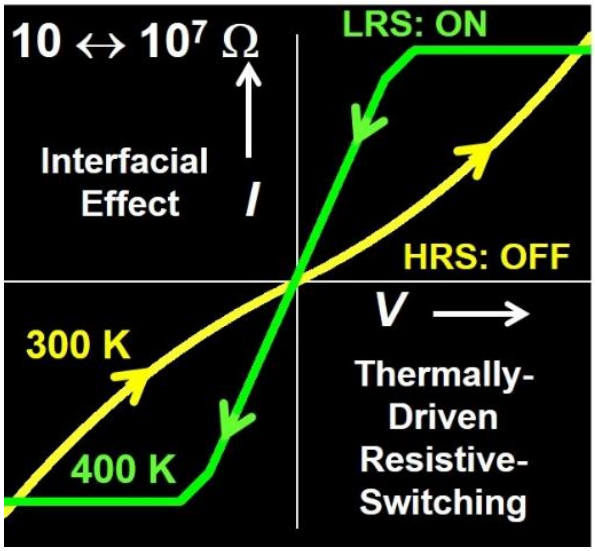

Scheme 4: *Variable temperature current-voltage (I-V) characteristics of Ag-TCNQ thin film.*

Publication from this chapter

1. Thermally Driven Resistive Switching in Solution-Processable Thin Films of Coordination Polymers .

   S. Rana, A. Prasoon, P. K. Jha, A. Prathamshetti, and N. Ballav.

   J. Phys. Chem. Lett., **2017**, *8*, 5008–5014.

Chapter 4. *Thin Films by Interfacial Chemical Reaction: Growth and Electrical Conductance in Cu(I)-HCF*

In this chapter, we have observed the spontaneous reduction of Cu(II) to Cu(I) at solid-liquid interface, upon dipping Cu(II) decorated MUDA/Au SAM into $K_4[Fe(CN)_6]$ solution—while a similar reduction was absent in liquid-phase reaction. This interfacial reduction reaction (IRR) results in the fabrication of high-quality thin films of coordination network having Fe(II)−CN−Cu(I) link on a functionalized Au substrate through LbL approach. Electron transfer from neither Fe(II) nor Au substrate was found to be responsible for the interfacial reduction. A confinement effect of restricted coordination at the interface is proposed to facilitate the reduction of Cu(II) to Cu(I). Also, here we have observed thermally driven reversible structural phase transition in thin film which, in turn modulated the electron transport property.

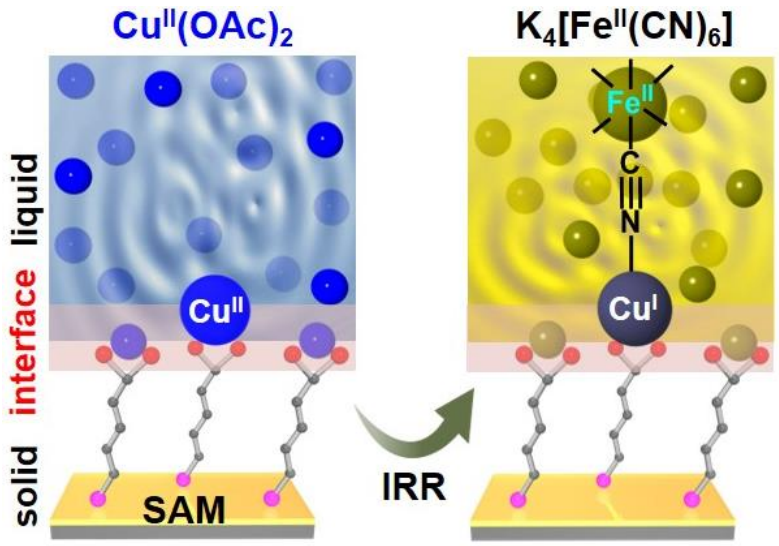

Scheme 5: Schematic illustration of spontaneous reduction of Cu(II) to Cu(I) at solid-liquid interface.

Publication from this chapter

2. Spontaneous Reduction of Copper(II) to Copper(I) at Solid–Liquid Interface.
   S. Rana, A. Prasoon, P. Sadhukhan, P. K. Jha, V. Sathe, S. R. Barman, and N. Ballav.
   J. Phys. Chem. Lett., **2018,** *9*, 6364–6371.

Glossary of Acronyms

C	Capacitance
V	Voltage
I	Current
eV	Electron Volt
TCNQ	7,7,8,8,-Tetracyanoquinodimethane
Cu-HCF	Copper Hexacyanoferrate
SAM	Self-assembled monolayer
MUDA	Mercaptoundecanoic acid
CPs	Coordination polymers
Ω	Ohm
LbL	Layer-by-Layer
CA	Contact angle
LMCT	Ligand to metal charge transfer
MLCT	Metal to ligand charge transfer
MMCT	Metal to metal charge transfer
°C	Degree Celsius
K	Kelvin
PMMA	Polymethylmethacrylate
HRS	High resistance state
LRS	Low resistance state
EDXS	Energy-dispersive X-ray spectroscopy
UV-vis	Ultraviolet-visible spectroscopy
FESEM	Field emission scanning electron microscopy
PXRD	Powder X-ray diffraction
TEM	Transmission electron microscopy
XPS	X-ray photoelectron spectroscopy
EPR	Electron paramagnetic resonance
EGaIn	Eutectic gallium indium

PB	Prussian Blue
PBAs	Prussian Blue Analogues
EtOH	Ethanol
M-TCNQ	Metal-Tetracyanoquinodimethane
CVD	Chemical Vapor Deposition
PVD	Physical Vapor Deposition
Cu	Copper
Ag	Silver
Au	Gold
FTO	Fluorine-doped Tin Oxide

Publications Included in Thesis

1. Spontaneous Reduction of Copper(II) to Copper(I) at Solid–Liquid Interface.
   S. Rana, A. Prasoon, P. Sadhukhan, P. K. Jha, V. Sathe, S. R. Barman, and N. Ballav.
   J. Phys. Chem. Lett., **2018,** 9, 6364–6371.
2. Thermally Driven Resistive Switching in Solution-Processable Thin Films of Coordination Polymers .
   S. Rana, A. Prasoon, P. K. Jha, A. Prathamshetti, and N. Ballav.
   J. Phys. Chem. Lett., **2017**, *8*, 5008–5014.
3. Highly Hydrophobic and Chemically Rectifiable Surface-Anchored Metal-Organic Framework Thin-Film Devices
   S. Rana, R. Rajendra, B. Dhara, P. K. Jha, and N. Ballav.
   Adv. Mater. Interfaces, **2016,** 3, 1500738-1500748.
4. Chemical Reduction at Solid-Liquid Interface
   S. Rana, P. Sindhu, and N. Ballav.
   2019 (submitted)
5. On Surface Transformation of Ag-TCNQ to AgI
   S. Rana, A. Prasoon, S. Bhand, and N. Ballav.
   2019 (submitted)

Other Publications

6. Stable Red Emission from Nanosheets of Molecularly Doped Hexagonal Boron Nitride
   V. Kumar, N. Joshi, B. Dhara, P. K. Jha, **S. Rana,** P. Ghosh, and N. Ballav.
   J. Phys. Chem. C, **2018,** 122, 21076–21082.
7. High-Level Supercapacitive Performance of Chemically Reduced Graphene Oxide
   P. K. Jha, S. K. Singh, V. Kumar, **S. Rana,** S. Kurungot, and N. Ballav
   Chem, **2017,** 3, 846-860.
8. Selective Sensing of Metal Ions and Nitro Explosives by Efficient Switching of Excimer-to-Monomer Emission of an Amphiphilic Pyrene Derivative

S. C. Deshmukh, **S. Rana,** S. V. Shinde, B. Dhara, N. Ballav, and P. Talukdar *ACS Omega*, **2016,** 1, 371–377.

9. Metamagnetism in Nanosheets of Co^{II}-MOF with T_N at 26 K and a Giant Hysteretic Effect at 5 K. K. Gupta, A. Dhadwal, **S. Rana,** P. K. Jha, A. Jain. S.M. Yusuf, P.A. Joy and N. Ballav*

Inorg. Chem. **2018,** 57, 15044-15047

CHAPTER 1

Introduction

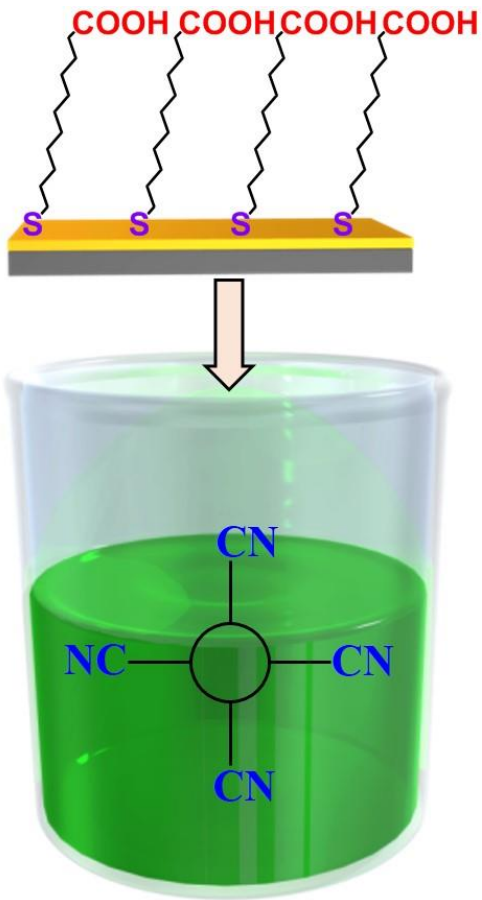

1.1 Surface and Interfaces

A common spatial boundary occupied by different matter or by matter in different physical state is called interface. An interface is a thin layer that has different properties than bulk material on its either side. One of the common examples include a glass of water, which has three interfaces: water – surrounding air, water – glass, and glass – surrounding air. Every object has one or more interfaces and these are certainly ubiquitous in nature. The evaporation of liquids, photosynthesis, adsorption of gases on metal surface, friction, the action of detergents and corrosion, refraction, are some of the common interfacial phenomena.[1-2] Interface between water and air, in a glass of water is almost flat while the same interface for a single drop of water is curved (Figure 1a).

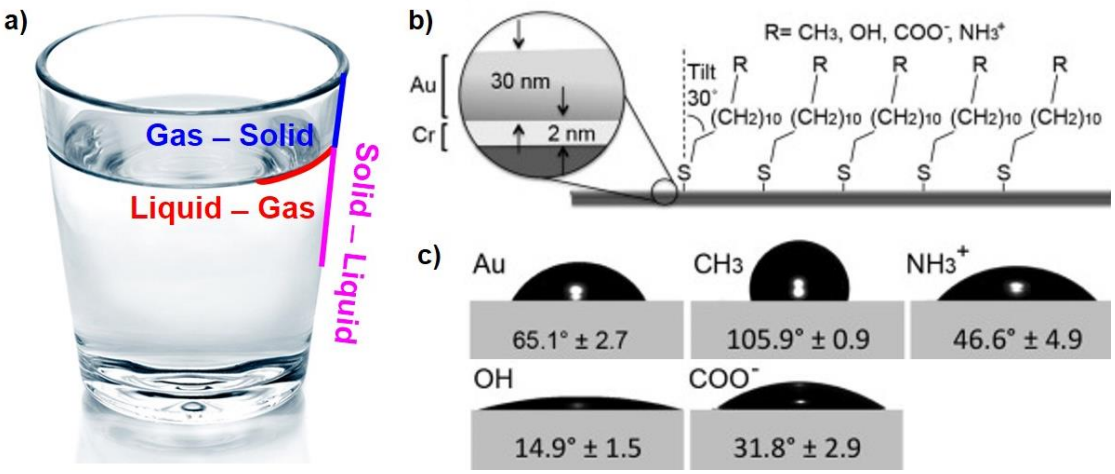

Figure 1: *(a) Optical image of a glass filled with water (interfaces are highlighted) (source google). (b) Schematic of alkane-thiol self-assembled monolayer (SAM) on Au substrate. (c) Optical images of water droplet on different functional group terminated SAM and their corresponding contact angle of air-water-surface (adopted from Ref. 3 @ Elsevier).*

How important is the interface? If we have carboxylate functionalized Au substrate, the solid-liquid interface is hydrophilic in nature as water contact angle (CA) comes ~20°, while it became hydrophobic upon changing the terminal group from carboxylate to methyl (water CA ~105°) (Figure 1b & 1c).[3] The understanding of the molecular-level chemistry that occurs at the interface is key to the development of many chemical, biological and physical systems, and is debatably the next big challenge for the surface-science community. Corrosion of metal

surfaces, the operation of electrochemical cells are some of the examples of chemical reactions occurring at the solid-liquid interface. However, it is not easy to investigate the chemical reactions occurring at interfaces on molecular level. Study of the interfacial reactions helps in determining the various factors which control the physico-chemical behavior of such systems and is important for optimizing the efficiency of their applications.[4] A large number of surface-sensitive techniques such as various spectroscopic [X-ray photoelectron spectroscopy (XPS), Raman spectroscopy, X-ray absorption spectroscopy (XAS), Infrared Reflection Absorption Spectroscopy (IRRAS)], and microscopic [Field Emission Scanning Electron Microscopy (FESEM), Scanning Tunneling Microscopy (STM), Atomic Force Microscopy (AFM)] techniques are required to study chemical reactions, structure, kinetics and charge-transfer dynamics at the interface which helps us to understand the interfacial chemistry.

In general, interface between two materials (oxides, organic molecule, metal chalcogenides, graphene, or MoS_2) can act as a host to a large range of interesting physics and chemistry related applications extending to magnetic and superconductvity.[5-6] The Interfacial properties substantially differ from their bulk counterparts, and are strongly depends on the nature of material, environmental conditions and morphological characteristics.[7] For example, the hetero-interface between two electrical insulating and non-magnetic perovskite metal oxides i.e. $LaAlO_3$ (LAO) and $SrTiO_3$ (STO) was observed to be metallic, magnetic, as well as superconducting (Figure 2a & 2b).[6, 8] A highly conductive layer containing the electron gas was formed between these two oxides (LAO and STO) at the interface and it was observed to be a two-dimensional (2D) superconductor.[9] This quasi-two-dimensional electron gas (q-2DEG) was majorly present at the hetero-interface between insulating oxides such as $LaAlO_3/SrTiO_3$, $LaVO_3/SrTiO_3$, and $LaTiO_3/SrTiO_3$ structures, and confined at the interface between LaO and TiO_2.[9-11] Interface between these oxides, provides a distinctive opportunity to control and enhance the effects by monitoring the interaction between layers. The interface between insulating organic crystals was also realized to be metallic in nature. Upon mechanically pressing two organic single crystals, TCNQ (7,7,8,8-tetracyanoquinodimethane) and TTF (tetrathiafulvalene), a highly conductive layer was formed between them with a remarkably high carrier density 10^{14} cm^{-2} (Figure 2c).[12] This metallic conduction at interface

arises mainly due to electron transfer from highest occupied molecular orbital (HOMO) of TTF to lowest unoccupied molecular orbital (LUMO) of TCNQ molecule.[12]

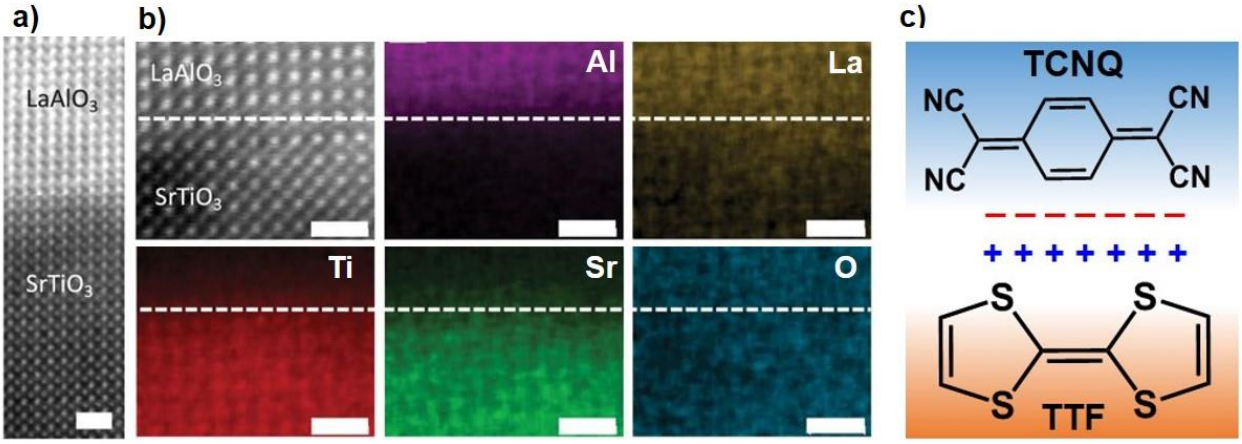

Figure 2: *(a) High resolution STEM image of $LaAlO_3/SrTiO_3$ interface. (b) High-magnification STEM image of $LaAlO_3/SrTiO_3$ interface, showing the detailed microstructures close to the interface and atomically resolved chemical mapping of Al, La, Ti, Sr, and O respectively. Scale bars are 1 nm for all images (adopted from Ref. 11 @ Nature Publishing Group). (c) Schematic of interface between two organic crystals (TCNQ and TTF) which is found to be superconductor.*

Interestingly, the surface/interface becomes more important in nanostructures as compared to bulk materials. In nanostructures, physical properties are majorly dependent upon their surface and interfacial environment as compared to bulk materials; this is due to the higher concentration of their constituent particles at surface. The gradient in properties is highest at surfaces and interfaces. Atoms/molecules present at surfaces/interfaces experiences a different kind of environment than those in bulk. Hence, at surface/interface constituent particles have different reactivity, free energies, structure and mobility etc. Knowledge of interfacial phenomenon is crucial for thin films because these are more often explored for their surface and interfacial properties.

1.2 Brief Overview on Thin Films

Thin films are well-ordered and densely packed thin layer of material (organic/inorganic) deposited on a suitable substrate. Thin film thickness ranges from 5 nm to 1 μm, while below 5 nm they are known as ultra-thin films and the one between 1-10 μm are called thick films.

An ultrathin film contains few layer/monolayer of atoms constituting the material, molecular self-assemblies, and epitaxial grown films by atomic layer deposition. But question arises *"Why thin films are so important?"*

1) Thin-film properties (optical, magnetic, electronic, thermal *etc.*) are significantly different from their corresponding bulk counterparts. This is due to their reduced size, dimensional constraint, microstructure and geometry.
2) In thin film, surface properties of the material often dominate over the conventional bulk properties. This is due to remarkable enhancement in their surface area-to-volume ratio brought by the dimensional restraints.
3) During growth of thin films, several defects can be incorporated which provide them different microstructure and unique properties, for example - intensification of resistivity in thin film.
4) It is easy to tailor characteristics of thin film to obtain desired properties. It thus formed a basis for improvement of several mechanical, active, and passive components of devices.
5) Thin films are used in almost all technological areas which make them so important.

Thin films find large number of application in our day-to-day life such as nanotechnology, catalysis, solar panel, thin film transistor, fuel cell, microelectronics, sensors, batteries, data storage, decorative and optical coatings. To study various physical, chemical and structural properties of thin films, sophisticated techniques are needed. Structure of thin film was determined by using grazing incidence x-ray diffraction (GIXRD), topography with scanning tunneling microscope (STM), surface structure with field emission scanning electron microscope (FESEM) as well as atomic force microscope; chemical analysis of thin film with X-ray photoelectron spectroscopy (XPS) and electron probe micro analyzer (EPM).

Fabrication of high-quality thin film is prerequisite for various technological applications. There exist numerous well-established methods to deposit thin films, yet there is significant interest in alternative methods which would be less expensive, more reliable, and capable of producing high quality films. All deposition techniques basically involve production of the constituent's species (atomic, molecular or ionic), transport of these species to a suitable

substrate, or deposition onto the substrate via direct condensation or chemical/electrochemical reaction.

Thin film deposition techniques are broadly classified into following three categories:

1. **Physical Vapor Deposition (PVD) Process:** In this method, the depositing material is vaporized into atomic or molecular species by physical means (laser ablation, ion bombardment, or evaporation). Vaporized species undergoes condensation on a substrate and no chemical reaction occurs in the entire process (Figure 3).
2. **Chemical Vapor Deposition (CVD) Process:** In this method, the vapors of depositing materials undergo chemical reaction to form solid film on a substrate. Generally, precursors are gaseous in nature and they are pumped in to a reaction chamber. Under the right conditions such as temperature and pressure, they undergo a reaction at the substrate. One of the products of the reaction gets deposited on the substrate (Figure 3).
3. **Chemical Solution Deposition Process:** In this method, precursor solution is coated on the substrate (Figure 3).

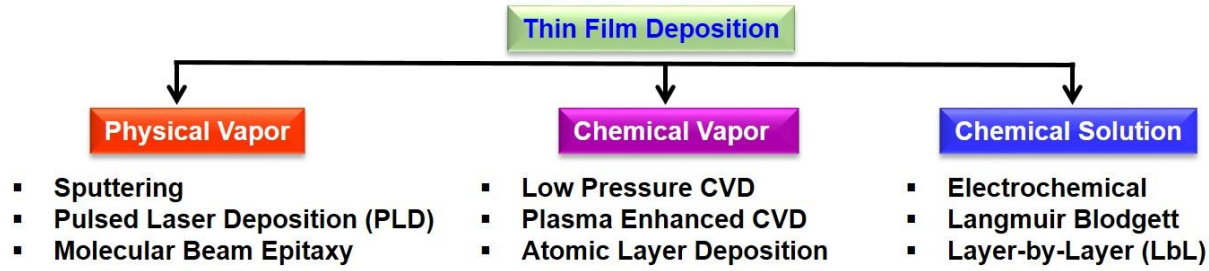

Figure 3: *Classification of various thin film deposition techniques.*

Note that this PhD work primarily deals with thin films grown by LbL method.

1.3 Functionalized Substrate: Self-assembled Monolayers (SAMs)

Self-Assembled Monolayer (SAM) is one molecule thick layer of material, formed spontaneously on a surface as result of physical or chemical adsorption during deposition process (Figure 4). Thiols and silanes can easily form SAMs by solution or vapor phase

deposition processes on Gold (Au) and Silicon (Si) substrates, respectively.[13] Once deposition occurs, a covalent (Au-S) bond formed with the surface which provide a permanent modification on surface of substrate.[13] The mostly studied SAMs are derived from adsorption of thiol on Au, Ag, Cu and Pt, because thiols have high affinity for the surfaces of noble and coinage metals.[14] Thiol SAMs have typical thickness in range of 1-3 nm which could be measured by ellipsometry and XPS.[13] SAMs are commonly used in nanoscience because (a) they are easy to prepare, just by dipping Au substrate into corresponding thiol solutions, do not require ultrahigh vacuum (UHV) or any particular instrument; (b) They can be made on differently sized objects and can modify surfaces; and (c) They couple the external environment to optical and electronic structure of metals.[15] The structure of a SAM is dependent on the chain length of adsorbate (thiol) molecule and the structure as well as orientation of the substrate. The molecules forming SAMs have a chemical functionality (head group) which have specific affinity for substrate (Figure 5). The most commonly used thiol molecules to functionalize Au substrate are Mercaptoundecanoic Acid (MUDA), Dodecanethiol (DDT), Mercaptoundecanol, Benzene-1,4-dithiol (BDT), and Biphenyl-4,4′-dithiol (BPDT).[13] The selective positioning of organic thiol molecule (patterning) on surfaces can be achieved by micro-contact printing (μCP), electron-beam lithography (EBL), photo lithography, and ink jet printing.[13, 16] SAMs are very important for nanoscience technology, used mainly for study interfacial phenomena such as wetting, corrosion, adhesion, nucleation and growth on surfaces, model surfaces for biochemistry and cell biology. They are now recognized as essential interlayers and electronically active layers in organic electronic devices, such as organic photovoltaics, non-volatile memories, and organic thin film transistors. Also, SAMs have been used as platform to study crystallization of calcium carbonate.[17] Various other applications of SAMs include protection of films from corrosion by chemical-etchants, adsorption of protein and to modify electrodes for electrochemistry (to control electron transfer).

Thiolated SAMs on Au with –COOH exposed functionality are primarily used as functionalized substrate for LbL growth.

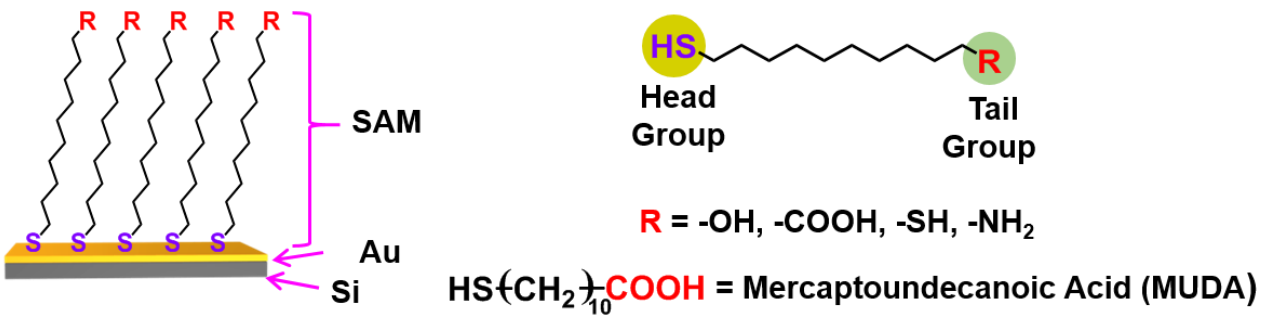

Figure 4: *Schematic of MUDA SAM on Au wafer and thiol molecule having different tail groups.*

1.4 Thin Films of Coordination Polymers by LbL Approach

The deposition of thin films through layer-by-layer approach involves sequential deposition of two or more materials that are physically bonded (Figure 5).[18] The techniques that are used for LbL assembly include successive spraying, immersion, spin coating, and electrochemical deposition.[19] LbL assembly through immersive techniques is most widely used and is typically executed by manually immersing a substrate into a solution of the desired material, followed by washing to remove unbound or unreacted material. Since last few decades, LbL approach of depositing thin films has been of significant interest because of its ability to have control over thickness of thin film, and the broad availability of functional materials for coating on substrates.

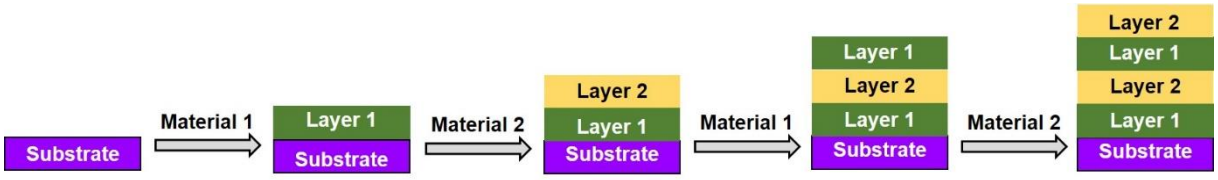

Figure 5: *Schematic of sequential deposition of two materials through LbL assembly.*

In recent years, LbL assembly through immersive technique has been extensively explored to grow thin film of coordination polymers (CPs) on top of conducting as well as non-conducting substrates (Figure 6).[20-21]

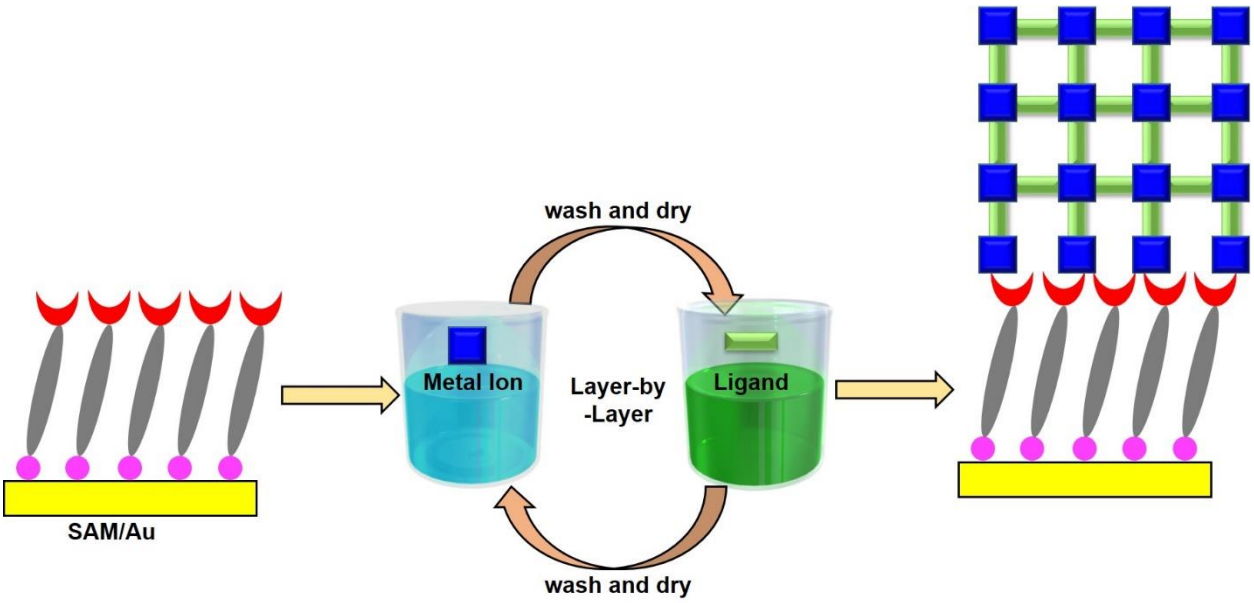

Figure 6: *Schematic of LbL approach to grow thin film of coordination polymers on SAM/Au template.*

Till date, majorly carboxylate or pyridine containing organic molecules (ligands) and Copper/Zinc (metal ions) are used to grow thin films of CPs through LbL approcah.[20] Commonly used substrates in this technique are functionalized Au substrate, SiO_2 coated silicon wafer, fluorine-doped tin oxide (FTO) and indium tin oxide (ITO) glass.[21] Growth of CPs through LbL approach generates highly oriented and homogenous thin film, also it prevents interpenetration of coordination network.

1.5 Coordination Polymers: M-TCNQs

Coordination compounds having one, two, or three dimensional (1D, 2D or 3D) polymeric structures consisting metal ions or clusters connected via organic linkers are called as Coordination Polymers (CPs).[22] Due to the easy tunability of their structure and availability of large number of metals and ligands, they can be used for variety of applications. Mostly oxygen and nitrogen based ligands have been used for the synthesis of CPs. One of the well-known nitrogen based ligand is 7,7,8,8-Tetracyanoquinodimethane (TCNQ). It is a planar organic molecule with D_{2h} symmetry and Π-conjugated system.[23] TCNQ is one of the synthetic

derivatives from the series of novel cyano-olefins.[23] It is a strong Π-acceptor, has high electron affinity (~2.8 eV), and forms stable molecular complexes containing radical monoanion ($TCNQ^{-}$) and dianion ($TCNQ^{2-}$).[24] Alkali metal-TCNQ (Na-TCNQ, K-TCNQ, Cs-TCNQ and Rb-TCNQ) are one-dimensional (1D) charge transfer complexes with isolated columns of TCNQ anion and alkali metal cation.[25] TCNQ is also known to form charge transfer complexes with transition metal ions (M-TCNQ; M= V, Fe, Co, Ni, Cu, Zn, Mn, Ag and Zn).[26-27] M-TCNQ complexes are majorly studied for their magnetic properties except Cu/Ag-TCNQ which are mostly explored for their unusual electrical properties.[26] Cu-TCNQ and Ag-TCNQ complexes are two dimensional (2D) organic semiconductors, bistable (exist in two phases), majorly used in memory storage devices, and have been extensively studied for their resistive switching behavior and field emission properties (Figure 7a & 7b).[28-30] So far, thin films of Cu/Ag-TCNQ complexes are fabricated by vapor deposition techniques (CVD, PVD); electro-crystallization; and by dipping Cu/Ag metal in TCNQ solution (Figure 7c).[30-31]

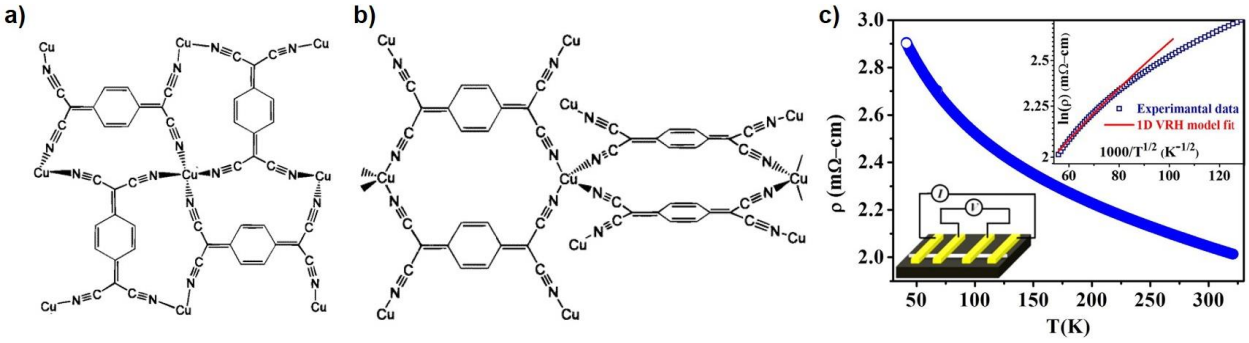

Figure 7: *(a) Schematic depicting bonding in Cu-TCNQ Phase-I (b) and Phase-II (c) (adopted from Ref. 31 @ American Chemical Society). (c) Temperature dependent resistivity of Cu-TCNQ nanowire (Lower Inset: Schematic of device used for measurement) (adopted from Ref. 30 @ Nature Publishing Group)*

1.6 Coordination Polymer: Cu-HCF

Copper Hexacyanoferrate (Cu-HCF) is one of the Prussian blue analogues (PBAs), which is majorly used as cathode material in batteries and for removal of toxic metal ions such cesium (Cs).[32-33] Prussian blue (PB) is a blue colored first modern synthetic pigment, with a chemical formula $Fe_4[Fe(CN)_6]_3 . xH_2O$ and majorly used in paints (Figure 8).[34] It is a mixed valence

compound, containing iron (Fe) in two different oxidation states i.e. +3 and +2. In 18th century, this compound was used to dye the uniform coats of the Prussian army, hence it is named as PB. Modifications (interstitial and substitutional) in PB generate a series of new complexes commonly called as Prussian blue analogs (PBAs), represented by the general formula $A_xM_A[M_B(CN)_6]_y.nH_2O$, where M_A and M_B are transition metal ions and A is an alkali metal ion.[34] In the last two decades, PBAs have attracted great attention because it is easy to tune their structural, chemical and magnetic properties by controlling the transition metal ions and their oxidation state.[35] PBAs find large number of applications such as electrode material in batteries, gas storage, ammonia sensor, and photo-switchable magnetic devices.[36-37] Nevertheless, thin film of PBAs are fascinating from technological as well as scientific point of view because of reduced dimensionality and the ability to tune their properties by changing various parameters such as preparation conditions, compositions, and film thickness. Earlier, an electrochemical deposition of the $Cr_{2.12}Cr(CN)_6$. zH_2O thin film onto SnO_2 coated glass substrate was successfully achieved and also electrochemically-induced magnetic switching between a ferromagnetic and a paramagnetic state in the thin film was observed.[38] Many remarkable properties and synergic effects could be expected in hetero-structures of PBAs due to interface and surface effects. To deposit thin films of PBAs, commonly used techniques are electrochemical deposition, Langmuir Blodgett method, spin coating or using sol-gel matrix.

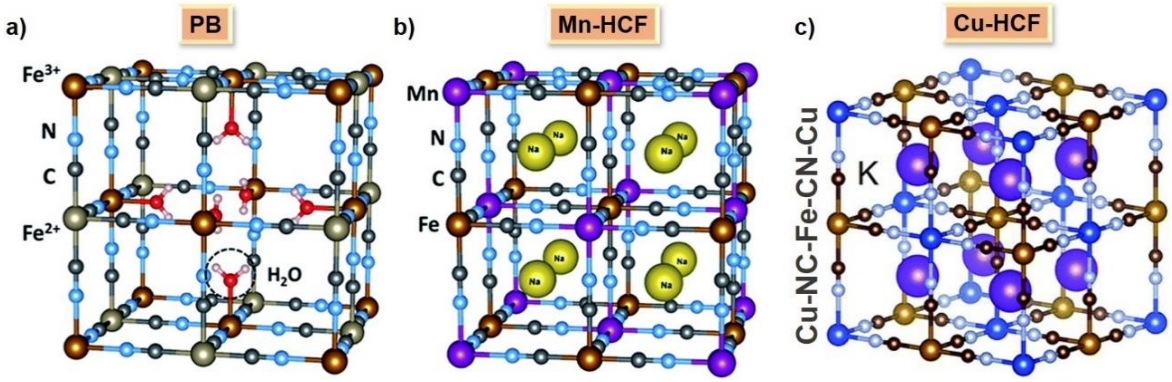

Figure 8: *(a) Unit cell of the PB $Fe_4[Fe(CN)_6]_3.nH_2O$ compound with defects. (b) Manganese-Hexacyanoferrate (Mn-HCF) $[Na_xMnFe(CN)_6]$ structure (adopted from Ref. 35 @*

Royal Society of Chemistry). (c) Copper-Hexacyanoferrate (Cu-HCF) $K_2Cu[Fe(CN)_6]$. (adopted from Ref. 33 @ Royal Society Chemistry)

1.7 Objectives of Thesis

Main objectives of thesis are following:

1. To investigate the metal-ligand coordination at solid-liquid interface where solid is functionalized Au/FTO substrate and solutions of metal salts as well as ligands were taken as liquids.
2. To grow thin films of Cu-TCNQ, Ag-TCNQ and Cu-HCF on functionalized Au substrate via layer-by-layer approach.
3. To fabricate proto-type thin film device by using photo-lithography and electron-beam lithography (EBL).
4. To study electrical conductance in thin films of Cu-TCNQ, Ag-TCNQ and Cu-HCF.
5. Modulation of electrical conductance in thin films by thermal and chemical stimuli.

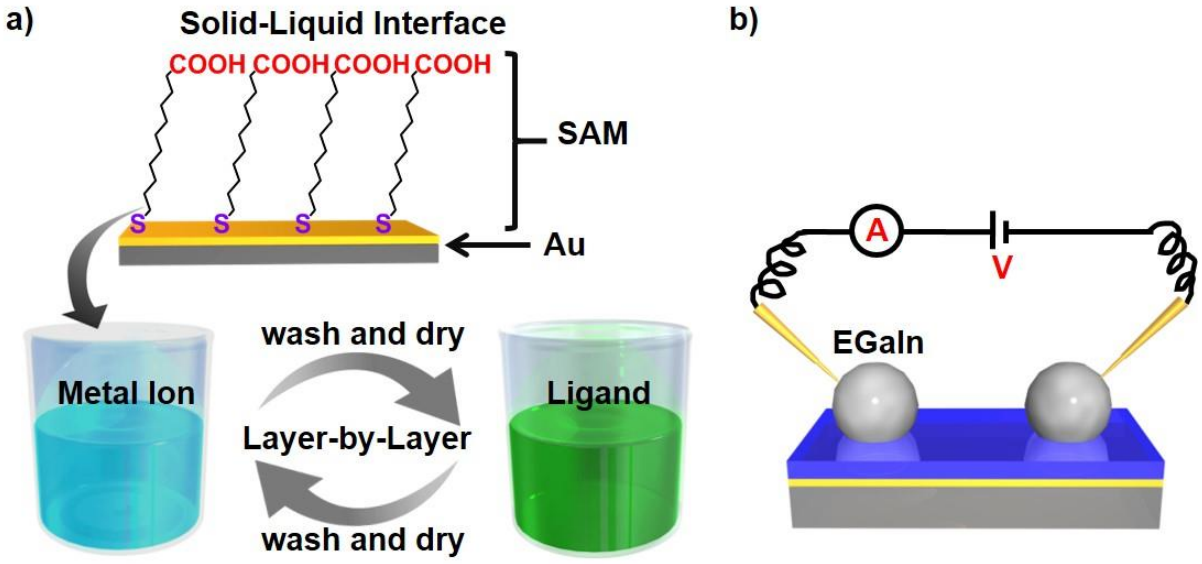

Figure 9: *(a) Schematic of MUDA SAM on Au substrate and LbL assembly. (b) Schematic of electrical measurement of thin film device with eutectic gallium indium (EGaIn) alloy as top electrode.*

1.8 References

(1) Kazemi, M. A.; Nobes, D. S.; Elliott, J. A. W., *Langmuir* **2017,** *33,* 4578-4591.

(2) Freund, H. J., *Angew. Chem. Int. Ed.* **1997,** *36,* 452-475.

(3) Rush, M. N.; Coombs, K. E.; Hedberg-Dirk, E. L., *Acta Biomater.* **2015,** *28,* 76-85.

(4) Astumian, R. D.; Chock, P. B., *J. Phys. Chem.* **1985,** *89,* 3477-3482.

(5) Song, T. T.; Yang, M.; Chai, J. W.; Callsen, M.; Zhou, J.; Yang, T.; Zhang, Z.; Pan, J. S.; Chi, D. Z.; Feng, Y. P.; Wang, S. J., *Sci. Rep.* **2016,** *6,* 29221-29229.

(6) Ohtomo, A.; Hwang, H. Y., *Nature* **2004,** *427,* 423-426.

(7) Zubko, P.; Gariglio, S.; Gabay, M.; Ghosez, P.; Triscone, J.-M., *Annu. Rev. Condens. Matter Phys.* **2011,** *2,* 141-165.

(8) Ohtomo, A.; Muller, D. A.; Grazul, J. L.; Hwang, H. Y., *Nature* **2002,** *419,* 378-380.

(9) Warusawithana, M. P.; Richter, C.; Mundy, J. A.; Roy, P.; Ludwig, J.; Paetel, S.; Heeg, T.; Pawlicki, A. A.; Kourkoutis, L. F.; Zheng, M.; Lee, M.; Mulcahy, B.; Zander, W.; Zhu, Y.; Schubert, J.; Eckstein, J. N.; Muller, D. A.; Hellberg, C. S.; Mannhart, J.; Schlom, D. G., *Nat. Commun.* **2013,** *4,* 2351-2355.

(10) Chen, Y.; Pryds, N.; Kleibeuker, J. E.; Koster, G.; Sun, J.; Stamate, E.; Shen, B.; Rijnders, G.; Linderoth, S., *Nano Lett.* **2011,** *11,* 3774-3778.

(11) Lu, H.-L.; Liao, Z.-M.; Zhang, L.; Yuan, W.-T.; Wang, Y.; Ma, X.-M.; Yu, D.-P., *Sci. Rep.* **2013,** *3,* 2870-2875.

(12) Alves, H.; Molinari, A. S.; Xie, H.; Morpurgo, A. F., *Nat. Mater.* **2008,** *7,* 574-580.

(13) Love, J. C.; Estroff, L. A.; Kriebel, J. K.; Nuzzo, R. G.; Whitesides, G. M., *Chem. Rev.* **2005,** *105,* 1103-1170.

(14) Vericat, C.; Vela, M. E.; Corthey, G.; Pensa, E.; Cortés, E.; Fonticelli, M. H.; Ibañez, F.; Benitez, G. E.; Carro, P.; Salvarezza, R. C., *RSC Advances* **2014,** *4,* 27730-27754.

(15) Arnold, R.; Azzam, W.; Terfort, A.; Wöll, C., *Langmuir* **2002,** *18,* 3980-3992.

(16) Kumar, A.; Biebuyck, H. A.; Whitesides, G. M., *Langmuir* **1994,** *10,* 1498-1511.

(17) Aizenberg, J.; Black, A. J.; Whitesides, G. M., *Nature* **1999,** *398,* 495-498.

(18) Richardson, J. J.; Cui, J.; Björnmalm, M.; Braunger, J. A.; Ejima, H.; Caruso, F., *Chem. Rev.* **2016,** *116,* 14828-14867.

(19) Richardson, J. J.; Björnmalm, M.; Caruso, F., *Science* **2015,** *348,* 2491-2503.

(20) Liu, J.; Woll, C., *Chem. Soc. Rev.* **2017,** *46,* 5730-5770.

(21) Zhuang, J.-L.; Terfort, A.; Wöll, C., *Coord. Chem. Rev.* **2016,** *307,* 391-424.

(22) Seth, S.; Matzger, A. J., *Cryst. Growth Des.* **2017,** *17,* 4043-4048.

(23) Acker, D. S.; Hertler, W. R., *J. Am. Chem. Soc.* **1962,** *84,* 3370-3374.

(24) Roberts, G. M.; Lecointre, J.; Horke, D. A.; Verlet, J. R. R., *Phys. Chem. Chem. Phys.* **2010,** *12,* 6226-6232.

(25) Funabiki, A.; Mochida, T.; Takahashi, K.; Mori, H.; Sakurai, T.; Ohta, H.; Uruichi, M., *J. Mater. Chem.* **2012,** *22,* 8361-8366.

(26) Vickers, E. B.; Giles, I. D.; Miller, J. S., *Chem. Mater.* **2005,** *17,* 1667-1672.

(27) Vickers, E. B.; Selby, T. D.; Thorum, M. S.; Taliaferro, M. L.; Miller, J. S., *Inorg. Chem.* **2004,** *43,* 6414-6420.

(28) Gu, Z.; Wu, H.; Wei, Y.; Liu, J., *J. Phys. Chem. C* **1993,** *97,* 2543-2545.

(29) Potember, R. S.; Poehler, T. O.; Benson, R. C., *Appl. Phys. Lett.* **1982,** *41,* 548-550.

(30) Basori, R.; Kumar, M.; Raychaudhuri, A. K., *Sci. Rep.* **2016,** *6,* 26764-26776.

(31) Heintz, R. A.; Zhao, H.; Ouyang, X.; Grandinetti, G.; Cowen, J.; Dunbar, K. R., *Inorg. Chem.* **1999,** *38,* 144-156.

(32) Wessells, C. D.; Huggins, R. A.; Cui, Y., *Nat. commun.* **2011,** *2,* 550.

(33) Takahashi, A.; Tanaka, H.; Minami, K.; Noda, K.; Ishizaki, M.; Kurihara, M.; Ogawa, H.; Kawamoto, T., *RSC Advances* **2018,** *8,* 34808-34816.

(34) Zakaria, M. B.; Chikyow, T., *Coord. Chem. Rev.* **2017,** *352,* 328-345.

(35) Paolella, A.; Faure, C.; Timoshevskii, V.; Marras, S.; Bertoni, G.; Guerfi, A.; Vijh, A.; Armand, M.; Zaghib, K., *J. Mater. Chem. A* **2017,** *5,* 18919-18932.

(36) Wang, B.; Han, Y.; Wang, X.; Bahlawane, N.; Pan, H.; Yan, M.; Jiang, Y., *iScience* **2018,** *3,* 110-133.

(37) Cafun, J.-D.; Champion, G.; Arrio, M.-A.; dit Moulin, C. C.; Bleuzen, A., *J. Am. Chem. Soc.* **2010,** *132,* 11552-11559.

(38) Sato, O.; Iyoda, T.; Fujishima, A.; Hashimoto, K., *Science* **1996,** *271,* 49-51.

CHAPTER 2

Thin Films by Interfacial Chemical Reaction

SECTION 2A

Growth of Cu-TCNQ

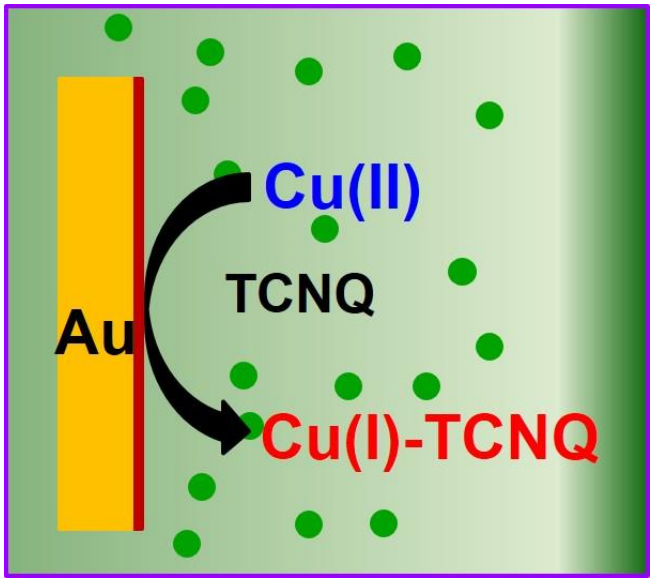

2A.1 Introduction

Functionalization of metallic or semiconducting surface with self-assembling, well-ordered, oriented, and porous layers of metal-organic coordination polymers (CPs) on self-assembled monolayer (SAM) templates—are promising candidates for variety of technological applications.[1] The rationale behind emergence of surface anchored thin film of CPs is their poor solubility in common organic solvents which heavily limits thin film processing on various support substrates for device fabrication. Cu-TCNQ is a well-known two dimensional (2D) semiconducting CP, which exhibit interesting properties such as resistive switching, and is used in memory devices.[2] So far, thin films of Cu-TCNQ were fabricated either by using vacuum deposition techniques or by dipping Cu metal source in TCNQ solution.[2] In this chapter, we have studied the chemical reactions at solid-liquid interface where functionalized Au substrate was used as a solid support and $Cu(OAc)_2$ / TCNQ solutions were used as liquids.

2A.2 Materials and Method

Copper Acetate ($Cu(OAc)_2.H_2O$), Gold (Au) coated silicon wafer, Mercaptoundecanoic Acid (MUDA), Copper Iodide (CuI), 7,7,8,8-Tetracyanoquinodimethane (TCNQ), Sulphuric Acid (H_2SO_4) and Hydrogen Peroxide (H_2O_2) were purchased from Sigma Adrich (India) and used without further purification. The morphology and thickness of thin films were recorded by using Carl Zeiss ULTRA Plus Field Emission Scanning Electron Microscope (FESEM) with Energy Dispersive X-ray Spectroscopy (EDXS) attachment. X-ray photoelectron spectroscopy (XPS) spectra was recorded by using ESCA0 (Omicron) equipped with monochromator source (Al K_α 1486.6 eV). X-ray Diffraction (XRD) patterns were recorded from a Bruker D8 Advance diffractometer using Cu K_α radiation (λ = 1.54 Å). Raman spectra (λ_{exc} = 633 nm) were recorded at Raman microscope (LabRAM HR, HorbiaJobinYvon) using a 60X objective lens. Contact angle was measured by using Holmarc's Contact Angle Goniometer.

Au substrate was cleaned by dipping into Piranha solution [H_2SO_4 (95%–98%)/H_2O_2 (30%) – 2:1] for 30 min, and was rinsed with milli-Q water and pure ethanol, finally dried under the stream of N_2 gas. Au substrate was functionalized by immersing into 1 mM solution of MUDA

thiol in ethanol and acetic acid (v:v = 9:1) for 48 hours, followed by washing with ethanol and dried under the stream of N_2 gas. Carboxyl functionalized Au substrate (MUDA/Au SAM) was dipped into $Cu(OAc)_2$ solution (1 mM in EtOH) followed by dipping into TCNQ solution (1 mM in EtOH) for 30 minutes in each solution. Both solutions were kept at room temperature. After each step, substrate was washed with ethanol and dried in stream of N_2 gas. Dipping once into metal ion and TCNQ solution constitute 1 cycle of LbL growth. Similar procedure was repeated up to fifty consecutive cycles to grow thin films of Cu-TCNQ.

2A.3 Results and Discussion

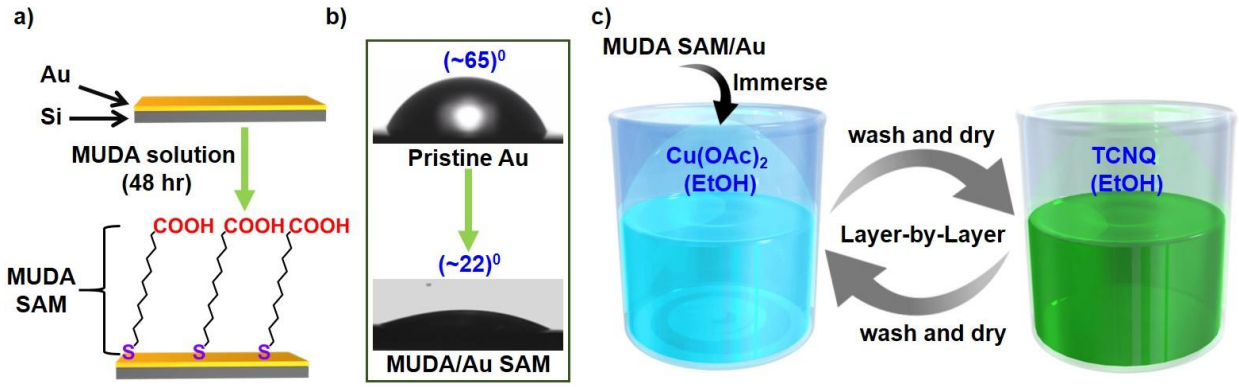

Figure 1: *(a) Schematic of pristine Au (top) and functionalized (MUDA SAM) Au substrate (down). (b) Optical image of water droplet on the surface of pristine Au (top) and MUDA/Au SAM (down). (c) Schematic illustration of LbL growth of Cu-TCNQ thin film on functionalized Au substrate.*

The MUDA/Au SAM formation on Au substrate was confirmed by measuring water contact angle (CA). The CA value of water significantly decreased from ~65° to ~22° upon dipping the Au substrate in to MUDA solution, which is characteristic of hydrophilic surfaces (Figure 1b).[3] Then, MUDA/Au SAM was dipped into $Cu(OAc)_2$ solution, referred as 0.5 cycle of LbL growth (Figure 1c). To determine the oxidation state and chemical identity of the thin film after 0.5 cycle, detailed XPS analysis was performed. The Cu 2p XPS spectrum showed Cu $2p_{3/2}$ peak at binding energy (BE) of ~934.2 eV along with a strong satellite feature at ~943.0 eV which indicates the predominant presence of Cu(II) ion (Figure 2b & 2c).[4-5] Hence, after 0.5 cycle, majorly Cu(II) was decorated on MUDA/Au SAM. Upon dipping this Cu(II) decorated SAM

into TCNQ solution (1 cycle), XPS analysis was performed again and the Cu $2p_{3/2}$ peak was observed to be red shifted to ~932.0 eV and also the satellite feature at ~943.0 eV disappeared after 1 cycle of LbL growth (Figure 2a).[5-6] Absence of satellite feature and Cu $2p_{3/2}$ peak at 932.0 eV, confirms the exclusive presence of Cu(I).[6] Hence, we observed spontaneous reduction of Cu(II) to Cu(I) upon dipping Cu(II) decorated MUDA/Au SAM into TCNQ solution.

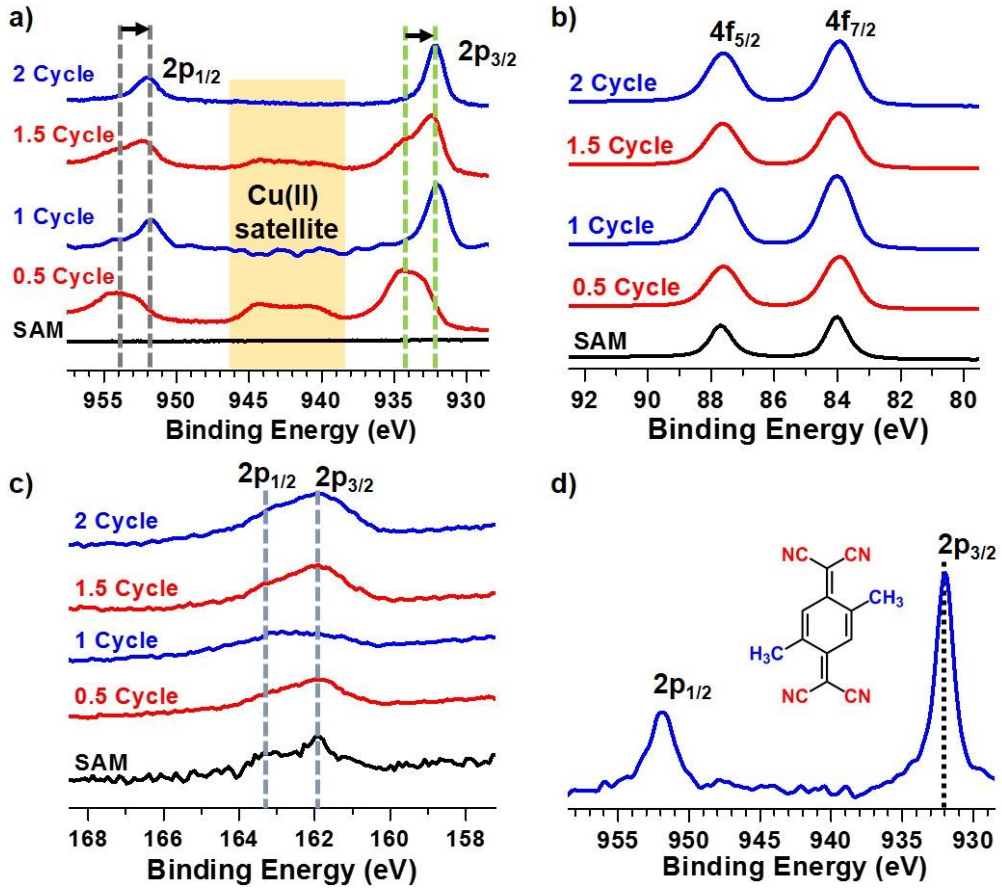

Figure 2: *(a) Cu 2p XPS spectra of MUDA/Au SAM and after 0.5, 1, 1.5, and 2 cycles of LbL growth. (b) Au 4f XPS spectra of MUDA/Au and after 0.5, 1, 1.5, and 2 cycles of LbL growth showing the $4f_{7/2}$ and $4f_{5/2}$ doublet peak due to spin orbit coupling. (c) S 2p XPS spectra of MUDA/Au and after 0.5, 1, 1.5, and 2 cycles of LbL growth. (d) Cu 2p XPS spectrum of Cu-$(CH_3)_2$TCNQ thin film after 2 cycles of LbL growth.*

Further this Cu(I) bearing substrate was again dipped into $Cu(OAc)_2$ solution (1.5 cycle) and XPS spectrum was recorded. Cu 2p XPS spectrum showed a broad peak in the BE range of 932-935 eV and a small satellite feature around ~943.0 eV, which indicates the presence of both Cu(I) as well as Cu(II).[5] Thus after 1.5 cycles, substrate has mixed oxidation state. Upon dipping into TCNQ solution again (2 cycles), Cu XPS spectrum showed the disappearance of satellite feature and presence of narrow $2p_{3/2}$ peak at BE ~932.2 eV, which indicates exclusive presence of Cu(I) (Figure 2c). Hence, chemical reduction of Cu(II) to Cu(I) was observed at solid-liquid interface upon dipping Cu(II) bearing solid functionalized Au substrate in to TCNQ solution.

To find the source of electron for conversion of Cu(II) to Cu(I), all the probable sources were probed including Au substrate and MUDA SAM. XPS spectra in the expected BE region of sulphur (S) and gold (Au) were measured after each step up to 2 cycles of LbL growth. In Au 4f XPS spectra, $4f_{7/2}$ peak was observed at BE ~83.9 eV at each step which rules out possibility of electron transfer from Au for interfacial reduction (Figure 2b).[7] The S 2p XPS spectra of functionalized Au substrate after each step from 0 to 2 cycles are presented in figure 2c. In pristine MUDA/Au SAM (0 cycle), the S $2p_{3/2}$ peak was observed at BE of ~161.9 eV which is characteristic of Au-S bond.[8-9] This peak position was consistently observed at same position up to 2 cycles of LbL growth indicating that most of thiolates are bound with Au surface. Interestingly, oxidized sulphur species which generally appear at BE of ~166.2 eV (due to sulfonic acid (SO_3^{2-}) groups) were also absent which suggest S is not acting as the reducing agent for interfacial reduction.[8] Thus, neither Au substrate nor S of SAM was accountable for the interfacial reduction of Cu(II) to Cu(I). Similar interfacial reduction of Cu(II) to Cu(I) was also observed with a TCNQ derivative i.e. 2,5-dimethyltetracyanoquinodimethane [$(CH_3)_2$TCNQ], where Cu 2p XPS spectrum after 1 cycle showed $2p_{3/2}$ peak at ~932.0 eV, signature of Cu(I) (Figure 2d).[6] Interestingly, liquid-phase reaction of $Cu(OAc)_2$ and TCNQ did not produce any kind of precipitate while under similar experimental condition, the reaction of CuI and TCNQ in liquid-phase generate Cu(I)-TCNQ complex (Figure 3a & 3b). In liquid-phase, Cu(II) did not react with TCNQ while Cu(I) can react, but at interface, Cu(II) decorated on top of functionalized Au substrate (solid) react with TCNQ solution (liquid) to generate Cu(I)-TCNQ complex.

Recently Prof. Mark D. Allendorf and coworkers showed that upon dipping Cu(II)-BTC (copper-benzenetricarboxylate) coordination polymer (CP) thin film into methanolic solution of TCNQ, a dense film of Cu(I)-TCNQ is formed.[10]

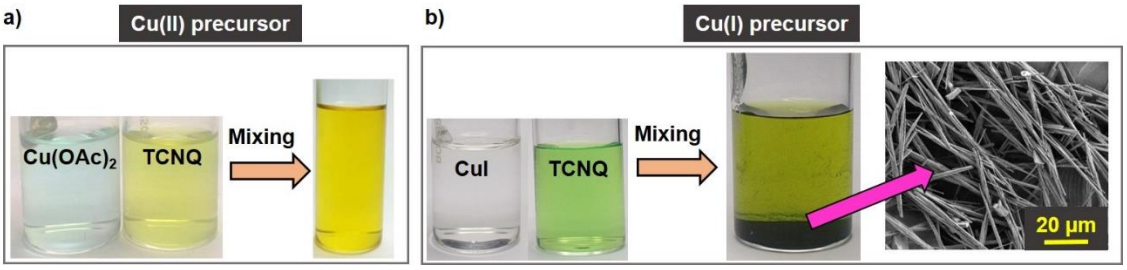

Figure 3: *(a) Optical images showing mixing of $Cu(OAc)_2$ and TCNQ solution, no precipitation was observed. (b) Optical images showing mixing of CuI and TCNQ solution, solid precipitate was formed (inset: FESEM image of corresponding precipitate).*

This chemical conversion is accompanied by enhancement of electrical conductivity by ~10 orders of magnitude and transformation of Cu(II) to Cu(I).[10] Electron for the reduction of Cu(II) to Cu(I) is probably due to methanol oxidation to formaldehyde or formic acid.[10] They have consistently observed such transformation in other protic solvents but this conversion was absent in aprotic and redox-inert solvents. Being inspired from this work, we have also checked interfacial reduction in acetone which is aprotic solvent.[10] Interestingly, after 1 cycle of LbL growth, Cu(II) was majorly present (Figure 4a). Hence interfacial reduction of Cu(II) to Cu(I) was absent in aprotic solvent. Based on these observations we have proposed a mechanism for interfacial reduction (Figure 4b).

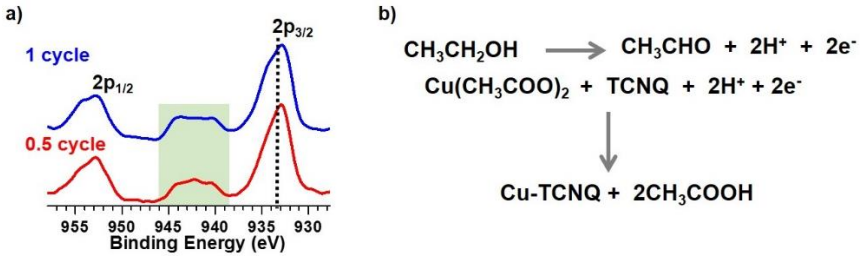

Figure 4: *(a) Cu 2p XPS spectra of MUDA/Au SAM after 0.5 and 1 cycle of LbL growth where both $Cu(OAc)_2$ and TCNQ solutions are in aprotic solvent i.e. acetone. (b) Proposed mechanism for interfacial reduction of Cu(II) to Cu(I).*

Upon performing fifty consecutive LbL cycles with Cu(II) and TCNQ solution, we have achieved a green colored thin film (Figure 5a) on functionalized Au substrate.[11] FESEM images of green thin film showed a high quality homogeneous thin film (Figure 5a). The water contact angle (CA) value was ~ 130° which is signature of hydrophobic surface (Figure 5a).[11] Out-of-plane X-ray diffraction pattern (XRD) of our green colored thin film was recorded and it almost matches to phase-I structure of bulk Cu(I)-TCNQ material (which was prepared by liquid-phase reaction of Cu(I) salt with TCNQ) (Figure 5b).[2] Average thickness of thin film was observed to be ~600 nm from cross-section height measurement with FESEM (Figure 5c).

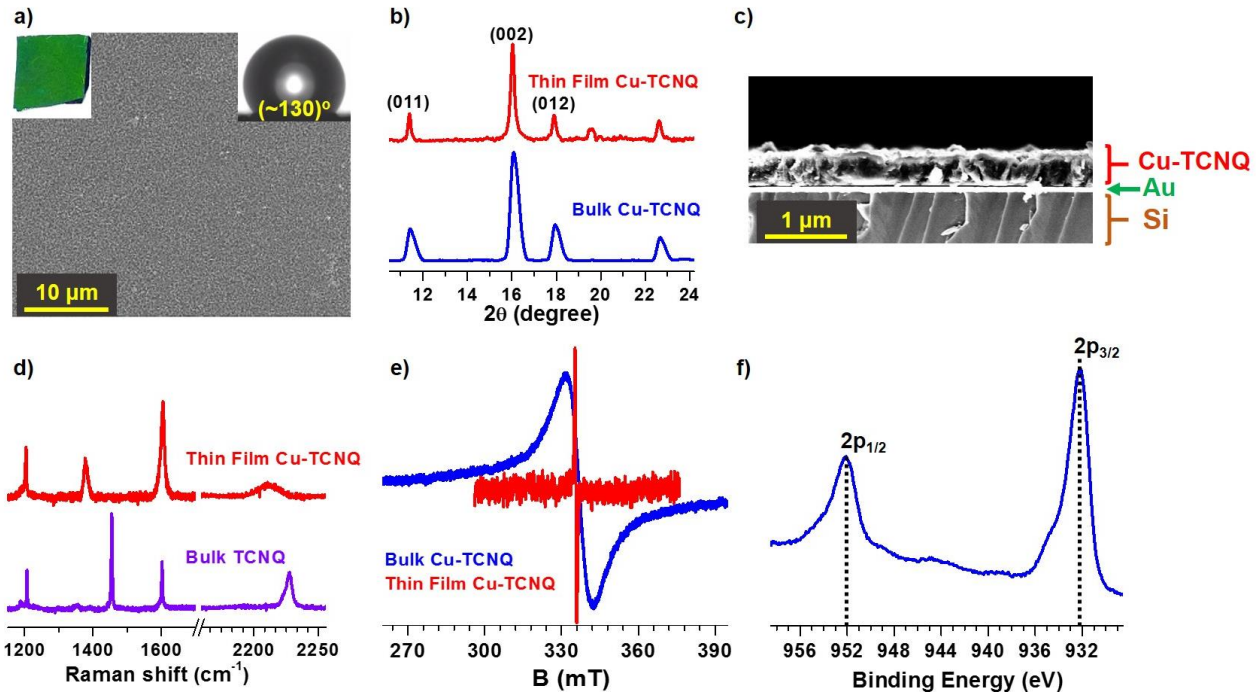

Figure 5: *(a) FESEM image of Cu-TCNQ thin film on functionalized Au substrate after fifty cycles of LbL growth (Inset: optical image of Cu-TCNQ thin film (green) and water droplet on surface showing contact angle ~130°). (b) Out-of-plane XRD pattern of bulk Cu-TCNQ and thin film of Cu-TCNQ on Au substrate after fifty cycles of LbL growth. (c) Cross-sectional FESEM image of showing thickness of Cu-TCNQ thin film of ~600 nm. (d) Raman spectra of bulk TCNQ and thin film of Cu-TCNQ. (e) EPR spectra of bulk and thin film Cu-TCNQ. (f) Cu 2p XPS spectrum of Cu-TCNQ thin film after fifty cycles of LbL growth.*

The C≡N stretching frequency is dependent on its coordination environment and charge on the counter ion. To know the chemical nature of TCNQ, Raman spectra of bulk TCNQ and our Cu-TCNQ thin film was recorded (Figure 5d). Vibrational bands in bulk TCNQ were observed at ~2228 cm^{-1}, ~1601 cm^{-1}, ~1453 cm^{-1} and ~1206 cm^{-1} which are characteristic of C≡N stretching modes, C=C ring stretching, C-CN wing stretching and C=C–H bending modes.[12] In case of our thin film, these peaks were observed at ~2206 cm^{-1}, ~1601 cm^{-1}, ~1374 cm^{-1} and ~1204 cm^{-1} which are characteristics of TCNQ radical monoanion (Figure 5d).[12] Hence in our Cu-TCNQ thin film, TCNQ exist as radical monoanion. Furthermore, reduction of Cu(II) to Cu(I) was also supported by electron paramagnetic resonance (EPR) measurements (Figure 5e). As Cu(II) ion is paramagnetic, and Cu(I) ion is diamagnetic, the latter species is EPR inactive and former is EPR active. In EPR spectra of our Cu-TCNQ thin film a single peak was observed at ~399 mT with g value 2.00, that is characteristic of organic-based radicals as in present case of TCNQ radical anion.[13] Interestingly, no signatures of Cu(II) could be observed which should appear at ~311 mT with g value 2.16.[13] Cu 2p XPS spectrum of our Cu-TCNQ thin film after fifty cycles of LbL growth showed Cu $2p_{3/2}$ peak ~932.1 eV along with a very small satellite feature at ~935 eV.[6] That means in our thin film Cu(I) was majorly present and Cu(II) was in small amount. Hence, we have successfully grown thin film of Cu-TCNQ first time on functionalized Au substrate through LbL approach by using Cu(II) precursor.

We have studied the effect of dipping time of functionalized Au substrate into precursors ($Cu(OAc)_2$ and TCNQ) solution on growth of Cu-TCNQ thin film. We have varied the dipping time from 0.25, 0.50, 1, 3, 5, 10, 15, to 30 minutes at each step in every precursor solution. Similar number of LbL cycles (fifty cycles) were performed at each time span and Cu-TCNQ thin films were fabricated. FESEM images recorded on each system showed a uniform growth of thin film except 0.25 minutes system (Figure 6a). A zoomed-in view FESEM image of each system confirmed the presence of highly oriented, vertically aligned and densely packed nano-crystallites of Cu-TCNQ except the one for 0.25 minutes (Figure 6a). The water contact angle value on the different system were in the range of 110° to 140° after fifty cycles of growth (Figure 6a & 6b). Average thickness of Cu-TCNQ thin films were estimated from the FESEM cross-sectional images after fifty cycles at different immersion time. With increasing the immersion time per cycle, average thickness of thin films enhances rapidly, but does not

match to thin films fabricated through ideal LbL approach where addition of precisely one monolayer in each growth cycle is predicted.

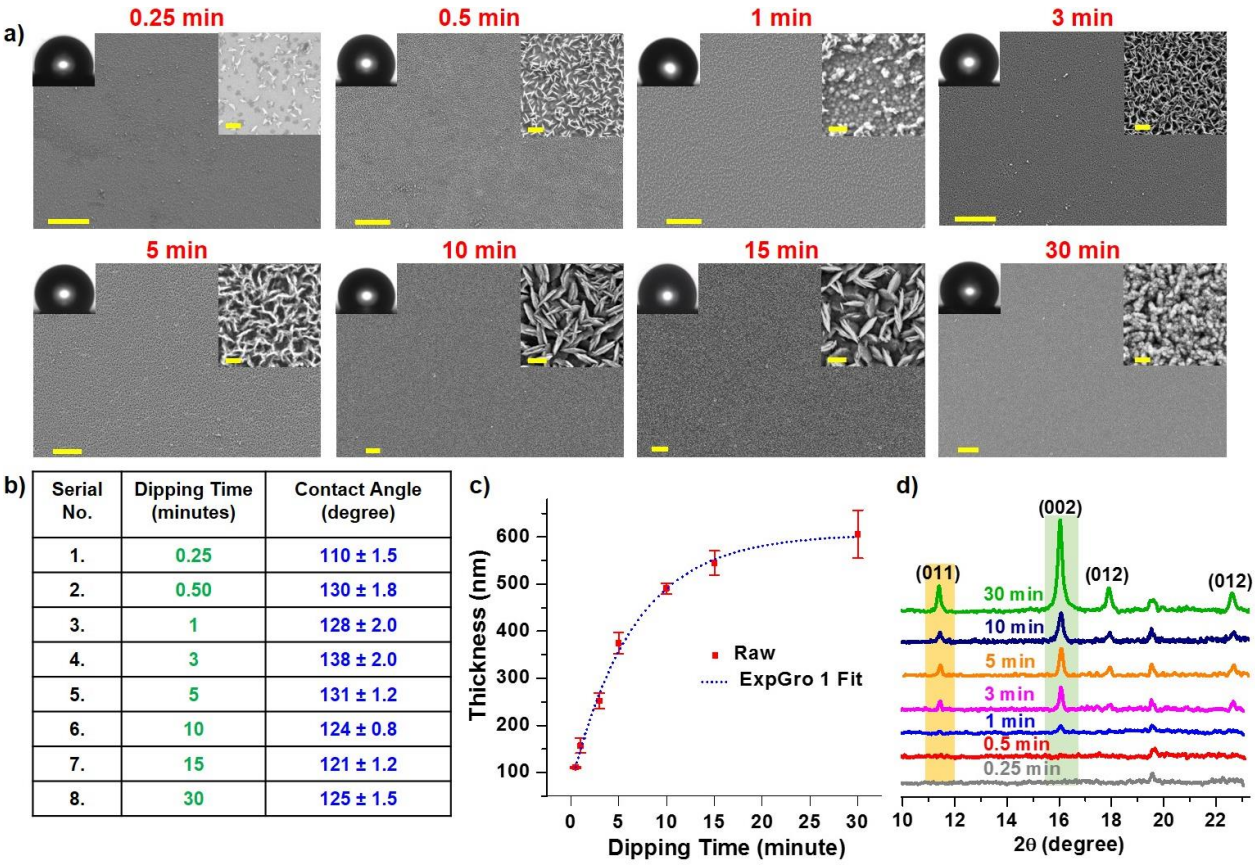

Serial No.	Dipping Time (minutes)	Contact Angle (degree)
1.	0.25	110 ± 1.5
2.	0.50	130 ± 1.8
3.	1	128 ± 2.0
4.	3	138 ± 2.0
5.	5	131 ± 1.2
6.	10	124 ± 0.8
7.	15	121 ± 1.2
8.	30	125 ± 1.5

Figure 6: *(a) FESEM image of Cu-TCNQ thin film on functionalized Au substrate after fifty cycles of LbL growth (Inset: water droplet on surface showing contact angle and zoomed-in FESEM images). (b) Water contact angle values for different dipping time. (c) Plot of cross-sectional height vs dipping time (fitted with exponential). (d) Out-of-plane XRD pattern of Cu-TCNQ grown at different dipping time after fifty cycles of LbL growth.*

That means the growth rate vastly exceeds and multi-layer growth happens with increasing immersion time. Overall the growth of thin film using the LBL method appears to be more complicated than that suggested by the idealized model. Therefore, the varying immersion time during LbL growth has great impact on growth of Cu-TCNQ, lesser immersion time (3 and 5 min) is better and can easily coat larger surfaces (Figure 6c). Hence immersing time has a remarkable influence on size of the Cu-TCNQ crystals, the surface coverage and thickness of

thin film. The out-of-plane XRD patterns of Cu-TCNQ thin film grown on MUDA/Au surface with different immersion time after fifty cycles were recorded. It shows predominant presence of (002) diffraction peak along with (011) and (012) signals of low intensity, which are characteristic signature of Cu-TCNQ phase-1 structure (Figure 6d). We deduce from the diffraction data that longer immersion time promotes Cu-TCNQ growth on MUDA/Au surfaces along the (002) direction. Hence, immersion time of substrate in different precursor solution has great impact on growth of Cu-TCNQ thin films.

2A.4 Conclusions

In conclusion, MUDA/Au SAM was alternatively dipped into $Cu(OAc)_2$ and TCNQ solutions. Upon dipping the Cu(II) decorated MUDA/Au SAM into TCNQ solution, spontaneous reduction of Cu(II) to Cu(I) was observed at solid-liquid interface. Similar reduction was absent in liquid-phase reaction of Cu(II) and TCNQ. This interfacial reduction lead to the formation Cu-TCNQ complex on top of functionalized Au substrate. Repeating the alternate dipping procedure up to fifty consecutive cycles of LbL growth, thin films of Cu-TCNQ was fabricated. Thickness of Cu-TCNQ thin film increases exponentially with increase in dipping time per cycle.

References

(1) Zhuang, J. L.; Terfort, A.; Wöll, C., *Coord. Chem. Rev.* **2016,** *307* 391-424.

(2) Heintz, R. A.; Zhao, H.; Ouyang, X.; Grandinetti, G.; Cowen, J.; Dunbar, K. R., *Inorg. Chem.* **1999,** *38* 144-156.

(3) Ballav, N.; Shaporenko, A.; Krakert, S.; Terfort, A.; Zharnikov, M., *J. Phys. Chem. C* **2007,** *111* 7772-7782.

(4) Ai, Z.; Zhang, L.; Lee, S.; Ho, W., *J. Phys. Chem. C* **2009,** *113* 20896-20902.

(5) Moulder, J. F.; Chastain, J., Physical Electronics Division, Perkin-Elmer Corporation: **1992**.

(6) Poulston, S.; Parlett, P. M.; Stone, P.; Bowker, M., *Surf. Interface Anal.* **1996,** *24* 811-820.

(7) Boyen, H.-G.; Kästle, G.; Weigl, F.; Koslowski, B.; Dietrich, C.; Ziemann, P.; Spatz, J. P.; Riethmüller, S.; Hartmann, C.; Möller, M.; Schmid, G.; Garnier, M. G.; Oelhafen, P., *Science* **2002,** *297* 1533-1536.

(8) Castner, D. G.; Hinds, K.; Grainger, D. W., *Langmuir* **1996,** *12* 5083-5086.

(9) Bourg, M.-C.; Badia, A.; Lennox, R. B., *J. Phys. Chem. B* **2000,** *104* 6562-6567.

(10) Thürmer, K.; Schneider, C.; Stavila, V.; Friddle, R. W.; Léonard, F.; Fischer, R. A.; Allendorf, M. D.; Talin, A. A., *ACS Appl. Mater. & Interfaces* **2018,** *10* 39400-39410.

(11) Rana, S.; Rajendra, R.; Dhara, B.; Jha, P. K.; Ballav, N., *Adv. Mater. Interfaces* **2016,** *3* 1500738-1500746.

(12) Gucciardi, P. G.; Trusso, S.; Vasi, C.; Patanè, S.; Allegrini, M., *Phys. Chem. Chem. Phys.* **2002,** *4* 2747-2753.

(13) Sutton, A. L.; Abrahams, B. F.; D'Alessandro, D. M.; Hudson, T. A.; Robson, R.; Usov, P. M., *CrystEngComm* **2016,** *18* 8906-8914.

CHAPTER 2

Thin Films by Interfacial Chemical Reaction

Section 2B

Growth of Ag-TCNQ

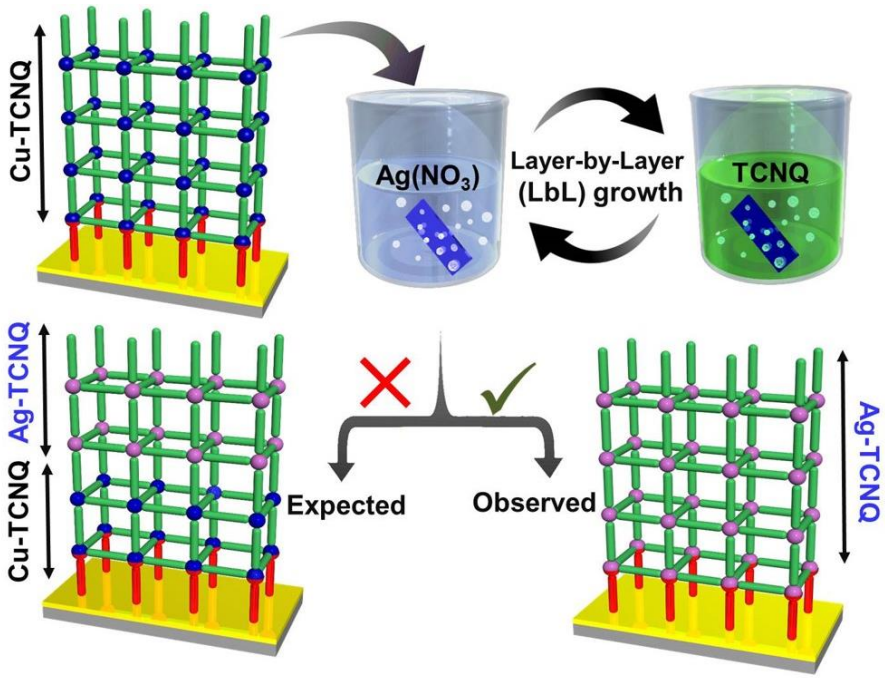

2B.1 Introduction

In chapter 2A, interfacial reduction reaction enabled us to grow thin film of Cu-TCNQ on functionalized Au substrate via layer-by-layer (LbL) approach. Silver (Ag) is present just below to copper (Cu) in same group of periodic table and is well known to form a complex with TCNQ. Till date, Ag-TCNQ thin films were grown either by using vacuum deposition (CVD or PVD) techniques or dipping Ag metal substrate in TCNQ solution.[1] We wanted to grow Ag-TCNQ thin film on functionalized Au substrate through LbL approach which was missing in previous reports. Herein, we have employed liquid-phase heteroepitaxy (LPH) approach to grow Ag-TCNQ thin films. In this technique, sequentially different coordination polymers (CPs) are deposited on a single-layered structure to allow the fabrication of several bilayered as well as trilayered thin films with similar as well as different lattice constants.[2-4] Herein, we have used the LPH approach to grow thin film of Ag-TCNQ by using Cu-TCNQ thin film as template.

2B.2 Materials and Method

Silver nitrate ($AgNO_3$), Copper acetate monohydrate $Cu(OAc)_2.H_2O$, Gold (Au) coated silicon wafer, Mercaptoundecanoic Acid (MUDA), and Tetracyanoquinodimethane (TCNQ) were purchased from Sigma Adrich (India) and used without further purification. Preparation of MUDA/Au SAM and characterization of all thin films are described in chapter 2A. Firstly, we have dipped MUDA/Au SAM into $AgNO_3$ followed by TCNQ solution, and similar procedure was repeated up to fifty cycles of LbL growth at room temperature.
In **step-I,** Cu-TCNQ thin films were fabricated by using LbL approach likewise chapter 2A but at an elevated temperature of 60 ^oC. This LbL process was repeated up to ten cycles to grow thick film. In **step-II**, thin films grown in step-I (Cu-TCNQ), were alternatively dipped into ethanolic solutions of $AgNO_3$ and TCNQ (30 minutes each) at higher temperature (60 ^oC) and similar LbL procedure was repeated up to ten consecutive cycles.

2B.3 Results and Discussion

Initially, the LbL approach was applied to grow Ag-TCNQ thin film on functionalized Au substrate by subsequently dipping MUDA/Au SAM into $AgNO_3$ and TCNQ solution. After fifty

cycles of LbL growth, FESEM images revealed that no thin film formation had occurred (Figure 1a). Even changing the terminal functional groups of SAMs from –COOH to $–NH_2$ or –SH (Figure 1b & 1c) did not help in the growth of Ag-TCNQ thin film. As a result, direct LbL growth of Ag-TCNQ thin film on MUDA/Au SAM was not possible.

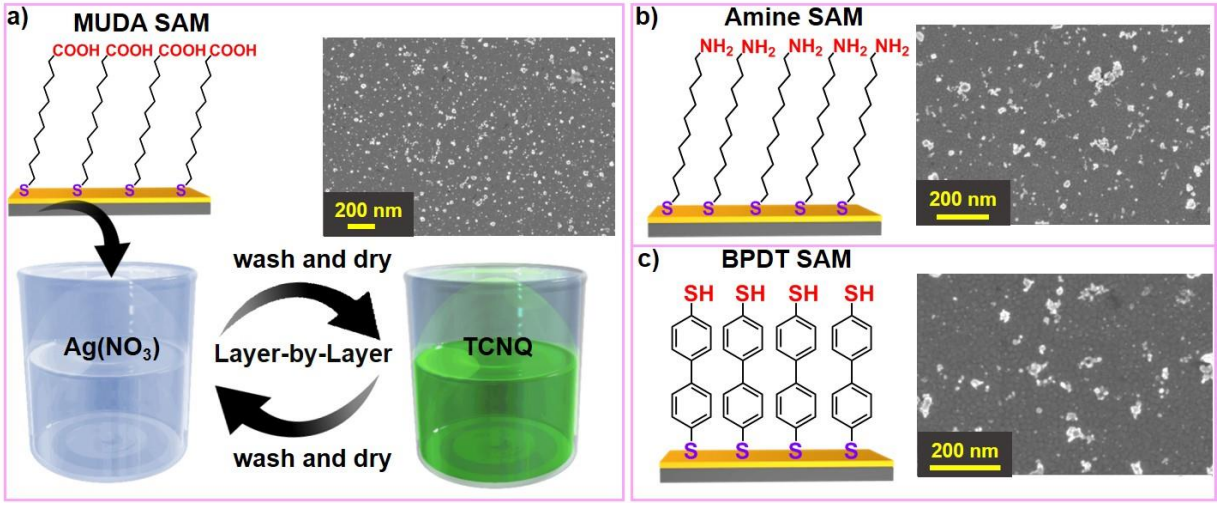

Figure 1: *(a) Schematic illustration of LbL growth of Ag-TCNQ on MUDA/Au SAM and respective FESEM image after fifty cycles. Schematic of -NH_2 (b) and –SH (c) terminated SAM and corresponding FESEM images fifty cycles of LbL growth.*

Liquid-phase heteroepitaxy approach was adopted to grow Ag-TCNQ on top of Cu-TCNQ thin film. Cu-TCNQ thin film (step-I) was grown via LbL approach on functionalized Au substrate. Followed by alternate dipping of Cu-TCNQ thin film $AgNO_3$ and TCNQ solution (step-II), and similar procedure was repeated up to ten consecutive cycles. A remarkable observation was change in color of initial thin film from dark green (step-I) to dark blue (step-II), which indicates that some chemical reaction has taken place (Figure 2a). To determine structural change during transformation from dark green to dark blue colored thin film, out-of-plane XRD measurements were performed at each step. The XRD pattern of the initial thin film (step-I) have peaks at 2θ values of 11.0°, 15.6°, and 17.4°, characteristic of Cu-TCNQ phase-I (Figure 2b).[5] With increasing number of cycles, the intensity of Cu-TCNQ patterns were gradually decreased from the 0^{th} cycle and finally almost vanished after 10^{th} cycle. Interestingly, new XRD peaks appeared at 2θ values of 10.25°, 14.5°, and 21.5° which

corresponds to (002), (022), and (004) planes of Ag-TCNQ phase-I, respectively (Figure 2b).[6] XRD measurements suggest the exclusive formation of Ag-TCNQ thin film in step-II.

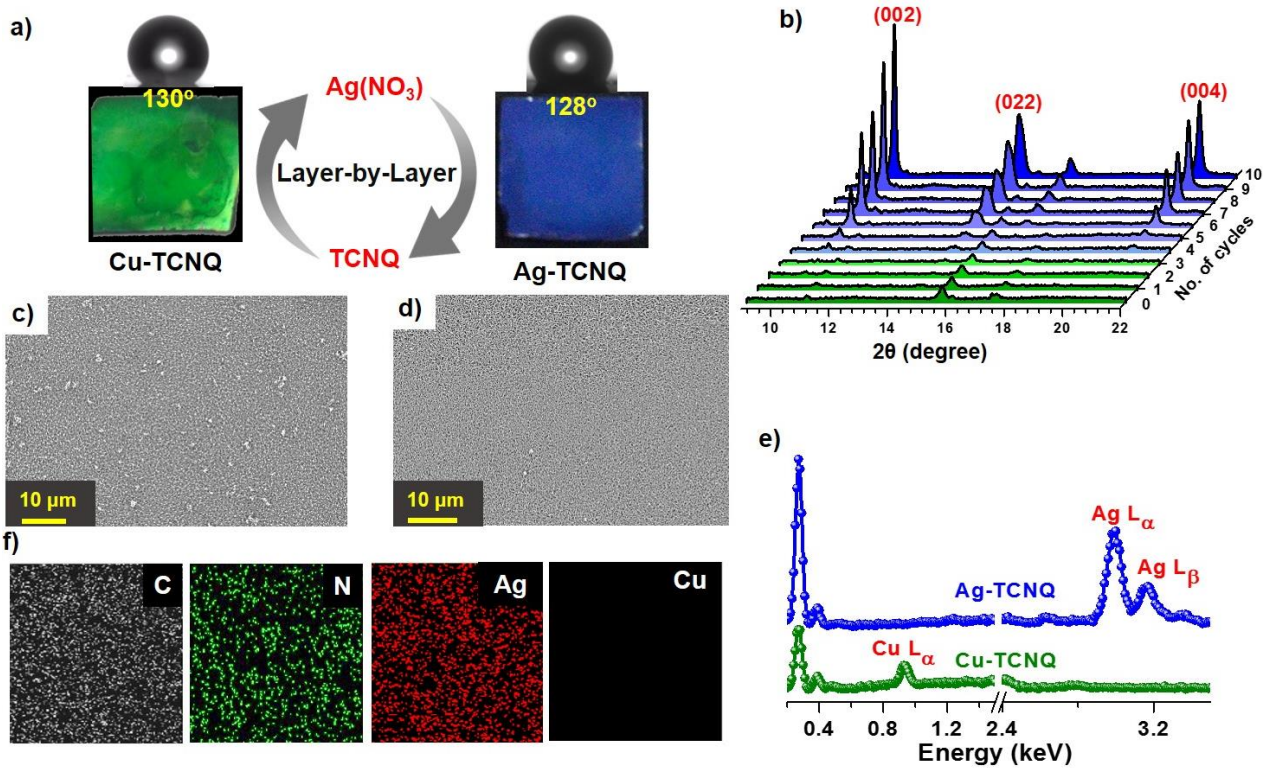

Figure 2: *(a) Optical images of Cu-TCNQ (green) thin film, Ag-TCNQ (blue) thin film and their corresponding water droplet on the surface of corresponding thin film. (b) Out-of-plane XRD patterns showing gradual transformation of Cu-TCNQ to Ag-TCNQ in thin film configurations. (c & d) FESEM image of Cu-TCNQ (step-I) and Ag-TCNQ thin film (step-II). (e) EDXS spectra Cu-TCNQ (step-I) and Ag-TCNQ thin film (step-II). (f) Elemental mapping of C, N, Cu, and Ag on the Ag-TCNQ thin film obtained in step-II.*

Hydrophobicity and uniformity of thin film were almost retained during transformation from Cu-TCNQ to Ag-TCNQ, as H_2O contact angle value did not change significantly, despite having different chemical identities (Figure 2a, 2c & 2d). Formation of Ag-TCNQ was further supported by EDXS analysis, showing the characteristic Cu L_α line at ~0.93 keV in Cu-TCNQ thin film (step-I), which disappeared in Ag-TCNQ thin film (step-II) (Figure 2e).[7] Also, Ag L_α (~2.93 keV) and Ag L_β (~3.15 keV) peaks were present in the final thin film (step-II), which

supports the exclusive presence of Ag (Figure 2e).[7] Elemental mapping also revealed homogeneous distribution of Ag, C, N across the final thin film and almost no traces of Cu. To further confirm the presence of Ag and absence of Cu, thorough cross-sectional EDXS analysis was performed at 7 different places in Ag-TCNQ thin film (step-II) which showed almost absence of Cu and predominant presence of Ag in Ag-TCNQ thin film (Figure 3b).

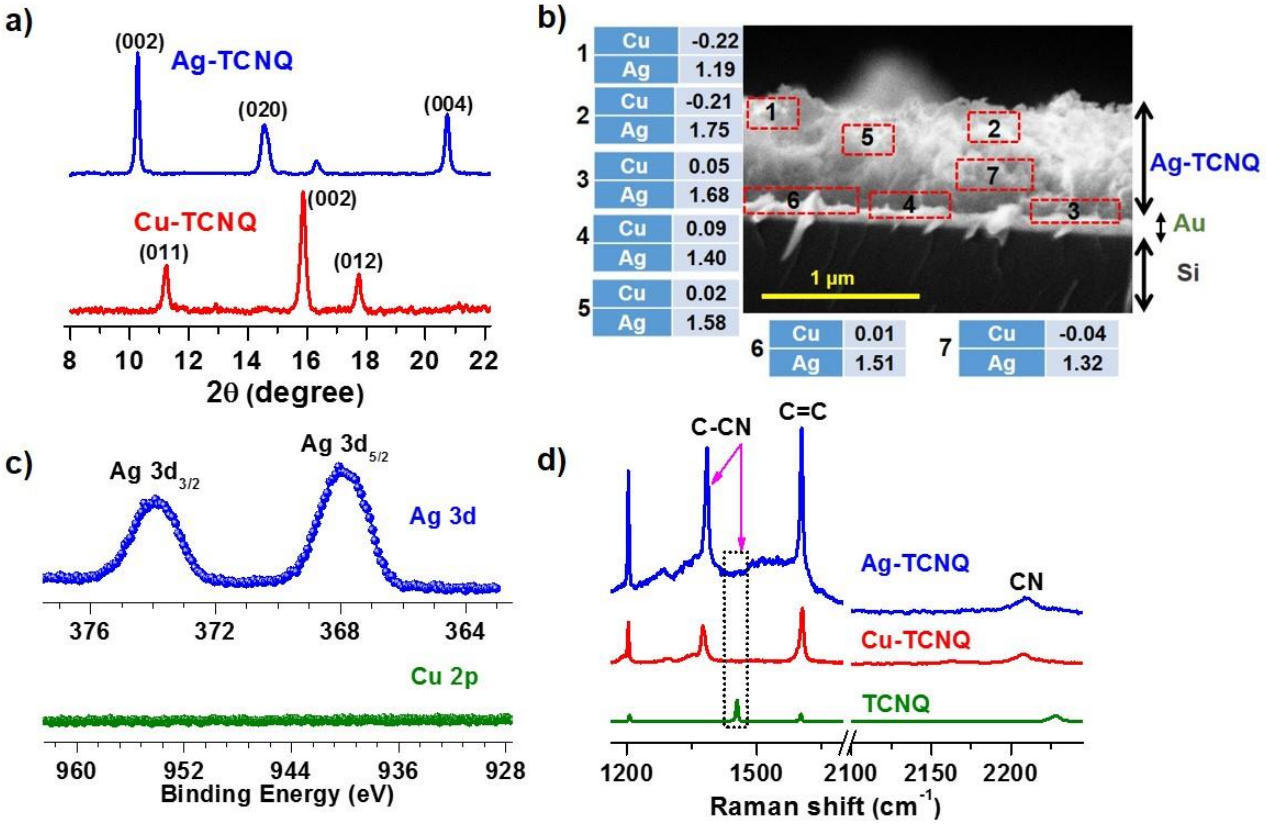

Figure 3: *(a) Out-of-plane XRD patterns of Cu-TCNQ (step-I), and Ag-TCNQ thin film (step-II). (b) Cross-sectional EDXS measurement of Ag-TCNQ thin film obtained in step-II. (c) Ag 3d and Cu 2p XPS spectra of Ag-TCNQ thin film obtained in step-II. (d) Raman spectra of bulk TCNQ, Cu-TCNQ (step-I), and Ag-TCNQ thin film (step-II).*

XPS analysis of thin film obtained in step-II was performed and the appearance of a strong Ag 3d photoemission signal at binding energy (BE) value of ~373.2 and ~367.53 eV confirmed the presence of Ag(I) majorly, which is typical of Ag-TCNQ (Figure 3c).[7] Interestingly, no reasonable Cu 2p photoemission signal was observed in the BE range of

930–960 eV.[7] Raman spectra of both initial and final thin films showed vibrational bands at ~1374 cm^{-1}, ~1602 cm^{-1} and ~2205 cm^{-1} which corresponds to C–CN stretching modes, C=C ring stretching, and C≡N stretching modes, which are characteristic of TCNQ mono-anion (Figure 3d).[8] Both Cu-TCNQ and Ag-TCNQ have almost similar lattice parameters, so formation of heterostructure Ag-TCNQ/Cu-TCNQ was expected. Unexpectedly, our Raman, EDXS, XPS, and XRD data, all together suggests exclusive formation of Ag-TCNQ thin film in step-II.

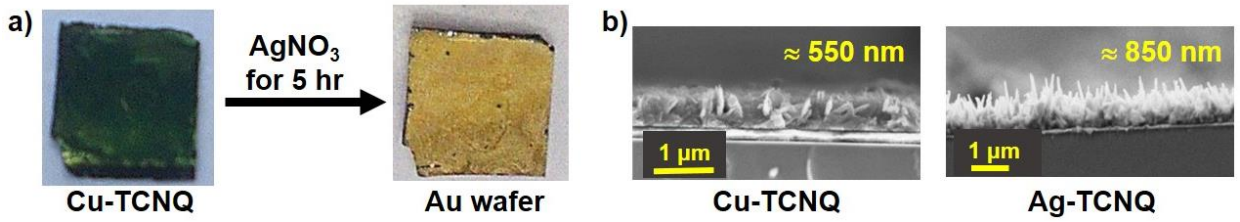

Figure 4: *(a) Optical images of Cu-TCNQ thin film before and after dipping into $AgNO_3$ solution for 5 hours which is showing the etching of Cu-TCNQ by $AgNO_3$. (b) Cross-sectional FESEM images of Cu-TCNQ (left) and Ag-TCNQ (right) thin films.*

The here revealed transformation from Cu-TCNQ to Ag-TCNQ in the thin film configuration seemingly appears to be typical ion-exchange phenomenon or post synthetic modification. $TCNQ^-$ being a soft base and both Cu(I) and Ag(I) ions being soft acids, can undergo kinetically labile metal–ligand exchange reaction, according to soft-hard acid-base (SHAB) theory.[9] But the following observations ruled out the possibility of an ion exchange process: (i) Typical ion-exchange process requires longer time, and we dipped the Cu-TCNQ thin film (step-I) into $AgNO_3$ solution for 5 h and it was completely etched away (Figure 4a) and (ii) thickness values of starting (step-I) and final (step-II) thin films were strikingly different (~850 nm for Ag-TCNQ at the cost of ~550 nm of Cu-TCNQ) (Figure 4b). To understand the origin of such an unusual transformation, we thoroughly investigated the growth of Ag-TCNQ thin film in each cycle of the LbL assembly by FESEM and EDXS analysis (Figure 5a, 5b, and 5c). After first cycle means dipping Cu-TCNQ thin film (step-I) into $AgNO_3$ and TCNQ solution (30 minutes each), FESEM images showed the formation of small Ag nanoparticles (NPs) which are distributed over the nanoflakes of Cu-TCNQ. EDXS analysis further confirmed the presence of Ag as well as Cu in the thin film after 1 cycle. The formation of Ag NPs was

further confirmed by XRD data where diffraction peaks around 38° and 45° matches to (111) and (200) planes of Ag NPs, respectively (Figure 5e and 5f).[10]

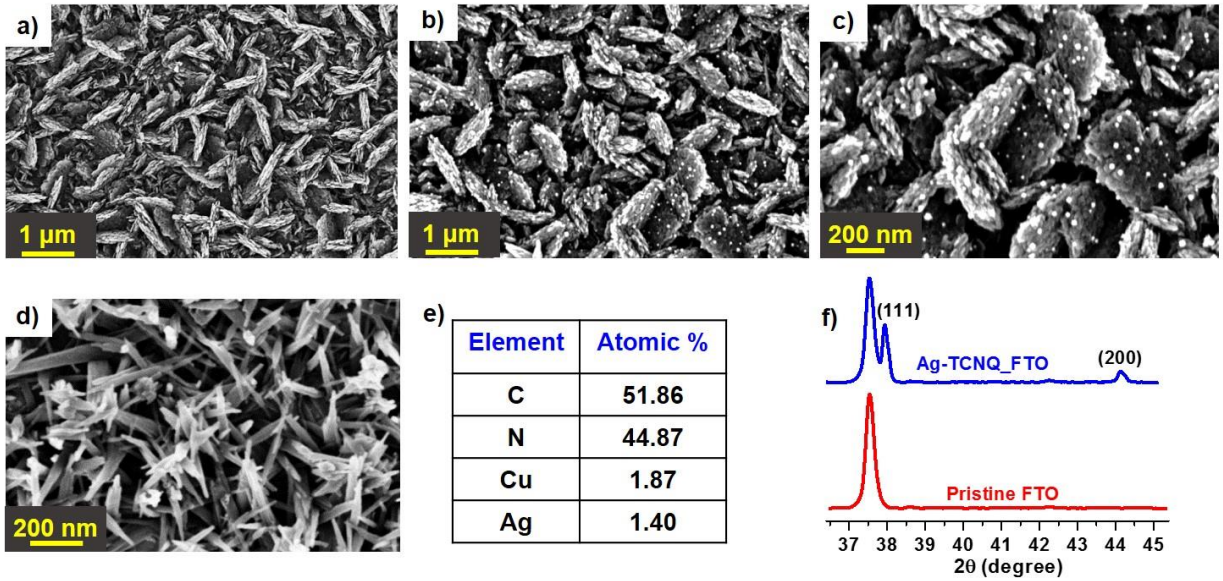

Element	Atomic %
C	51.86
N	44.87
Cu	1.87
Ag	1.40

Figure 5: *(a) FESEM image of Cu-TCNQ thin film (step-I). High resolution (b) and zoomed-in (c) FESEM image of Cu-TCNQ thin film after 1 cycle (dipping once in to $AgNO_3$ and TCNQ solution) of LbL growth. (d) FESEM image of Ag-TCNQ thin film (step-II). (e) EDXS measurement of Cu-TCNQ thin film after 1 cycle of LbL growth. (f) Out-of-plane XRD patterns of pristine FTO and Ag-TCNQ/FTO (step-II) thin film.*

Upon continued cycling, Cu-TCNQ nanoflakes slowly disappeared and ultimately Ag-TCNQ nanorods were formed, thereby justifying the role of Cu-TCNQ as a sacrificial layer in the growth of Ag-TCNQ via the LbL approach. The reactions behind the sacrificial growth of Ag-TCNQ were proposed as

$$\text{Cu-TCNQ} + AgNO_3 \longrightarrow Cu^{2+} + Ag^0 + NO_3^- + TCNQ^-$$

$$Ag^0 + TCNQ \longrightarrow \text{Ag-TCNQ}$$

Reduction potential of Ag(I) ion ($E^0_{Ag(I)/Ag}$) is equal to + 0.80 V and Cu(I) ion ($E^0_{Cu(II)/Cu(I)}$) is 0.16 V, so Cu(I) ion can act as the reducing agent for Ag(I) ions, thus sacrificing to form Cu(II) ions.[11] Interestingly, as we have shown in chapter 2A, upon mixing Cu(II) solution with TCNQ

solution – no product formation was observed. However, if we mix Cu(I) ion solution with TCNQ we could isolate some solid precipitate of Cu-TCNQ, perhaps due to the fact that the Cu(II) ion is a borderline acid, while Cu(I) ion is a soft acid. Thus, our sacrificial LPH approach yielded high quality Ag-TCNQ thin film on the SAM template.

2B.4 Conclusions

We have successfully grown Ag-TCNQ thin film through LbL approach. The transformation of Cu-TCNQ to Ag-TCNQ on the surface was realized to be sacrificial growth and not an ion exchange process. Cu-TCNQ thin film gets sacrificed to grow Ag-TCNQ thin film. The here presented sacrificial liquid-phase heteroepitaxial approach appears to be the first report on successful growth of Ag-TCNQ thin films on organically modified non Ag substrates.

References

(1) Liu, H.; Zhao, Q.; Li, Y.; Liu, Y.; Lu, F.; Zhuang, J.; Wang, S.; Jiang, L.; Zhu, D.; Yu, D.; Chi, L., *J. Am. Chem. Soc.* **2005,** *127,* 1120-1121.

(2) Wannapaiboon, S.; Tu, M.; Fischer, R. A., *Adv. Funct. Mater.* **2014,** *24,* 2696-2705.

(3) Wang, Z.; Liu, J.; Lukose, B.; Gu, Z.; Weidler, P. G.; Gliemann, H.; Heine, T.; Wöll, C., *Nano Lett.* **2014,** *14,* 1526-1529.

(4) Tu, M.; Fischer, R. A., *J. Mater. Chem. A* **2014,** *2,* 2018-2022.

(5) Heintz, R. A.; Zhao, H.; Ouyang, X.; Grandinetti, G.; Cowen, J.; Dunbar, K. R., *Inorg. Chem.* **1999,** *38,* 144-156.

(6) Zheng, W.; Li, Z.; Yang, F.; Song, X.; Zhang, H.; Liu, Y.; Wang, C., *Mater. Lett.* **2008,** *62,* 1448-1450.

(7) Pearson, A.; Ramanathan, R.; O'Mullane, A. P.; Bansal, V., *Adv. Funct. Mater.* **2014,** *24,* 7570-7579.

(8) Rana, S.; Rajendra, R.; Dhara, B.; Jha, P. K.; Ballav, N., *Adv. Mater. Interfaces* **2016,** *3,* 1500738-1500746.

(9) Pearson, R. G., *J. Am. Chem. Soc.* **1963,** *85,* 3533-3539.

(10) Jyoti, K.; Baunthiyal, M.; Singh, A., *J. Radiat. Res. Appl. Sci.* **2016,** *9,* 217-227.

(11) J. E. Huheey, E. A. K., R. L. Keiter and O. K. Medhi, *Pearson Education* **2006**.

CHAPTER 3

Electrical Conductance in Thin Films of Cu/Ag-TCNQ

Section 3A

Chemical Effect

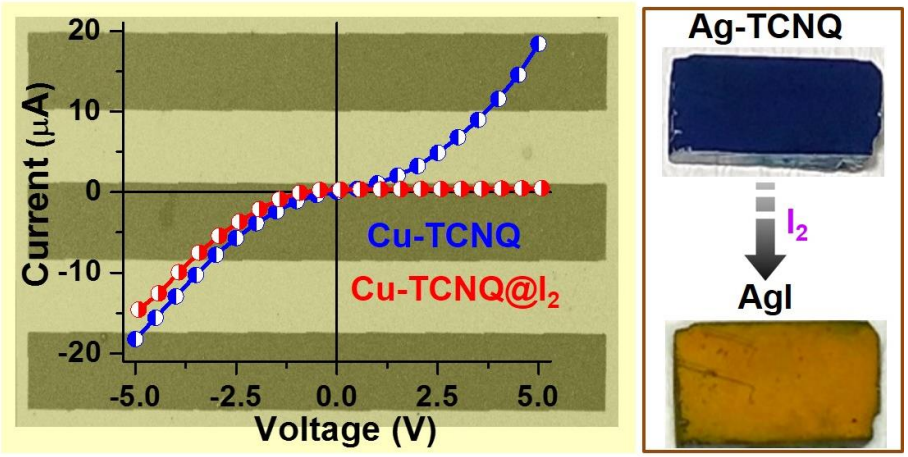

3A.1 Introduction

In the previous chapter, thin films of Cu-TCNQ and Ag-TCNQ were fabricated on functionalized Au substrate via LbL approach. As both Cu-TCNQ and Ag-TCNQ are semiconductors so it would be interesting to check the effects of external chemical stimuli on their electrical conductance and structure. To investigate the effect of chemical stimuli on structure and electrical conductance of Cu-TCNQ and Ag-TCNQ thin film, we have dosed iodine (I_2) due to its strong affinity towards Cu(I) and Ag(I).[1] Iodine is a strong oxidizing agent and easily sublimes to violet gas at room temperature.[1] Herein, we have exposed both Cu-TCNQ and Ag-TCNQ thin films to I_2 vapors and investigate the effect on structure and electrical conductance. The I_2 dosing to Ag-TCNQ thin film does not form heterostructure, rather it leads to the formation of AgI thin film. So far, patterning techniques such as irradiation-promoted exchange reaction (IPER), micro-contact printing (μCP) and dip-pen nanolithography (DPN) were used to make patterned thin film devices of coordination polymers (CPs).[2-4] We have fabricated thin film devices of Cu-TCNQ by employing electron-beam lithography (EBL).

3A.2 Materials and Method

Fluorinated Tin Oxide (FTO) glass, Iodine (I_2), Poly (methyl methacrylate) (PMMA), Isopropyl Alcohol (IPA), Methyl Isobutyl Ketone (MIK) were purchased from Sigma Aldrich (India) and used without further purification. Patterning (Electron-beam lithography) of thin film devices were performed in Zeiss Ultra Plus Field Emission Scanning Electron Microscope (FESEM). The electrical conductivity of thin films was measured by two-probe technique MODEL 4200-Semiconductor Characterization System (SCS), connected with everbeing probe station. Synthesis of MUDA/Au SAM, various other chemicals and instruments used in this chapter are already described in Chapter 2.

Fabrication of thin film devices by using electron-beam (e^- beam) lithography (EBL) is described below:

1. Firstly, 4 wt% PMMA solution was spin coated onto a clean Au substrate at 8000 rpm for 1 minute followed by baking for 5 minutes at 180 ^oC.

2. PMMA was irradiated with electron-beam at 20 keV, and then the substrate was dipped into developer solution (isopropanol + methylisobutylketone) to get patterned substrate.
3. Subsequently, the patterned substrate was dipped into thiol (MUDA) solution to grow SAM at the irradiated zones.
4. Now, Cu-TCNQ crystallites were grown upon subsequently dipping patterned substrate having MUDA SAM into $Cu(OAc)_2$ and TCNQ solution up to 40 cycles of LbL growth.
5. In the last step, the substrate was dipped in acetone and ultra-sonicated to remove unwanted Cu-TCNQ crystallites and PMMA. Micro (length 1000 µm X width 100 µm) as well as nano patterns were fabricated on both Au and FTO substrates.

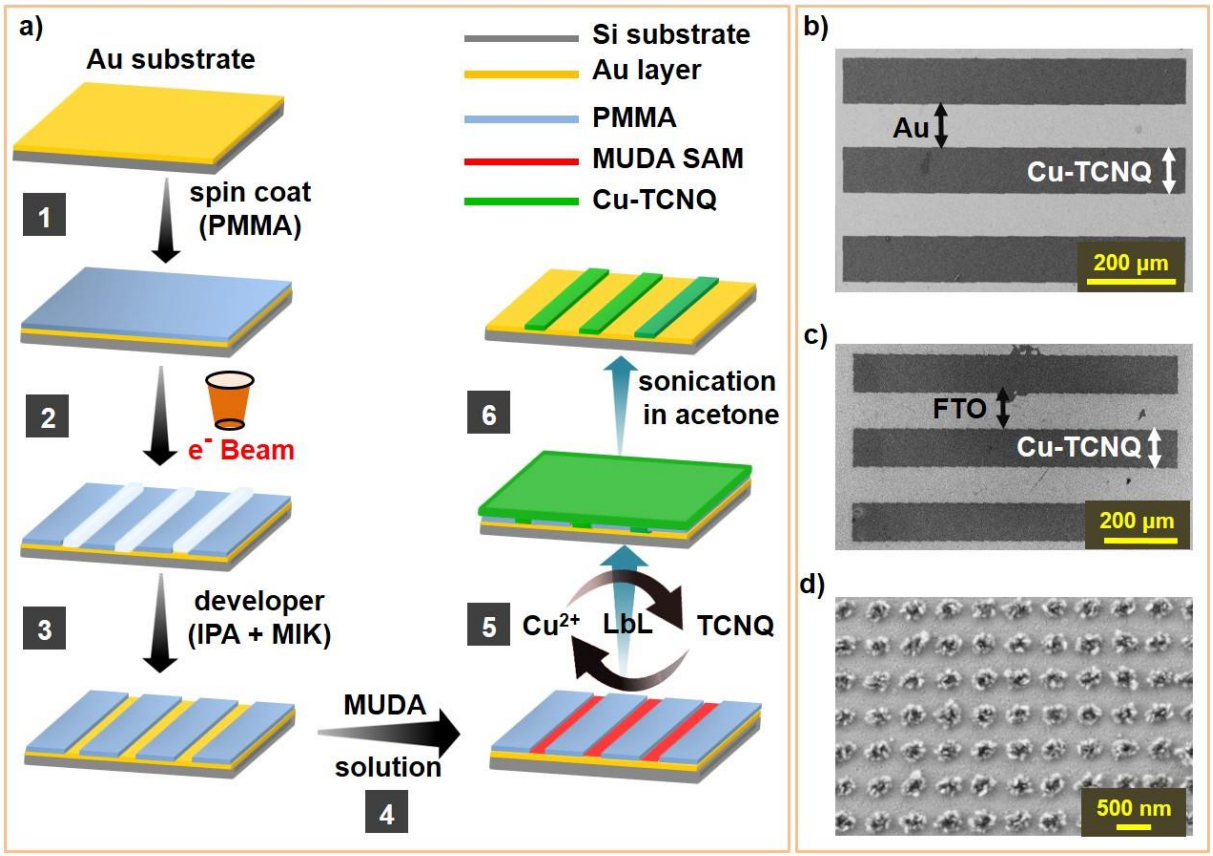

Figure 1: *Patterned growth of Cu-TCNQ thin film device: (a) step-1: spin coating of PMMA on clean Au (or FTO) substrate; step-2: exposure of PMMA to e⁻ beam; step-3: development by dipping into mixture of IPA + MIK solvent; step-4: formation of MUDA SAM by dipping into thiol*

solution; step-5: fabrication of Cu-TCNQ through LbL approach; step-6: lift-off PMMA and unwanted Cu-TCNQ crystallites by dissolving in acetone. (b & c) FESEM images of micro-patterns of Cu-TCNQ on Au and FTO substrates, respectively. (d) FESEM image of nano-patterned Cu-TCNQ on Au substrate.

3A.3 Results and Discussion

3A.3.1 Iodine Dosing to Cu-TCNQ

The micro-patterns of Cu-TCNQ were fabricated on Au and FTO substrates by using EBL technique (Figure 1). The electrical performance of Cu-TCNQ/Au and Cu-TCNQ/FTO devices were conducted with standard two-probe *I–V* technique (inset Figure 2a). Noticeable feature was the non-linear type of electrical conductance in Cu-TCNQ devices with a conductivity value in the range of ~10^{-5} S cm^{-1} on both Au and FTO substrates (Figure 2a & 2b).

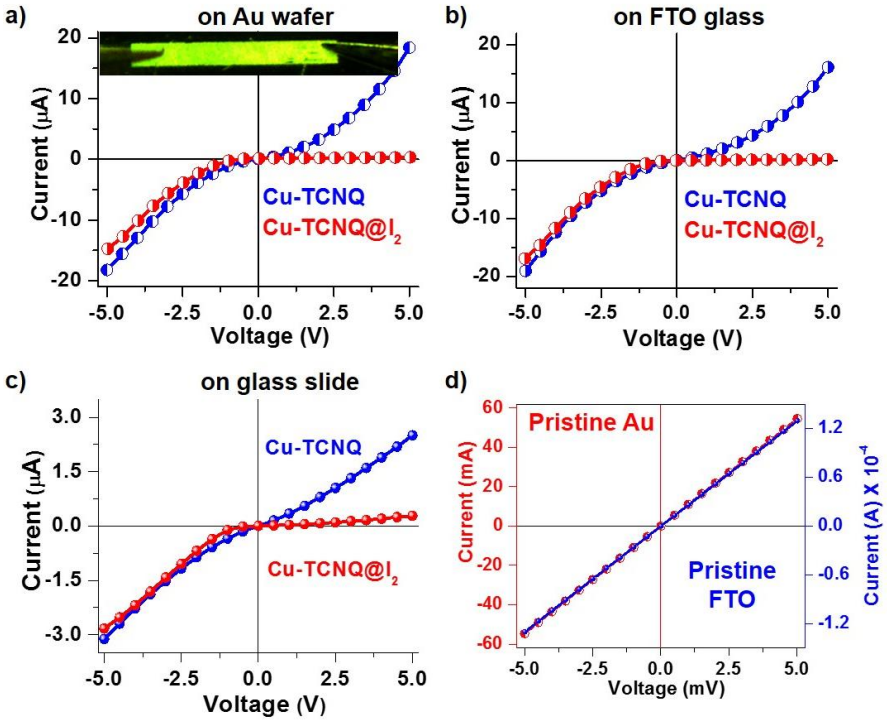

Figure 2: *I–V characteristics of Cu-TCNQ on Au (a) (inset: an optical image of two-probe measurement), FTO (b) and non-conducting glass (c) substrate before (blue) and after (red) dosing I_2 gas. (d) I-V characteristics of pristine Au (red) and pristine FTO (blue).*

Since non-linear *I-V* characteristics of semiconductors are prone to external stimuli, we exposed these Cu-TCNQ devices to iodine (I_2) vapors for 48 hours. These devices were thoroughly washed with chloroform to remove unreacted I_2 from the surface of Cu-TCNQ. Now, again *I–V* characteristics were recorded. A remarkable observation was the electrical rectification in electrical conductance of Cu-TCNQ-I_2 system on both FTO and Au substrates which is characteristic of a p–n junction diode. This electrical rectification was observed in Cu-TCNQ thin films grown on ordinary non-conductive glass substrates (Figure 2c). The possibility of leakage current in the devices could be cast-off due to the following reasons: (i) the Ohmic type *I-V* characteristics on both pristine Au and FTO substrate and their corresponding conductivity values were in the range of 10^{-3} and 10^{-2} Scm^{-1}, respectively (Figure 2d); (ii) the conductivity values of different batches of the device were consistently observed to be in the range of $\approx 10^{-5}$ Scm^{-1} (Figure 3a to 3d) and electrical rectification was also highly reproducible (Figure 3e to 3h).

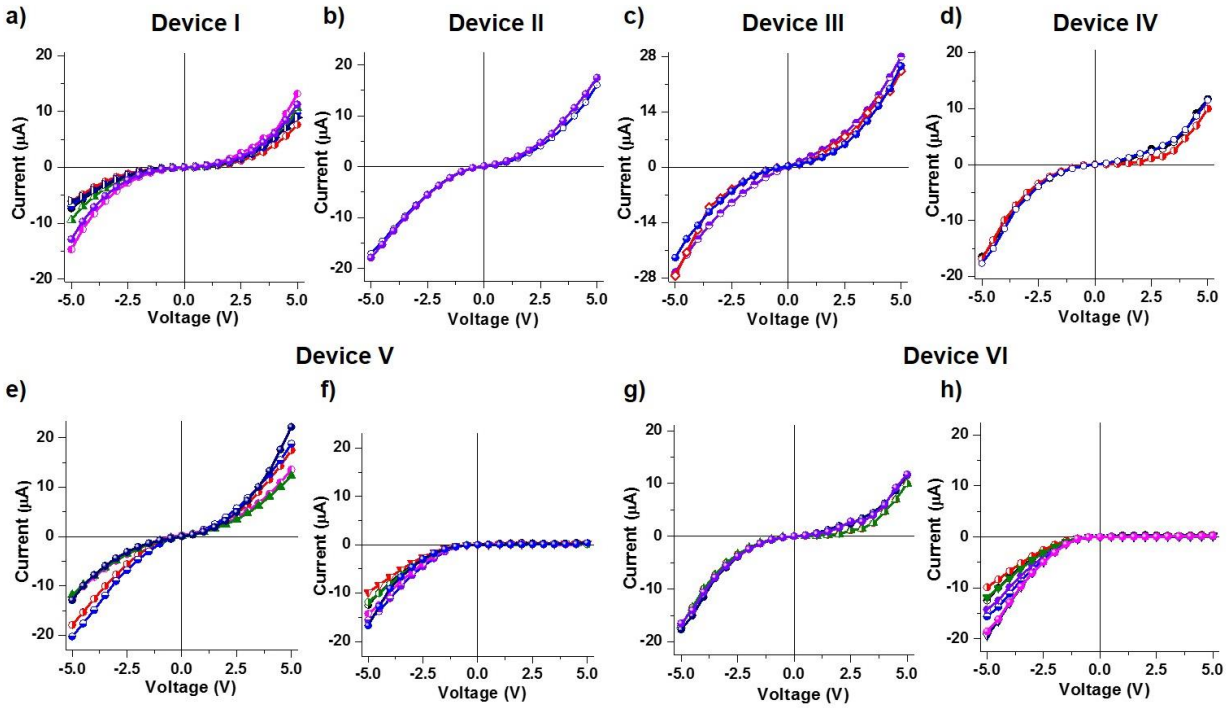

Figure 3: *(a, b, c & d) I-V characteristics of four different Cu-TCNQ thin-film devices. I-V characteristics of Cu-TCNQ thin-film devices (device 5 & device 6) before (e & g) and after (g & h) dosing I_2 vapors.*

To find out the reason of such unusual electrical rectification, we have performed Raman spectroscopy, Electron Paramagnetic Resonance (EPR) and XRD measurements on Cu-TCNQ thin films before and after I_2 dosing. TCNQ is a redox-active organic molecule which exists in three stable forms neutral, radical monoanion and dianion, all of them having distinctive Raman vibrational bands (Figure 4a).[5] Raman spectra of Cu-TCNQ thin film exhibited bands at ~1202, ~1380, ~1602, and ~2205 cm^{-1} corresponding to C=C−H bending, C−CN stretching, C=C ring stretching, C≡N stretching vibrational modes, indicating the presence of TCNQ radical monoanion (Figure 4b).[6]

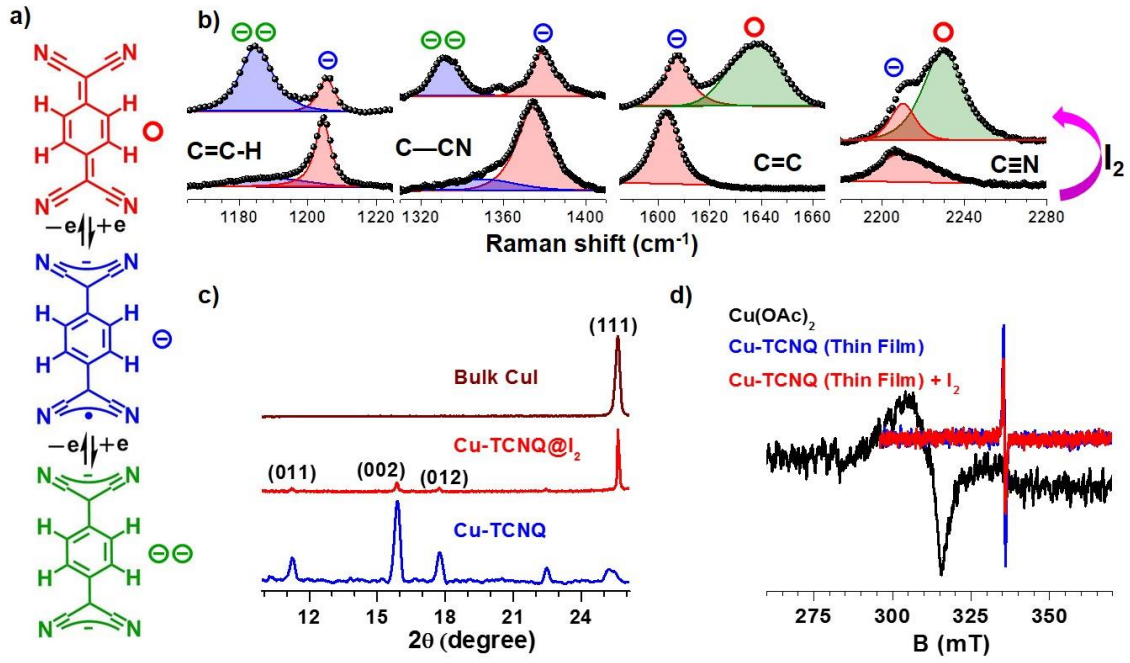

Figure 4: *a) Molecular schemes of neutral (red circle), radical anion (blue circle), and dianion (green circles) forms of redox-active TCNQ. (b) Raman spectra of Cu-TCNQ thin film before (bottom panels) and after (upper panels) dosing I_2 vapors. (c) out-of-plane XRD pattern of bulk CuI, Cu-TCNQ thin film before and after dosing I_2 vapors. (d) Room temperature EPR spectra of $Cu(OAc)_2$, Cu-TCNQ and Cu-TCNQ upon dosing I_2 vapors.*

After I_2 dosing, four new bands appeared, two at ~1638, ~2228 cm^{-1} and another two at ~1184, ~1332 cm^{-1} in Raman spectra which are characteristics of neutral and dianion forms

of TCNQ, respectively (Figure 4b).[7] This means that TCNQ radical monoanion in Cu-TCNQ thin-film was disproportionately converted to neutral and dianion moieties of TCNQ, after dosing I_2 vapors. I_2 vapors acts as an oxidizing agent to convert TCNQ radical monoanion to neutral TCNQ thus producing iodide anion (I^-) ion in the system. Coordination of I^- to Cu(I) ion is further supported by an additional peak in XRD pattern of Cu-TCNQ-I_2 system at $2\theta \approx 26°$ which indicates the formation of CuI (Figure 4c).[8-9] To detect change in the oxidation state of Cu ion upon I_2 dosing, we have employed EPR spectroscopy. As we know, Cu(I) is diamagnetic hence EPR inactive, while Cu(II) being paramagnetic is an EPR active species (Figure 4d). EPR spectra confirmed the absence of Cu(II) after I_2 dosing in thin film of Cu-TCNQ as typical peak of Cu(II) should appear at ~311 mT with $g \approx 2.162$, while EPR peak in Cu-TCNQ comes at ~339 mT which is characteristic of organic radicals like TCNQ radical monoanion (so-called free electron with $g \approx 2.00$). Thus, upon I_2 dosing redox reaction did not convert the Cu(I) to Cu(II) and also a significant portion of TCNQ radical monoanion was retained. Hence, here reported electrical rectification is mainly due to the formation of heterostructrure i.e. CuI/Cu-TCNQ upon I_2 dosing in the Cu-TCNQ system.

3A.3.2 Iodine Dosing to Ag-TCNQ

In the above section, we have exposed I_2 vapors to Cu-TCNQ which results in the heterostructure formation and electrical rectification in *I-V* characteristics. To study the similar effect on Ag-TCNQ, we have exposed Ag-TCNQ thin film to I_2 vapors for just 3 minutes and thoroughly washed with chloroform to remove unreacted I_2 from the surface. Interesting observation was the remarkable change in color of thin film from blue to golden yellow (Figure 5a). To probe structural change, we have performed out-of-plane XRD measurements, before and after dosing I_2 vapors. Peaks in XRD pattern corresponding to Ag-TCNQ structure almost disappeared and new peaks appeared around ~22.5° and ~24°, characteristic of (100) and (002) plane of β-phase of silver iodide (β-AgI), respectively (Figure 5b). The exclusive presence of AgI was further supported by solid state UV and Raman measurements of thin film. Solid-state UV spectra of Ag-TCNQ-I_2 system and bulk AgI was almost similar (Figure 5c). Most interesting observation was the disappearance of characteristic Raman peaks of TCNQ in range of 1200-2230 cm^{-1} and appearance of new broad peak in range of 100-250 cm^{-1} which

almost matches to bulk β-AgI (Figure 5d). Further, Ag 3d photoemission signal (XPS) of Ag-TCNQ@ I_2 thin film appeared at binding energy (BE) of ~367 eV ($3d_{5/2}$) and ~373 eV ($3d_{3/2}$) which are characteristic of +1 oxidation state of Ag (Figure 6a).

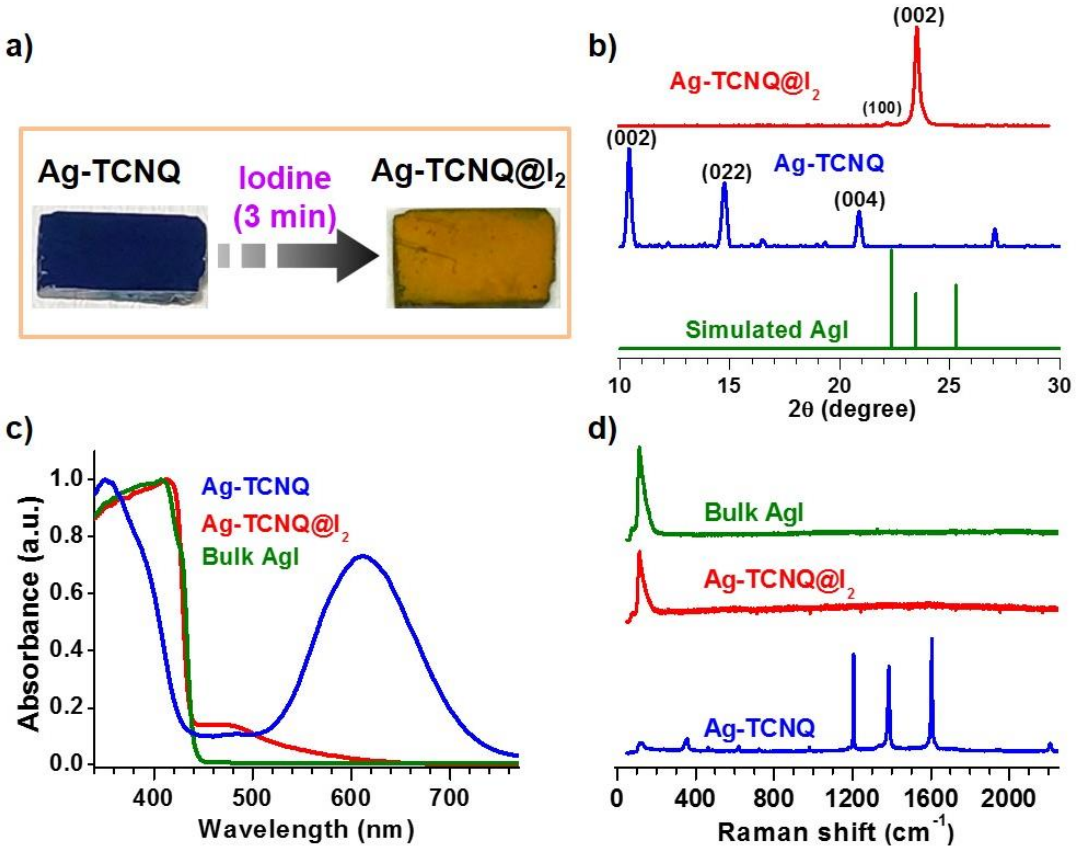

Figure 5: *(a) Optical image of Ag-TCNQ on Au substrate before and after dosing I_2 vapors. (b) Out-of-plane XRD patterns of simulated AgI, Ag-TCNQ thin film before and after I_2 dosing vapors. Solid-state UV (c) and Raman (d) spectra of bulk AgI, Ag-TCNQ thin film before and after I_2 dosing vapors.*

Iodine (I) 3d XPS spectra showed peaks at binding energy (BE) of ~619 eV ($3d_{5/2}$) and ~631 eV ($3d_{3/2}$) which indicates the presence of iodide anion (I^-) (Figure 6b). FESEM image of Ag-TCNQ thin film after dosing I_2 vapors, showed homogeneous thin film of AgI (Figure 6c). The water contact angle (CA) values of Ag-TCNQ-I_2 system was ~130° which almost matches to CA value of Ag-TCNQ system (inset Figure 6c). Elemental mapping showed homogeneous

distribution of Ag and I throughout the thin film sample and elemental ratio of Ag:I is almost close to 1:1, which also suggest formation of AgI (Figure 6d). Furthermore, we have also studied time dependent I_2 dosing to Ag-TCNQ thin films which is monitored by XRD and Raman measurements. We exposed Ag-TCNQ thin film to I_2 vapor and after every 20 seconds washed with chloroform and recorded XRD pattern. Within 60 seconds, peaks corresponding to Ag-TCNQ almost vanished and new peaks of β-AgI appeared (Figure 6e).

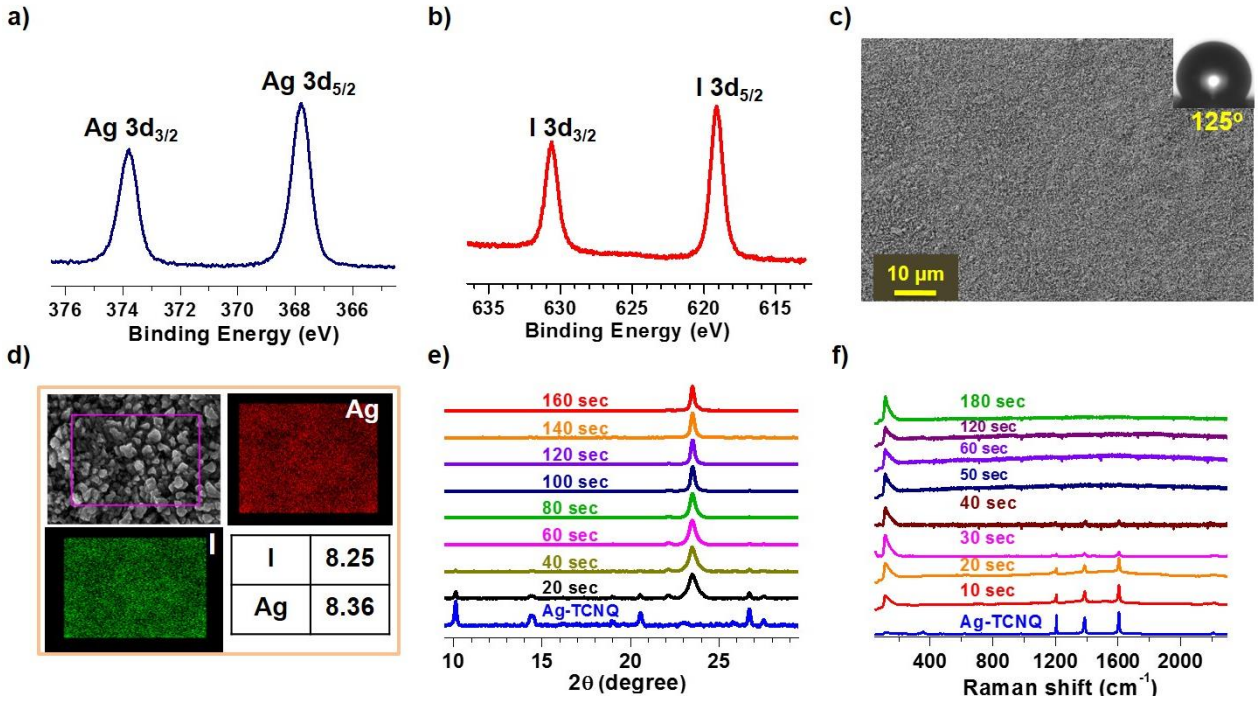

Figure 6: *Ag 3d (a) and I 3d (b) XPS spectra of Ag-TCNQ thin film after dosing I_2 vapors. (c) FESEM image of Ag-TCNQ thin film after dosing I_2 vapors (inset: optical image of water droplet on surface). (d) Elemental mapping and EDX of Ag-TCNQ thin film after dosing I_2 vapors. Out-of-plane XRD pattern (e) and Raman spectrum (f) of Ag-TCNQ thin film and after dosing I_2 vapors for different time intervals.*

3A.4 Conclusions

In conclusion, Cu-TCNQ thin film devices were fabricated by employing EBL technique. The Cu-TCNQ thin film devices exhibited non-Ohmic *I-V* characteristics. Upon dosing I_2 vapors, a

remarkable rectification in the electrical conductance was observed which was attributed to the formation of heterostructure i.e. CuI/Cu-TCNQ system. I_2 dosing to Ag-TCNQ thin film lead to the formation of AgI thin film with retention of hydrophobicity and homogeneity of thin film.

3A.5 References

(1) Kobayashi, Y.; Jacobs, B.; Allendorf, M. D.; Long, J. R., *Chem. Mater.* **2010,** *22,* 4120-4122.

(2) Gassensmith, J. J.; Erne, P. M.; Paxton, W. F.; Valente, C.; Stoddart, J. F., *Langmuir* **2011,** *27,* 1341-1345.

(3) Carbonell, C.; Stylianou, K. C.; Hernando, J.; Evangelio, E.; Barnett, S. A.; Nettikadan, S.; Imaz, I.; Maspoch, D., *Nat. Commun.* **2013,** *4,* 2173-2179.

(4) Ballav, N.; Shaporenko, A.; Terfort, A.; Zharnikov, M., *Adv. Mater.* **2007,** *19,* 998-1000.

(5) Tseng, T.-C.; Urban, C.; Wang, Y.; Otero, R.; Tait, S. L.; Alcamí, M.; Écija, D.; Trelka, M.; Gallego, J. M.; Lin, N.; Konuma, M.; Starke, U.; Nefedov, A.; Langner, A.; Wöll, C.; Herranz, M. Á.; Martín, F.; Martín, N.; Kern, K.; Miranda, R., *Nat. Chem.* **2010,** *2,* 374-379.

(6) Heintz, R. A.; Zhao, H.; Ouyang, X.; Grandinetti, G.; Cowen, J.; Dunbar, K. R., *Inorg. Chem.* **1999,** *38,* 144-156.

(7) Batten, S. R.; Champness, N. R.; Chen, X.-M.; Garcia-Martinez, J.; Kitagawa, S.; Öhrström, L.; O'Keeffe, M.; Suh, M. P.; Reedijk, J., *Cryst. Eng. Commun.* **2012,** *14,* 3001-3004.

(8) Rochford, L. A.; Keeble, D. S.; Holmes, O. J.; Clarkson, G. J.; Jones, T. S., *J. Mater. Chem. C* **2014,** *2,* 6056-6060.

(9) Miyao, K.; Funabiki, A.; Takahashi, K.; Mochida, T.; Uruichi, M., *New. J. Chem.* **2014,** *38,* 739-743.

CHAPTER 3

Electrical Conductance in Thin Films of Cu/Ag-TCNQ

Section 3B

Thermal Effect

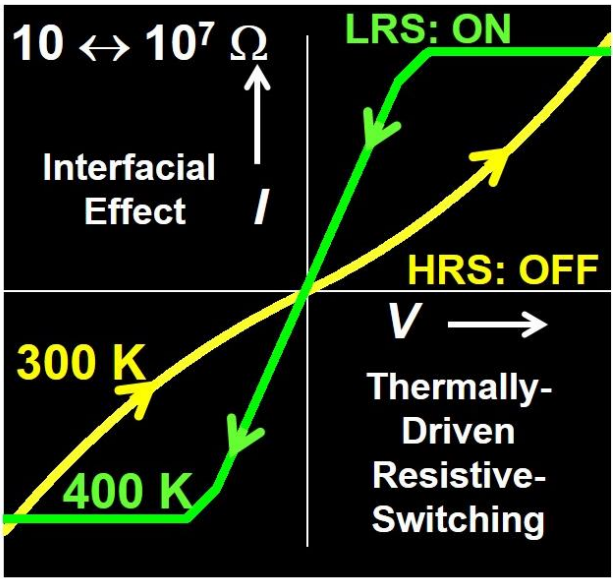

3B.1 Introduction

Metal-TCNQs solids are an interesting class of air-stable semiconducting coordination polymers (CPs) with unusual magnetic properties (long-range ordering at high temperatures). Among various M-TCNQ complexes, Cu-TCNQ and Ag-TCNQ are well known for their bipolar resistive switching behavior.[1] Resistive switching is the ability of system to change from high resistance state (OFF state) to low resistance state (ON state) under the influence of a strong external electric field or current or light and the change of resistance is non-volatile as well as reversible.[2] An interesting application of resistive switching is the fabrication of non-volatile random-access memories (RAM).[2] A material which exhibit high ON/OFF current ratio, large cycling durability and low threshold voltage for switching is required for engineering memory devices.[3] So far only electrical field and light induced resistive switching is reported in Cu-TCNQ and Ag-TCNQ complexes.[1] In this chapter, we have investigated thermal effect on the electrical transport of Cu-TCNQ and Ag-TCNQ thin films.

3B.2 Materials and Method

Fabrication of thin films of Cu-TCNQ and Ag-TCNQ was already discussed in Chapter 2A and 2B, respectively. Various other chemicals and instruments used are already described in Chapter 2. Top contacts of Titanium (Ti) and Platinum (Pt) on thin film were deposited by using photolithography (LW405 Laser writer) and sputtering of metals (LTE sputter 080). The electrical conductance of thin films was measured in Keithley two-probe (MODEL 4200-SCS) attached to Ever-being probe station equipped with thermal chuck. Electrochemical measurements (CV) on thin films were performed by Galvanostat/Potentiostat PARSTAT, PMC 2000 with scan rate of 10 mV/s.

3B.3 Results and Discussion

Electrical transport in the Ag-TCNQ thin film was initially investigated by using eutectic gallium indium (EGaIn) alloy as top electrodes (Figure 1a).[4] The appreciable feature was nonlinear current−voltage (*I*–*V*) characteristics of the metal/semiconductor (EGaIn/Ag-TCNQ) interface at room-temperature (300 K) and initial resistance of the system was ~10^6 Ω (Figure 1b). System was initially in a high-resistance state (HRS). Upon gradual increase in temperature

from 300 K to 400 K; resistance value was decreased to ~10 Ω and the system was in low-resistance state (LRS) (Figure 1b). Hence there is transformation from HRS to LRS upon gradual increasing temperature. Also, upon cooling back the system to room temperature (300 K), the system comes back to HRS. Thus, there is complete transformation of the LRS to HRS occurs, which is a clear signature of thermally-driven resistive switching (HRS ↔ LRS), as shown in Figure 1b.

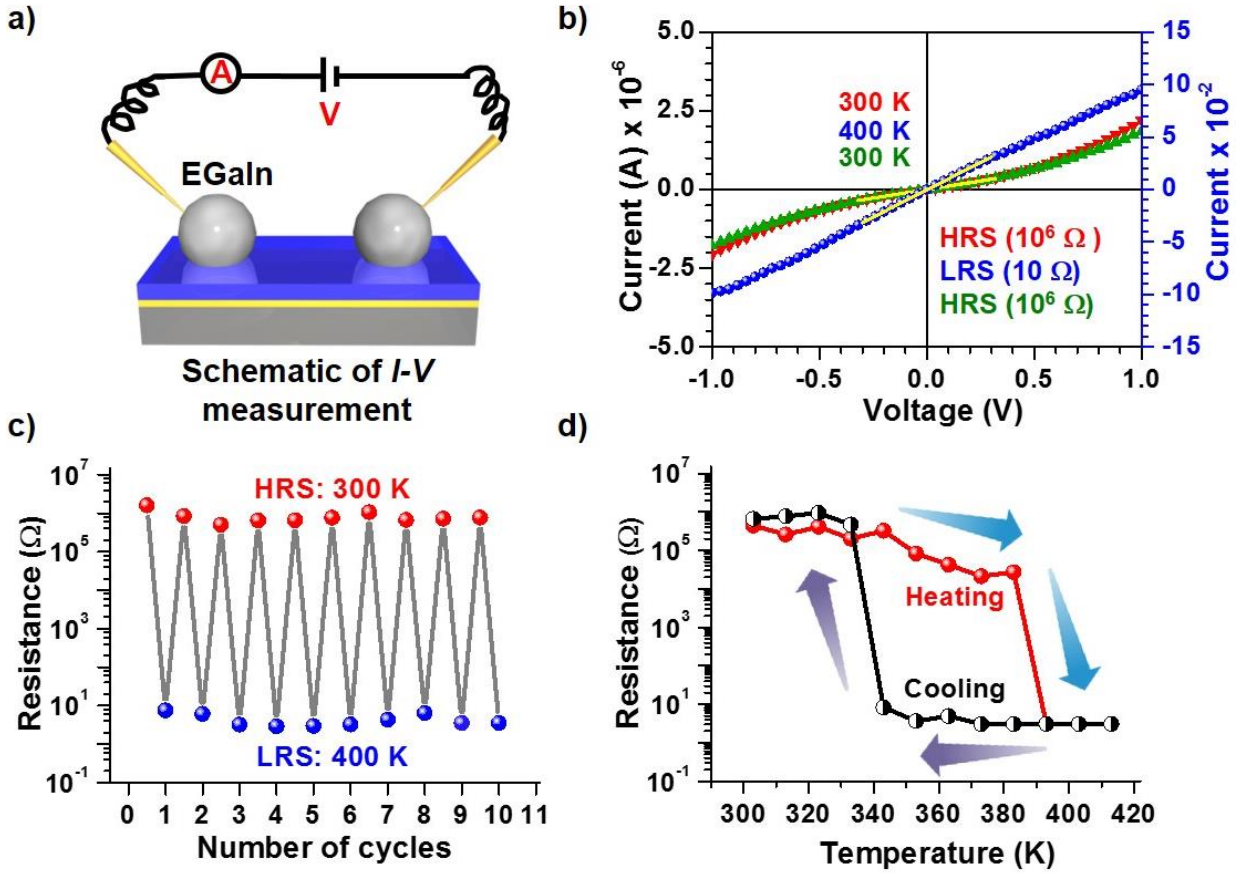

Figure 1. *(a) Schematic of the electrical transport measurement on Ag-TCNQ thin films by using EGaIn as the top–electrode. (b) I–V characteristics of Ag-TCNQ thin film at variable temperature, 300 K (red), 400 K (blue), and 300 K (green). To calculate resistances* R_{HRS} *and* R_{LRS}*, I−V curves were fitted linearly (yellow lines) in the voltage range of −0.3 to +0.3 V and respective values are provided. The black colored current axis is for both plots recorded at 300 K and the blue colored current axis is for the 400 K plot. (c) Plot of resistance values at HRS and LRS during heating-*

cooling processes versus the number of cycles. (d) Heating and cooling curves of resistance versus temperature clearly show a hysteresis loop.

A significant enhancement in the electrical conductance by a record factor of ~10^5 appears relatively better than earlier reports on the electric field-induced resistive switching in Ag-TCNQ.[5] To test the robustness of our thermally-driven resistive switching in Ag-TCNQ thin films, heating and cooling processes were executed up to 10 consecutive cycles. Excellent retention of the electrical conductance values at both the HRS and LRS was observed in the cycling process (Figure 1c). Also, a prominent hysteresis loop was appeared in the heating–cooling path which is characteristic of the memory effect (Figure 1d).

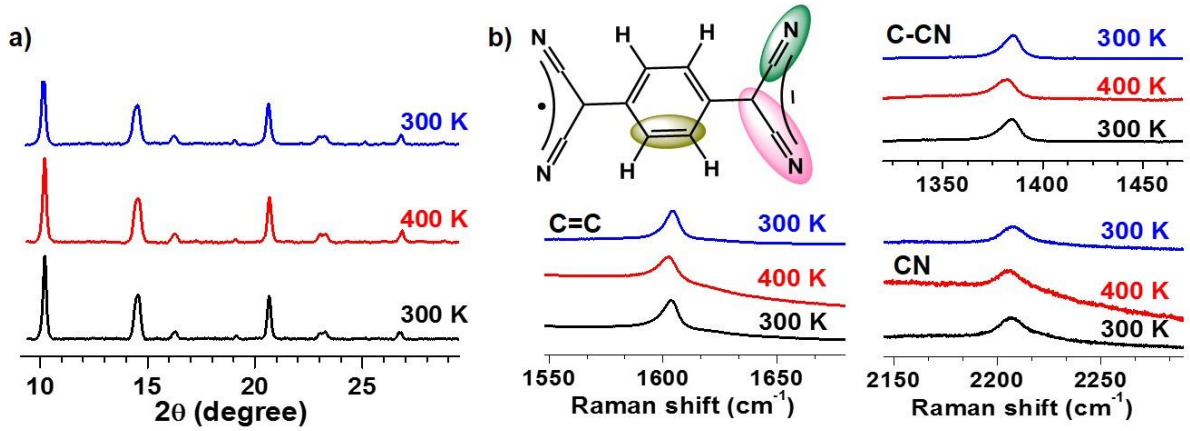

***Figure 2**. (a) Variable-temperature XRD patterns (a) and Raman spectra (b) of the Ag-TCNQ thin film.*

The distinct transition between the LRS and HRS can be assigned to OFF and ON states of resistive switching, thus making our Ag-TCNQ thin film a promising candidate for the development of temperature-dependent memory devices. A large number of mechanisms are proposed for the resistive switching in metal oxides as well as metal–organics.[2, 6] In a broad sense, it is largely either physical (structural/ conductive path via defect migration) or chemical (conductive path via filament formation/ charge transfer). The electrical field induced resistive switching in the Ag-TCNQ was due to the formation and rupture of electronically conductive filaments (CFs), which is well-established via the following charge transfer.[7]

$$[\text{Ag-TCNQ}]_n \text{ (HRS)} \longleftrightarrow x\text{Ag}^0 + x\text{TCNQ}^0 + [\text{Ag-TCNQ}]_{n-x} \text{ (LRS)}$$

To investigate the mechanism of our thermally-driven resistive switching in Ag-TCNQ thin film, we have recorded the variable temperature out-of-plane XRD patterns and Raman spectra (Figure 2a). At 300 K, the XRD pattern of our Ag-TCNQ thin film suggests a phase-I structure.[8] XRD pattern of our Ag-TCNQ thin film sample at room temperature (300 K) and high temperature (400 K) are almost similar, no reasonable change was observed, thereby ruling out the possibility of structural phase transition to be in the origin of thermally-driven resistive switching.[8] In Raman spectra of our Ag-TCNQ thin film at room temperature (HRS), the appearance of vibrational bands at ~2206 cm^{-1} (C≡N stretching), ~1603 cm^{-1} (C=C ring stretching), and ~1374 cm^{-1} (C−CN stretching) are characteristics of a TCNQ radical anion (Figure 2b).[9]

We have recorded the variable temperature Raman spectra of our Ag-TCNQ thin film. The spectral fingerprints of TCNQ radical anion are remained similar at both 300 K (HRS) and 400 K (LRS), and specifically the appearance of new bands at ~1457 cm^{-1} and ~2229 cm^{-1}, characteristics of neutral TCNQ, were not observed. Also, with subsequent cooling down the system to 300 K, spectral features were retained. Therefore, our Raman data clearly suggest that thermally-driven resistive switching in Ag-TCNQ thin film was not due to the formation of conductive filaments involving charge transfer, as discussed earlier. Markedly, in a recent article on the electric field-induced resistive switching in thin films of CPs, formation of conductive filaments was also excluded. Alternative cause of the resistive switching could be the metal-semiconductor interface, the so-called interface-type.[6] In order to investigate the role of contact resistance, we have used Ti and Pt micropads as top electrode in addition to EGaIn drops, for electrical measurements on the Ag-TCNQ thin films. Ag-TCNQ is an n-type semiconductor and having work function value (φ) of ~1.19 eV.[10] Due to the lower work function of Ag-TCNQ as compared to those of EGaIn (φ ~ 4.2 eV), Ti (φ ~ 4.3 eV), and Pt (φ ~ 6.3 eV), at metal-semiconductor interfaces, formation of a Schottky-type barrier is expected, which is giving rise to a depletion layer due to a band bending phenomenon (Figure 3a).

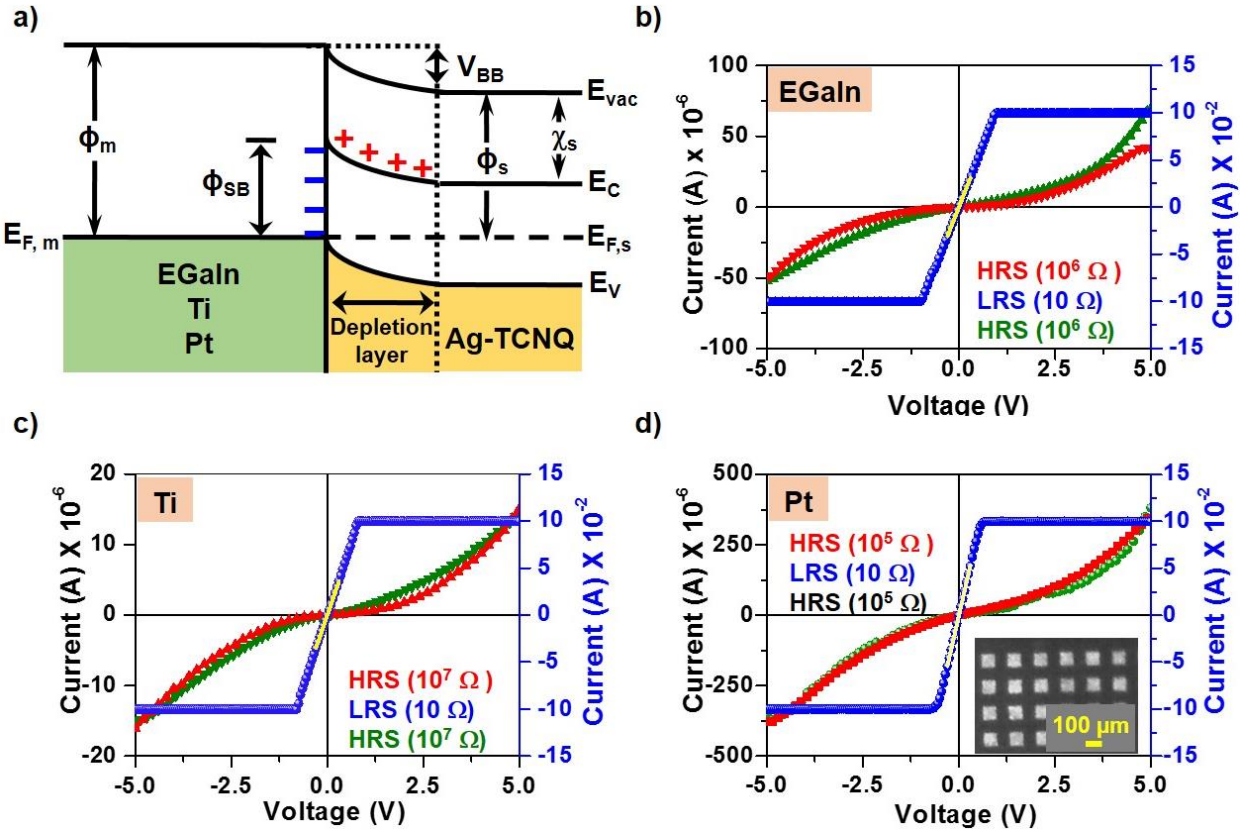

Figure 3. *(a) Schematic of the energy diagram of the metal-semiconductor interface. Here, semiconductor represents Ag-TCNQ (n-type) and metal represents EGaIn or Pt or Ti, where ϕ_s is the semiconductor work function, ϕ_m is the metal work function, ϕ_{SB} is the Schottky barrier, E_c is the energy of the conduction band minimum, χ_s is the electron affinity of the semiconductor, E_v is the energy of the valence band maximum, and E_{vac} is the vacuum energy. I−V characteristics of Ag-TCNQ thin films by using different top electrodes such as EGaIn (b), Ti (c), and Pt (d) at 300 (red), 400 (blue), and 300 K (green). (Inset in d: optical image of Pt contact pads on a Ag-TCNQ thin film). The blue colored current (I) axis is for the 400 K plot, and the black colored current (I) axis is for both plots recorded at 300 K (b−d).*

Indeed, *I*−*V* characteristics (−5 to +5 V) were recorded at different interfaces (EGaIn/Ag-TCNQ, Ti/Ag-TCNQ, and Pt/Ag-TCNQ), consistently showed non-ohmic characteristics at 300 K (Figure 3c−3d). Upon heating the different interfacial systems to 400 K, non-ohmic characteristics consistently switched to ohmic, and again, cooling down the systems to 300

K, non-ohmic nature consistently reappeared. To calculate the contact resistance values at each temperature, data points in the *I*–*V* curves were fitted linearly in low-voltage regions (−0.3 to +0.3 V) (Figure 3b–3d, yellow lines). The respective values at 300 K and 400 K for different top electrodes were found to be ~10^6 and ~10 Ω (EGaIn); ~ 10^7 and ~10 Ω (Ti); and ~10^5 and ~10 Ω (Pt). Depending on the metallic contact, the increment factor in electrical resistance ranged from ~10^4 to ~10^6. Generally, the contact resistance is estimated to increases with increasing the work function of metal in the case of metal/n-type semiconductor interfaces. Though, in the current study, no correlation among contact resistance values and the work function values of metals was observed, which strongly suggests that the Fermi levels of various metals on Ag-TCNQ are pinned, possibly due to creation of metal-induced gap states.

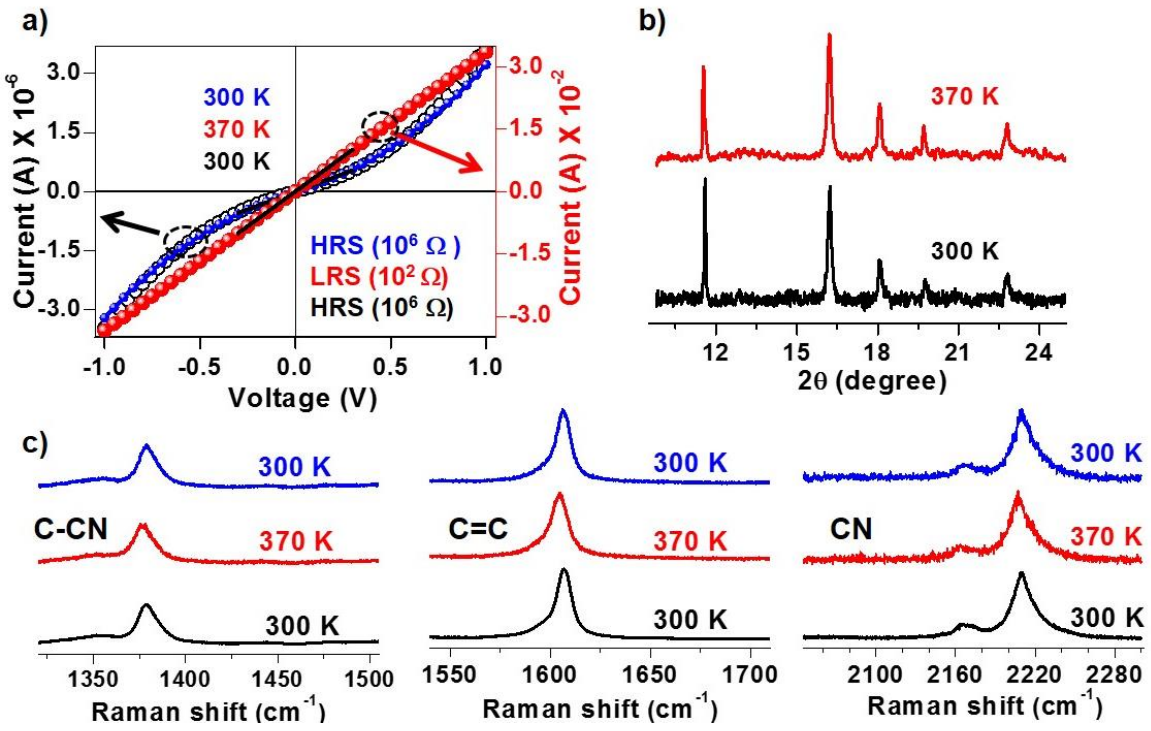

Figure 4: *I-V characteristics of Cu-TCNQ thin films at 300 K (black), heating at 370 K (red) and cooling back to 300 K (blue) showing resistive switching (HRS and LRS) with an enhancement of ~10^4 in electrical resistance value (a). Variable temperature out of plane X ray diffraction patterns of Cu-TCNQ thin film configurations (b). Variable temperature Raman spectra recorded on Cu-TCNQ thin films (c).*

This thermally-driven resistive switching effect is not specific not only for the Ag-TCNQ system; Cu-TCNQ thin films grown on SAM templates by LbL approach also showed similar effects (Figure 4a). As no appreciable change in the temperature dependent XRD patterns and Raman data on the Cu-TCNQ thin films was observed, the formation of CFs as the driving mechanism for the thermally-driven resistive switching can be excluded (Figure 4b & 4c).

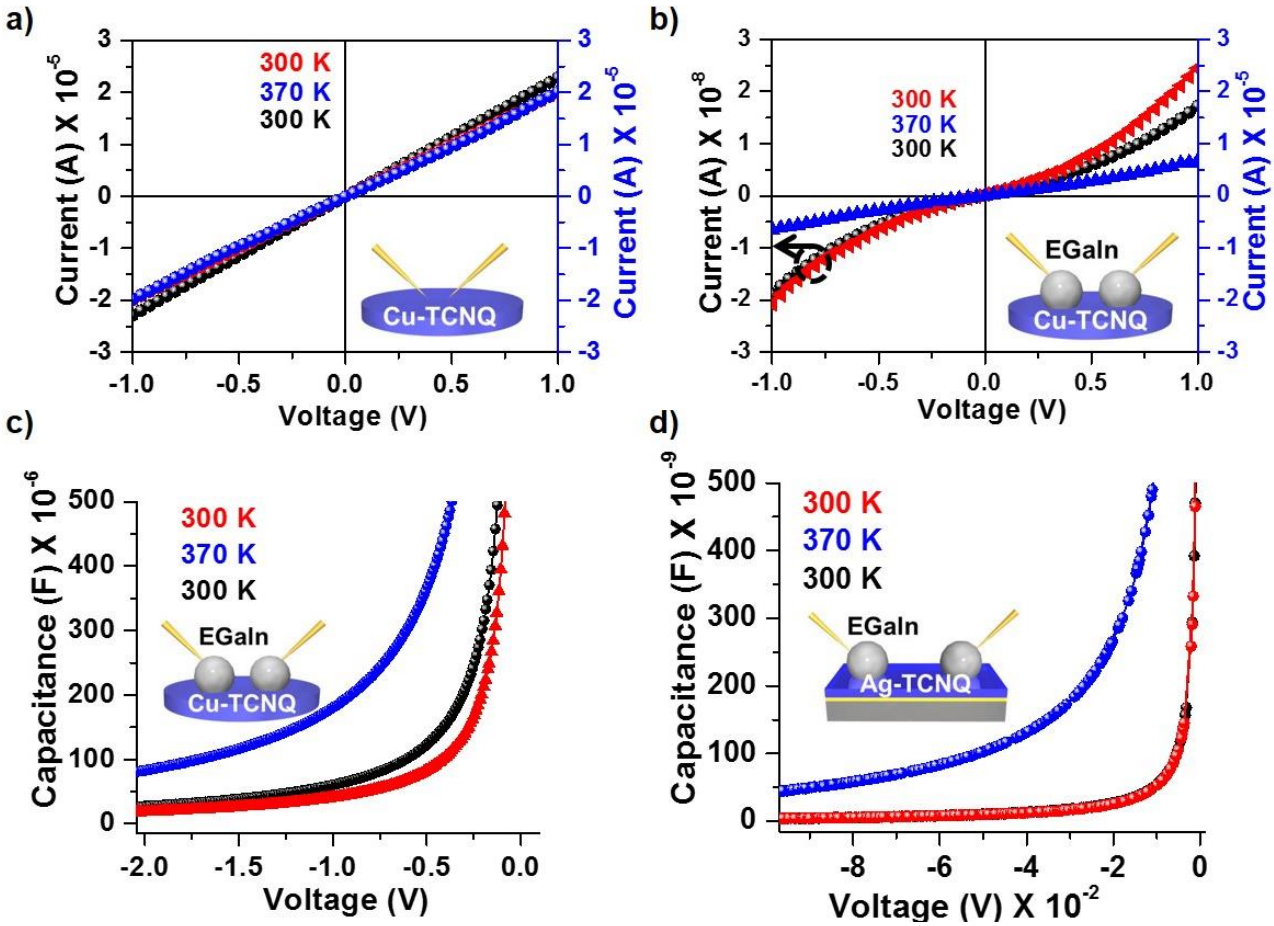

Figure 5. *(a) I–V plots of bulk Cu-TCNQ (in pellet form) recorded at different temperatures, 300 (red), 370 (blue), and 300 K (green), with direct contacts of pins, the so-called two-probe. (b) I–V plots of the Cu-TCNQ pellet recorded at different temperatures, 300 (red), 370 (blue), and 300 K (green), with EGaIn as the top electrodes. The blue colored current (I) axis is for the 400 K plot, and the black colored current (I) axis is for both plots recorded at 300 K (a, b). (c) C–V curves recorded on a Cu-TCNQ pellet at different temperatures, 300 (black), 370 (blue), and 300 K (red),*

with EGaIn as the top electrodes. (d) C−V curves recorded on Ag-TCNQ thin films at different temperatures, 300 (black), 370 (blue), and 300 K (red), with EGaIn as top electrodes.

To further strengthen our claim of thermally-driven resistive switching as an interfacial effect, we performed *I-V* measurement on pressed pellets of Cu-TCNQ powder at various temperatures with and without using EGaLn as the top contacts (Figure 5a, & 5b). *I−V* features in both the systems were remarkably different: (i) Whereas we see the presence of ohmic Characteristics at both 300 and 370 K in the former system, the latter is characterized by presence of non-ohmic and ohmic characteristics at 300 K and 370 K respectively; (ii) contact resistance at 300 K across the EGaIn/Cu-TCNQ interface is significantly higher (by a factor of $\sim 10^3$) than the direct contact resistance; and (iii) a clear onset of thermally-driven resistive switching only at the EGaIn/Cu-TCNQ interface with an enhancement factor of $\sim 10^3$ in the electrical resistance value. Thus, the observed thermally-driven resistive switching originates mainly from lowering of the Schottky barrier at the metal/semiconductor interface with increase in temperature and is not a bulk property of the material itself. The Schottky barrier height can be approximated with the following equation: $\Phi_{SB}(300K) = \Phi_{SB}(300\ K) + \alpha(T - 300\ K)$, where α is a temperature coefficient term (eV/K) and for n-type semiconductors such as Ag-TCNQ and Cu-TCNQ exhibit negative α values. We have estimated potential profiles of the depletion layer by recording capacitance−voltage (*C−V*) plots at 300 and 370 K. C is inversely proportional to the depletion layer width and thus, is expected to be larger in the LRS than that in the HRS in a conventional Schottky model.[6] Indeed, our preliminary C−V results recorded on both EGaIn/Cu-TCNQ (pellet) and EGaIn/Ag-TCNQ (thin film) interfaces showed larger C values at high temperatures (LRS) compared to the values at room temperature (HRS) (Figure 5c & 5d). However, to conclude on the temperature dependency of the Schottky barrier height from C−V measurements, more analysis is needed.

3B.4 Conclusions

In conclusion, we have successfully demonstrated resistive switching in thin films of CPs upon alternation of the Schottky barrier at the metal−semiconductor interfaces by thermal energy. Specifically, thin films of Ag-TCNQ and Cu-TCNQ consistently showed reversible switching

between the HRS and LRS at elevated temperatures (400 K for the former and 370 K for the latter). A remarkable enhancement factor in the electrical conductance with an excellent switching durability is observed.

3B.4 References

(1) Gu, Z.; Wu, H.; Wei, Y.; Liu, J., *J. Phys. Chem.* **1993,** *97*, 2543-2545.

(2) Zhu, L.; Zhou, J.; Guo, Z.; Sun, Z., *J. Materiomics* **2015,** *1*, 285-295.

(3) Waser, R.; Aono, M., *Nat. Mater.* **2007,** *6*, 833-840.

(4) Chiechi, R. C.; Weiss, E. A.; Dickey, M. D.; Whitesides, G. M., *Angew. Chem. Int. Ed.* **2008,** *47*, 142-144.

(5) Yang, F.; Zhao, Q.; Xu, C.; Zou, Y.; Dong, H.; Zheng, Y.; Hu, W., *Adv. Mater.* **2016,** *28*, 7094-100.

(6) Sawa, A., *Mater. Today* **2008,** *11*, 28-36.

(7) Rosner, B.; Ran, K.; Butz, B.; Schmidt, U.; Spiecker, E.; Fink, R. H., *Phys Chem Chem Phys* **2015,** *17*, 18278-18281.

(8) Zheng, W.; Li, Z.; Yang, F.; Song, X.; Zhang, H.; Liu, Y.; Wang, C., *Mater. Lett.* **2008,** *62*, 1448-1450.

(9) Rana, S.; Rajendra, R.; Dhara, B.; Jha, P. K.; Ballav, N., *Adv. Mater. Interfaces* **2016,** *3*, 1500738-1500748.

(10) Liu, H.; Zhao, Q.; Li, Y.; Liu, Y.; Lu, F.; Zhuang, J.; Wang, S.; Jiang, L.; Zhu, D.; Yu, D.; Chi, L., *J. Am. Chem. Soc.* **2005,** *127*, 1120-1121.

CHAPTER 4

Thin Films by Interfacial Chemical Reaction: Growth and Electrical Conductance in Cu(I)-HCF

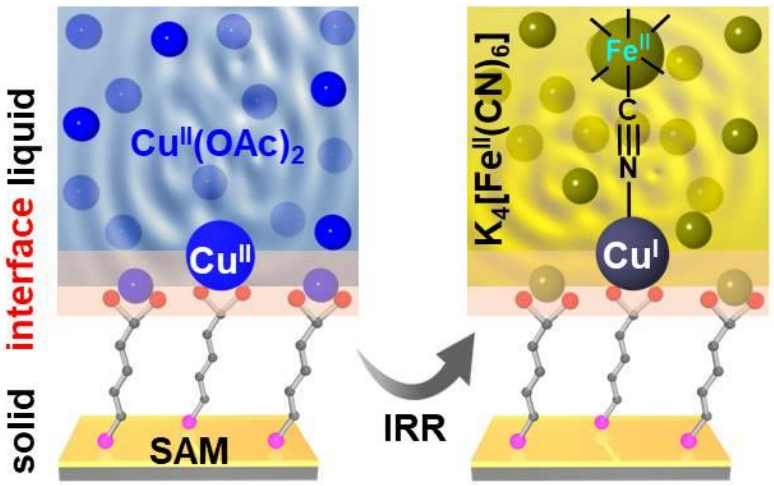

4.1 Introduction

In chapter 2A, we have observed the interfacial reduction of Cu(II) to Cu(I) by TCNQ which results in the fabrication of high-quality thin film of Cu-TCNQ. TCNQ is an organic molecule which contains four nitrile (-CN) groups. To examine the significance of -CN functional group on the interfacial reduction of Cu(II), a redox-active metal ion i.e. Fe(II) attached with -CN group (as a spectroscopic marker) was used as a ligand. For this, $K_4[Fe(CN)_6]$ molecule was chosen, and thin films were fabricated on functionalized Au substrate through layer-by-layer (LbL) approach. This $K_4[Fe(CN)_6]$ molecule, is a major precursor for Prussian Blue (PB), upon mixing with Fe(III), gives a blue colored product. [1] PB is known as the first modern synthetic compound and its analogues (PBAs) are well explored for a large number of applications such as detection of toxic metal ions, rechargeable batteries, gas storage, and photo-magnetic devices.[1] Herein, we have grown thin film of Copper-Hexacyanoferrate (Cu-HCF) via LbL approach and study the interfacial reduction.

4.2 Materials and Method

Potassium ferrocyanide ($K_4[Fe(CN)_6]$), Copper acetate ($Cu(OAc)_2.H_2O$), Cuprous Chloride (CuCl) and Au coated silicon wafer were purchased from Sigma Adrich (India) and used without further purification. X-ray Photoelectron spectra (XPS) spectra were recorded by using Scienta R4000 analyzer and a monochromatic Al K_α source. Solid state UV-vis absorption spectra were recorded on Shimadzu UV- 3600 UV VIS-NIR spectrophotometer. Thin film was gently peeled off and dispersed in ethanol, then drop casted on TEM grid and examined under FE TECNAI G2 F20 microscope. Fabrication of MUDA/Au SAM on Au substrate and various other instruments used for characterization of thin films are as described in Chapter 2.

To grow thin films, MUDA/Au SAM was alternatively dipped into $Cu(OAc)_2$ (1 mM in EtOH) and $K_4[Fe(CN)_6].3H_2O$ (0.7 mM in H_2O/EtOH (v/v = 1:2)) solution (30 minutes in each) to complete 1 cycle of layer-by-layer growth. Both precursor solutions were kept at an elevated temperature of 60 ^oC. Similar procedure was repeated up to 20 consecutive cycles. Thin film was thoroughly washed with ethanol and dried under the stream of N_2 gas after each step.

Bulk Copper-Hexacyanoferrate (Cu-HCF) was synthesized by a simple mixing of aqueous solutions of $K_4[Fe(CN)_6].3H_2O$ (0.5 M) and $Cu(OAc)_2.H_2O$ (1 M) at room temperature under constant stirring in a beaker containing 20 ml of distilled water.[2] Then, this solution was left undisturbed 4 hours and finally, brown colored precipitate was formed appeared which was thoroughly washed with water and dried at 100 ^oC in vacuum oven for 2 hours.

4.3 Results and Discussion

4.3.1 Interfacial Reduction

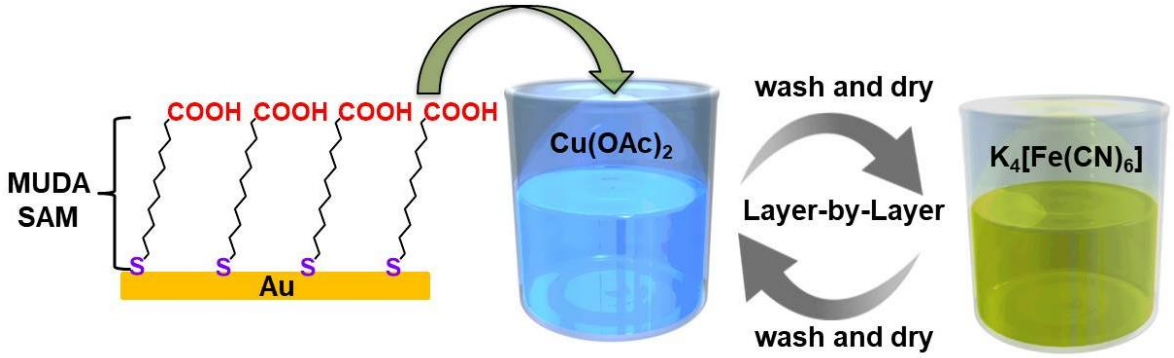

Figure 1: *Schematic illustration of Cu-HCF thin film by LbL growth on thiol functionalized Au substrate.*

After 2 cycles of LbL growth, thin film was first examined with photoelectron spectroscopy to determine the oxidation states of various elements. The Cu 2p XPS spectrum of thin film sample showed a strong $2p_{3/2}$ peak at binding energy (BE) of ~932.0 eV, which is characteristic of Cu(I) species (Figure 2b).[3] The Fe $2p_{3/2}$ photoemission signal at BE of ~708.4 eV confirmed the major presence of Fe(II) species in thin film sample (Figure 2c).[4] The presence of Cu(I) as well as low-spin Fe(II) was further supported by the absence of satellite features in the photoemission signals of Cu 2p and Fe 2p.[3] After 0.5 cycles, majorly Cu(II) is present as shown in chapter 2A, however after 2 cycles, Cu(I) is observed on MUDA/Au SAM surfaces. Hence, here again we have observed an interfacial reduction of Cu(II) to Cu(I), likewise in chapter 2A where TCNQ has caused similar chemical reduction. Now, the question arises, what is the source of electron for this interfacial reduction of Cu(II) to Cu(I)? What is the nature (oxidation state) of Au and S during this reduction process? To

address these questions, core-level photoemission signal of Au substrate and S of SAM were recorded on the same sample. The Au 4f XPS spectrum showed a single $4f_{7/2}$ peak at BE of ~83.9 eV which ruled out the possibility of an electron transfer from the Au substrate causing the reduction of Cu(II) to Cu(I) at solid-liquid interface (Figure 2d).[5-6]

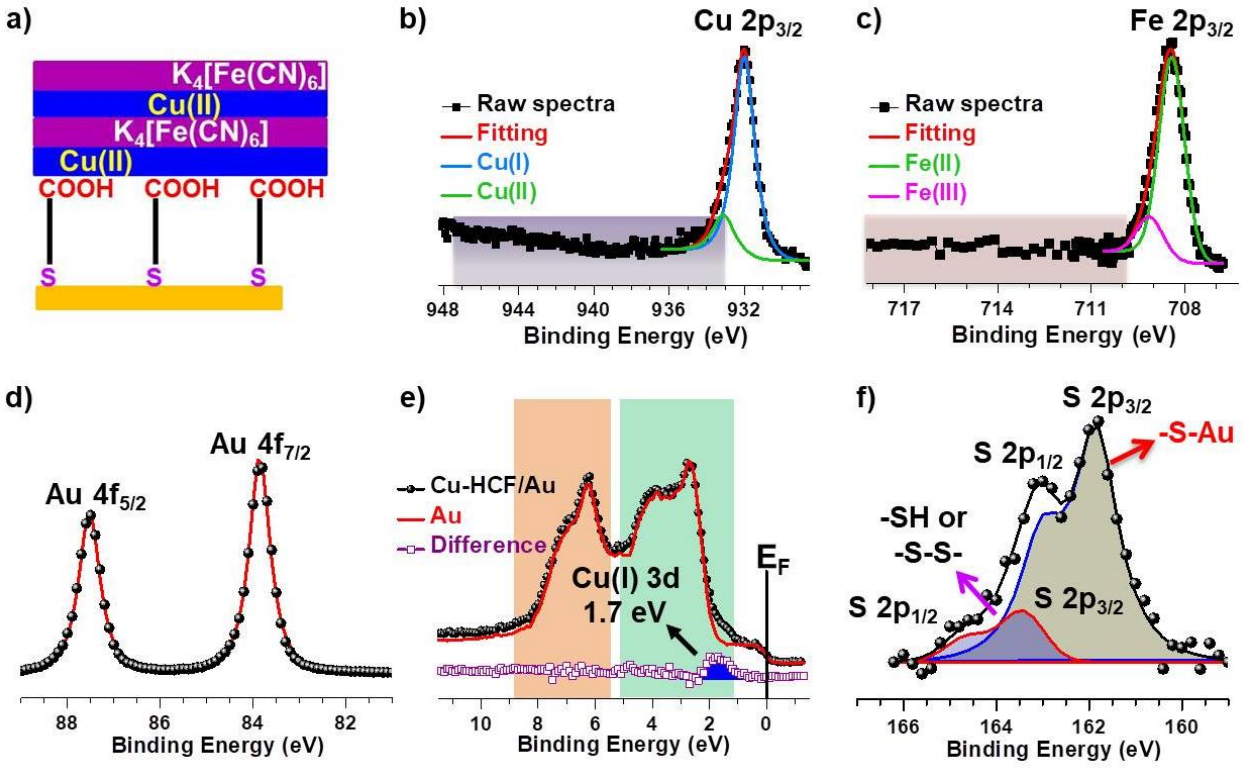

Figure 2: *(a) Schematic of thin film after 2 growth cycles which was further characterized by XPS. (b, c) High-resolution Cu 2p and Fe 2p XPS spectra of thin film. Respective satellite zones corresponding to Cu(II) and low-spin Fe(III) are marked by color shades. (d) Au 4f XPS spectrum of thin film showing the $4f_{7/2}$ and $4f_{5/2}$ doublet peak (due to spin-orbit coupling). (e) Valence band (VB) spectra recorded on the thin film and on pristine Au substrate showing the 5d (orange shades) and 6s (green shade) states of Au. Cu(I) 3d state is clearly visible (blue fill) in the difference spectrum. Fermi level (E_F) was represented by solid black line. (f) High-resolution S 2p XPS spectrum of thin film. Specific bonding scenario of S is marked*

Presence of Cu(I) and intactness of Au substrate was also supported by valence-band (VB) photoemission signals from the same sample. Presence of Fermi edge at 0 eV in VB signal indicates the absence of oxidized Au and a significant peak could be realized at ~1.7 eV upon subtraction of sample from pristine Au which is characteristics of photoemission from Cu 3d states of Cu(I) species (Figure 2e).[3] Furthermore, photoemission signal of S on the same sample clearly revealed that the thiolate (Au−S) bond was almost intact and S was not oxidized (Figure 2f).

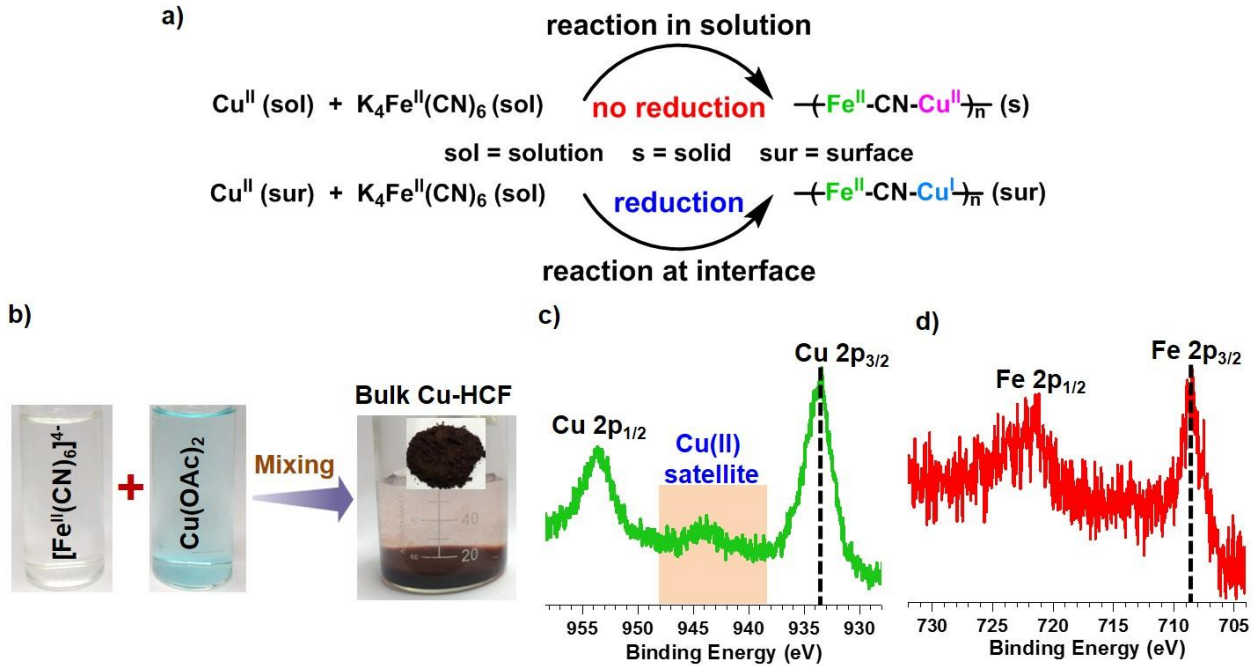

Figure 3: *(a) Schematic illustration of different reactivity of surface supported Cu(II) and liquid-phase Cu(II) with liquid $K_4[Fe(CN)_6]$ solution. (b) Upon mixing Cu(II) and $K_4[Fe(CN)_6]$ solution, a brown colored precipitate was formed (liquid-phase reaction) and named it as bulk Cu-HCF. (c, d) Cu 2p and Fe 2p XPS spectrum of bulk Cu-HCF showing major presence of Cu(II) and Fe(II). Satellite feature of Cu(II) was highlighted with orange shade.*

Thus, Au substrate and S of the SAM was not the source of electron for interfacial reduction of Cu(II) to Cu(I). Interestingly, reduction of Cu (II) to Cu(I) was almost absent in a liquid-phase reaction of Cu(II) with $K_4[Fe(CN)_6]$. Upon mixing solutions of $Cu(OAc)_2$, and $K_4[Fe(CN)_6]$, a brown colored product formed, in which Cu(II) and Fe(II) was predominantly

present as evident from the corresponding XPS spectra of bulk Cu-HCF (Figure 3b). It has been observed the longer exposure of sample to X-rays during XPS measurement, can potentially induce the reduction of Cu(II) to Cu(I).[7] Therefore, a nondestructive spectroscopic technique i.e. Raman was employed for the probing of interfacial reduction. The C≡N

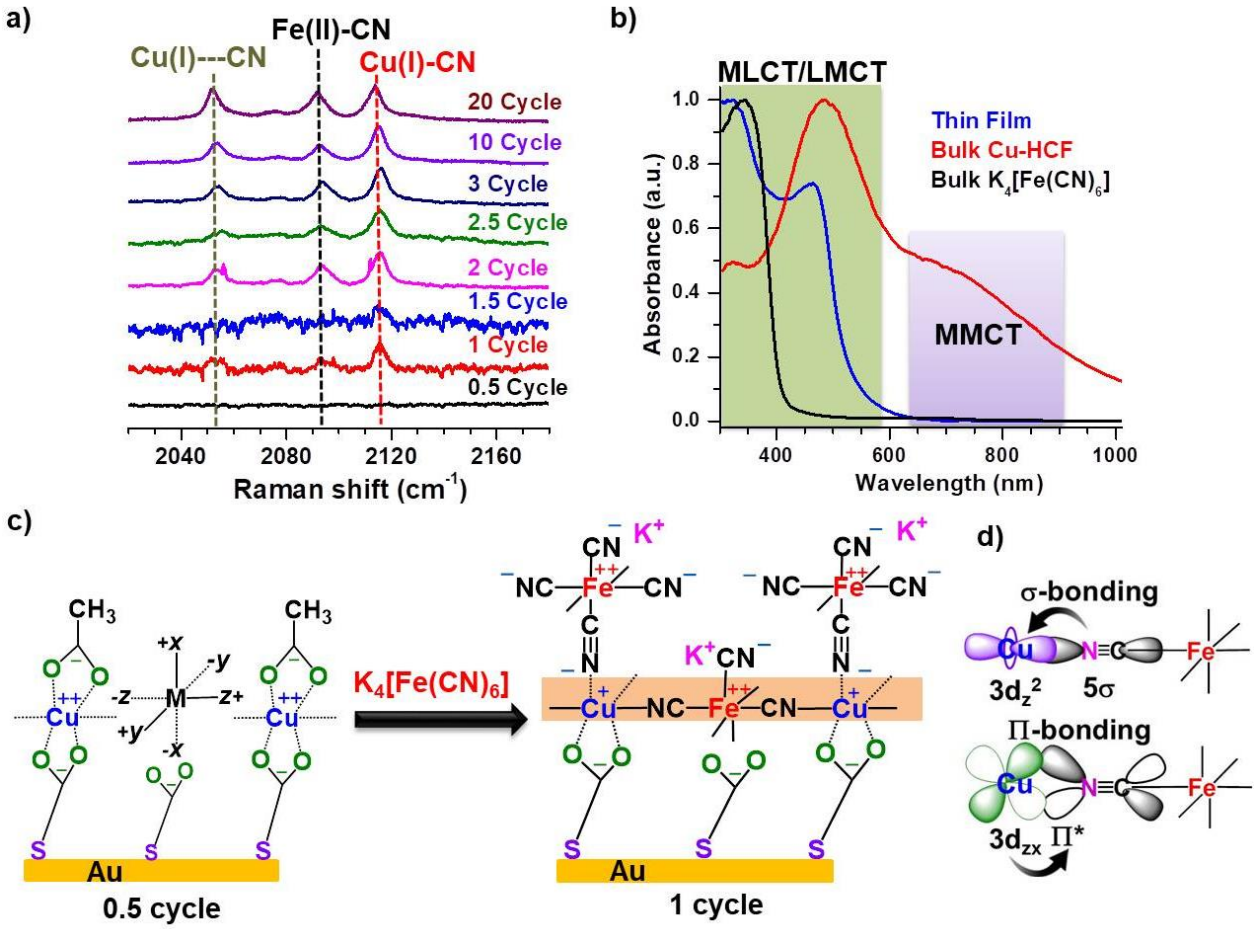

Figure 4: *(a) Raman spectra recorded stepwise in the LbL growth. Distinctive bonding scenario was also indicated with dashed line. (b) Solid state UV-vis spectra of bulk Cu-HCF, thin film of Cu-HCF and pure bulk $K_4[Fe(CN)_6]$. Respective, MLCT/LMCT and MMCT bands are highlighted. (c) Schematic showing anchoring of the Cu(II) on surface of MUDA/Au SAM template (0.5 cycle of the LbL growth). As a guide to eye, six approaching directions of ligands to a metal ion M is provided. Addition of $K_4[Fe(CN)_6]$, leads to reduction of Cu(II) to Cu(I) at the interface by the CN ligand (1 cycle of LbL growth). (d) Illustration of a synergistic Cu−CN bonding driving the interfacial reduction of Cu(II) to Cu(I): σ-bonding upon overlapping of filled*

5σ orbital of CN ligand and partially filled $3d_z^2$ orbital of Cu and π-back bonding from the filled $3d_{zx}$ orbital of Cu to the empty π orbital of CN.*

stretching frequency relatively depend on the counter ion and its coordination environment, for example, the CN stretching bands at ~2093 and ~2135 cm^{-1} distinctively revealed the presence of Fe(II)-CN and Fe(III)-CN bonds in $K_4[Fe(CN)_6]$ and $K_3[Fe(CN)_6]$, respectively.[8-9] Here, Raman spectra were recorded at each step of cycles (initially) during the LbL growth of thin film. After 1 cycle of LbL growth (dipping the Cu(II) ions decorated SAM into $K_4[Fe(CN)_6]$ solution), three characteristic Raman bands appeared at ~2053, ~2093, and ~2115 cm^{-1} which correspond to Cu(I)---CN (weak interaction), Fe(II)−CN, and Cu(I)−CN (strong interaction) bonding scenario (Figure 4a).[10] All three unique peaks were consistently observed up to 20 consecutive cycles. Remarkably, characteristic Raman band of Cu(II)−CN (2153 cm^{-1}) and Fe(III)−CN (2135 cm^{-1}) bonding scenario were not observed, which support the claim of interfacial reduction.[10] The distinctive bonding scenario of biredox link allows metal-to-ligand, ligand-to-metal, and metal-to-metal charge transfer (MLCT, LMCT and MMCT) interactions in PBAs.[1] Among various CT interactions, MMCT band was majorly observed in the partially reduced system [(Cu(II)-CN-Fe(II)] and was almost absent in fully reduced [(Cu(I)-CN-Fe(II)] or fully oxidized [(Cu(II)-CN-Fe(III)] system of PBAs.[11] Solid state UV−vis absorption spectrum of thin film and bulk $K_4[Fe(CN)_6]$ samples didn't show ~700 nm peak characteristic of MMCT transition (Figure 4b).[11] Absence of MMCT transition in thin film again confirmed the presence of fully reduced Fe(II)−CN−Cu(I) state in our thin film. Based on Raman data of thin film, we have proposed a mechanism for LbL growth of coordination network bearing Fe(II)−CN−Cu(I) link (Figure 4c). During growth of coordination network at solid-liquid interface, two attacking directions (-x and +y of d orbital) at Cu(II) are preoccupied upon surface anchoring to SAM surface, so CN ligand can approach towards Cu(II) from only the remaining four directions – +x, -y, +z and -z. As, Cu(II) has partially filled $3d_z^2$ orbital in the z-direction, the CN ligands approaching in ± z direction will transfer electron density from its filled sigma (5σ) orbital and reduce Cu(II) to Cu(I). All 3d-orbitals are filled upon formation of Cu(I), and then there is a synergistic backfilling of electron density from its filled $3d_{zx}$ orbital to empty π* orbital of CN which stabilizes the Cu−CN bond (Figure

4d). Two more CN approaching from remaining directions (+x and −y) will interact in a nonlinear fashion with Cu(I), leading to the formation of weaker Cu---CN bond. On the other hand, in a liquid-phase reaction, ideally six CN ligands of ferrocyanide can approach Cu(II) from all six directions of an octahedral geometry (±x, ±y, and ±z), without any confinement effect and as a result, coordination network bearing Fe(II)−CN−Cu(II) link could easily be precipitated without causing the reduction of Cu(II) to Cu(I). Thus, geometrical constraints at the solid-liquid interface will make two types of Cu(I)−CN bonds, one at ~2115 cm^{-1} (linear) and another at ~2053 cm^{-1} (nonlinear) as is clearly evident from the Raman spectra. Such distinguishing Cu−CN bonding is further supported by the gradual variation of the intensity of the Raman bands at ~2115 and ~2053 cm^{-1} beyond 1 cycle of LbL growth. The Raman band at ~2053 cm^{-1} was almost diminished while the intensity of Raman band at ~2115 cm^{-1} was greatly reduced after 1.5 cycles of LbL growth. Successive dipping of substrate into $K_4[Fe(CN)_6]$ solution (2 cycle of LbL growth) again generated both aforementioned Raman bands of Cu(I)−CN and Cu(I)---CN bonds. Hence, the Raman spectra not only compliments the XPS data but also exclude the possibility of reduction of Cu(II) to Cu(I) by secondary electrons during XPS measurements.

Typically, the next nearest neighbor distance of S/Cu atoms in thiolate SAMs on Au surface is ~10 Å which almost matches to the distance between two Fe ions in PBAs (~10 Å) and thereby allowing metal-ligand coordination vis-à-vis maximization of charge neutrality at the confined environment-resembling various enzymatic reactions. We have recorded the UV-vis spectra of $K_4[Fe(CN)_6]$ solution before and after 20 cycles of LbL growth and realized an oxidation of $K_4[Fe(CN)_6]$ to $K_3[Fe(CN)_6]$ in solution which could be the probable source of electron causing the reduction of Cu(II) to Cu(I) at solid−liquid interface (Figure 5a). Furthermore, reaction of CuCl (Cu(I) ion) and $K_4[Fe(CN)_6]$ in a liquid-phase as well as at a solid−liquid interface did not result in the formation of the expected Fe(II)−CN−Cu(I) coordination link (Figure 5b-f). Thus, IRR is anticipated to be very useful in generating new materials that are otherwise difficult to achieve via conventional liquid-phase reactions.

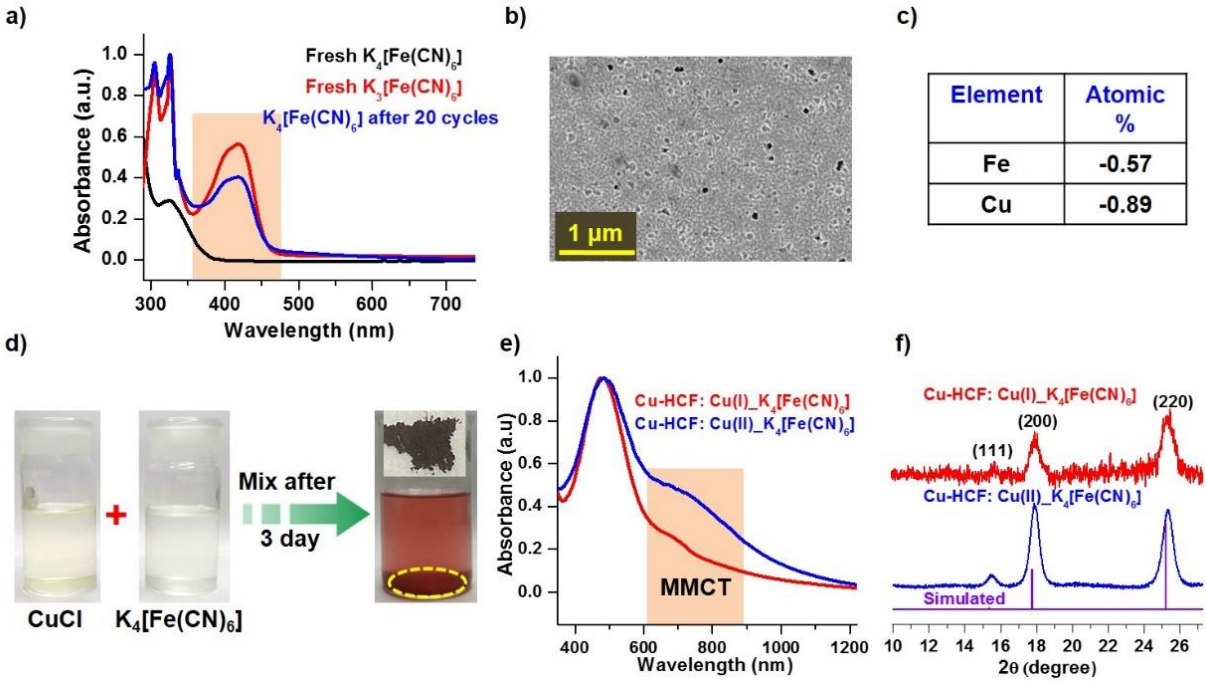

Figure 5: *(a) UV-vis spectra of fresh $K_4[Fe(CN)_6]$, fresh $K_3[Fe(CN)_6]$ and $K_4[Fe(CN)_6]$ solution after 20 cycles of LbL growth. (b) FESEM image of functionalized Au substrate after 20 cycles of LbL with Cu(I) salt as a precursor, showing bare Au which means thin film was not grown. (c) EDXS analysis showing absence of Cu and Fe on Au substrate. (d) Optical images showing reaction of CuCl and $K_4[Fe(CN)_6]$ solution. After mixing two solutions, brown colored precipitate was formed after three days. (e) Solid state UV-vis spectra of bulk Cu-HCF obtained by using Cu(I) (red line) and Cu(II) (blue line) salts as precursors and both spectra matched well and MMCT transition (~700 nm) was visible. (f) Out-of-plane XRD pattern of bulk Cu-HCF obtained by using Cu(I) (red line), Cu(II) (blue line) precursors and simulated pattern of Cu-HCF (PDF no-75-0023). All these samples showed cubic phase of Cu-HCF.*

4.3.2 Generation of New Material with Interfacial Reduction Reaction

We were able to successfully grow thin film of Cu-HCF consisting Fe(II)−CN−Cu(I) coordination link by interfacial reduction. FESEM images showed homogeneous and high quality thin film which is prerequisite for practical applications (Figure 6a). Elemental mapping of the Cu-HCF thin film by using EDXS analysis showed uniform distributions of

various elements – K, Cu, and Fe, throughout the thin film (Figure 6a). The out-of-plane X-ray diffraction (XRD) measurements of thin films was recorded and compared with that of bulk Cu-HCF. XRD pattern of bulk Cu-HCF sample showed two peaks at $2\theta \approx 15.3°$ and 17.9° which corresponds to cubic phase of PBAs (Figure 6b).[2] Interestingly, three prominent peaks at $2\theta \approx 14.8°$, 19.5°, and 21.3° were observed in case of thin film which were characteristics of rhombohedral phase of PBAs (Figure 6b).[12] Thus, the thin film sample showed presence of rhombohedral phase, while cubic phase was present in bulk sample. Transmission electron microscopy (TEM) measurement along with selected area electron diffraction (SAED) pattern of the thin film material, suggested high degree of crystallinity and supported the major presence of rhombohedral phase in thin film sample (Figure 6c). Overall, solid-liquid interfacial reaction generates rhombohedral phase while liquid-phase reaction produces cubic phase of PBAs.

Now the question arises, how the different phases of PBAs are getting stabilized from same precursor solutions in liquid-phase and at the interface? PBAs have the general formula $A_xM_A[M_B(CN)_6]_y{\cdot}nH_2O$, where M_A and M_B are transition metal ions and A is an alkali metal ion. The structure is perfect cubic (without any vacancy defect) if the ratio of M_A/M_B is equal to 1, and upon deviation of this ratio from 1, the $[M_B(CN)_6]$ vacancies will distort the structure from perfect cubic.[12] Also, the nano-pores of PBAs were occupied by some fraction of water molecules and alkali metal ions; and the remaining fraction of water molecules reside in the vacancy of the $[M_B(CN)_6]$ site and coordinate to the M_A site. In our Cu-HCF thin film, the ratio of M_{Cu}/M_{Fe} is around 3 which clearly indicates the presence of enormous vacancy defects in the material.[12] It is reported in the literature that higher alkali metal ion concentration also induces phase transition from cubic to rhombohedral and fully reduced biredox state (Fe(II)−CN−Fe(II)) favors rhombohedral phase in PBAs.[13] Thorough EDXS analysis of our Cu-HCF thin film showed higher K^+ ion concentration (Figure 6d). Hence, fully reduced state (Fe(II)−CN−Cu(I)) (from XPS and Raman) and higher concentration of K^+ ion in Cu-HCF thin film justify the formation of rhombohedral phase from an interfacial growth. Also, formation of linear and nonlinear Cu(I)−CN bonds at solid−liquid interface−as was evidenced from our Raman data−could lead to rhombohedral structure in the thin film material. Interestingly, in

our bulk Cu–HCF sample, the amount of K^+ ion was found to be very small (< 0.3%) which supported the cubic phase structure (Figure 6e).

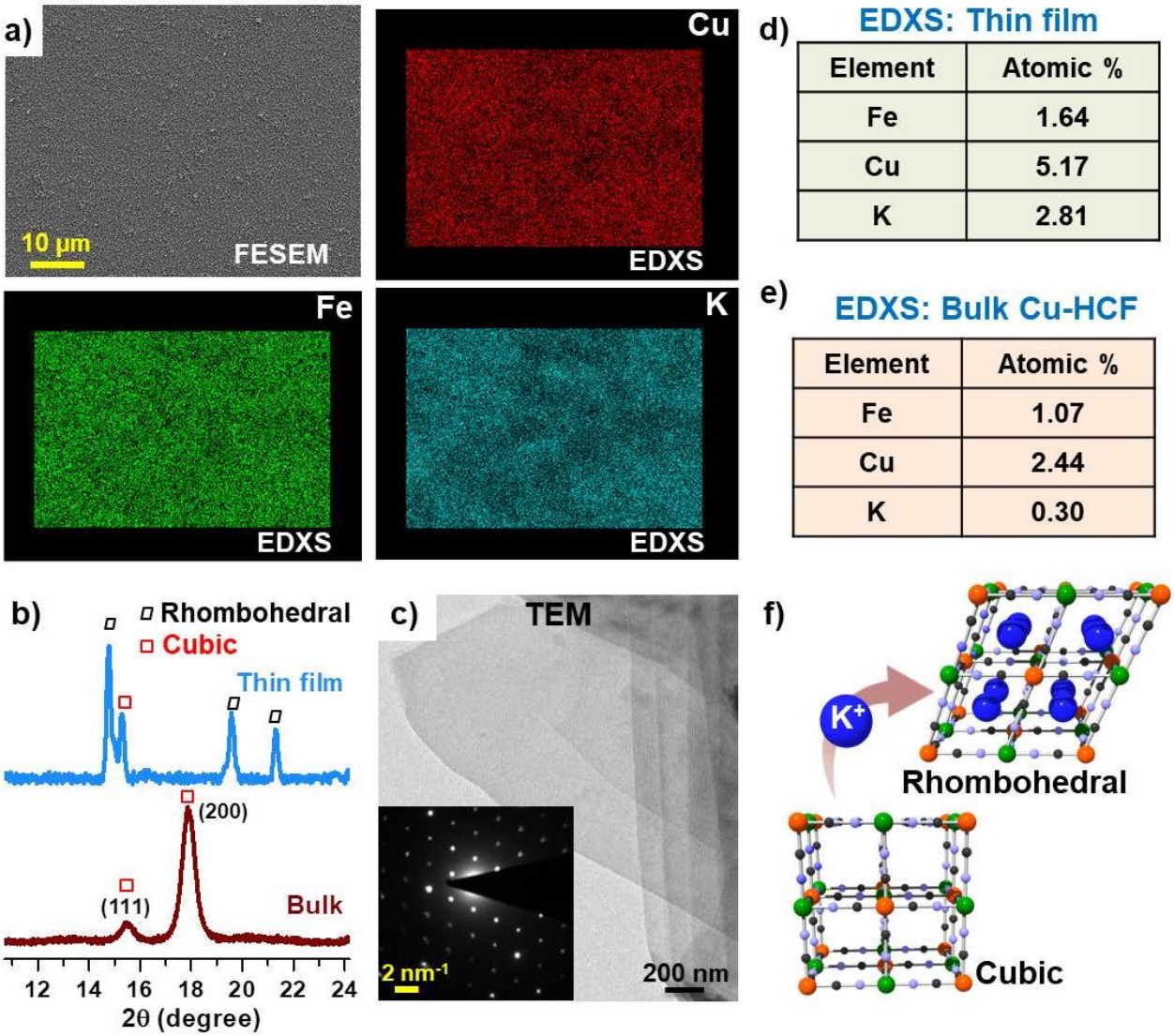

Figure 6: *(a) FESEM image and EDXS mapping (elements are mentioned) of the Cu-HCF thin film sample. (b) XRD pattern of bulk and thin films samples of Cu–HCF. (c) TEM image of materials extracted from Cu-HCF thin film (inset: corresponding SAED pattern representing rhombohedral phase). (d) EDXS analysis of thin film after twenty cycles. (e) EDXS analysis of bulk Cu-HCF. (f) Schematic representation of cubic to rhombohedral phase transformation upon insertion of potassium ions in PBAs.*

4.3.3 Thermo Responsive Cu-HCF Thin Film

In PBAs, insertion and elimination of water molecule as well as alkali metal ions are known to induce structural phase transition in the material.[14] However, thermally-driven reversible structural phase transition in PBAs are rare unlike flexible coordination polymers. To examine structural dynamics in our Cu-HCF thin film having fully reduced Fe(II)−CN−Cu(I) coordination link, we have recorded variable temperature XRD pattern and a remarkable change in the XRD patterns was observed. At high temperature of 400 K, characteristic diffraction peak of the rhombohedral phase at $2\theta \approx 14.8°$ disappeared and a new diffraction peak appeared at $2\theta \approx 16.3°$ which we would like to assign to a modified-rhombohedral and/or orthorhombic phase of PBAs (Figure 7a).[12] Upon cooling down the sample temperature from 400 K to 300 K, the original diffraction peaks reappeared which revealed a stimuli-responsive nature of our Cu-HCF thin film. We have also performed variable temperature Raman measurement to investigate the cause of such reversible structural phase transition. The peaks corresponding to Fe---O (~476, ~510, and ~590 cm^{-1}) and Cu---O (~350 cm^{-1}) bonds almost vanished at higher temperature (400 K) and reappeared upon cooling down the system to room temperature (300 K) (Figure 7b).[15-16] Thus, structural phase transition in our Cu-HCF thin film is due to loss of water molecule from coordination network. Generally, structural phase transition in a material is accompanied by a change in the physical property and therefore we have also performed variable temperature current-voltage (*I*−*V*) characteristics across the thin film by using eutectic gallium indium alloy (EGaIn) as a top electrode. Indeed, upon increasing the temperature from 300 K to 400 K, electrical conductance of Cu-HCF thin film was enhanced by two orders of magnitude which was observed to be reversible, thereby corroborating the reversible structural phase transition in the Cu-HCF thin film (Figure 7c). To probe charge-transfer during thermally driven structural phase transition in such as biredox link, we again recorded temperature-dependent Raman spectra and examined the C≡N stretching vibrations (Figure 7d). Interestingly, intensity of all Raman bands were significantly decreases at high temperature, the zoomed in view of Raman spectrum at high temperature (400 K) showed a band at ~2103 cm^{-1}, which was originally present at ~2093 cm^{-1} (room temperature). Also, shoulder peaks appeared at ~2130 cm^{-1} and around ~2150 cm^{-1} at

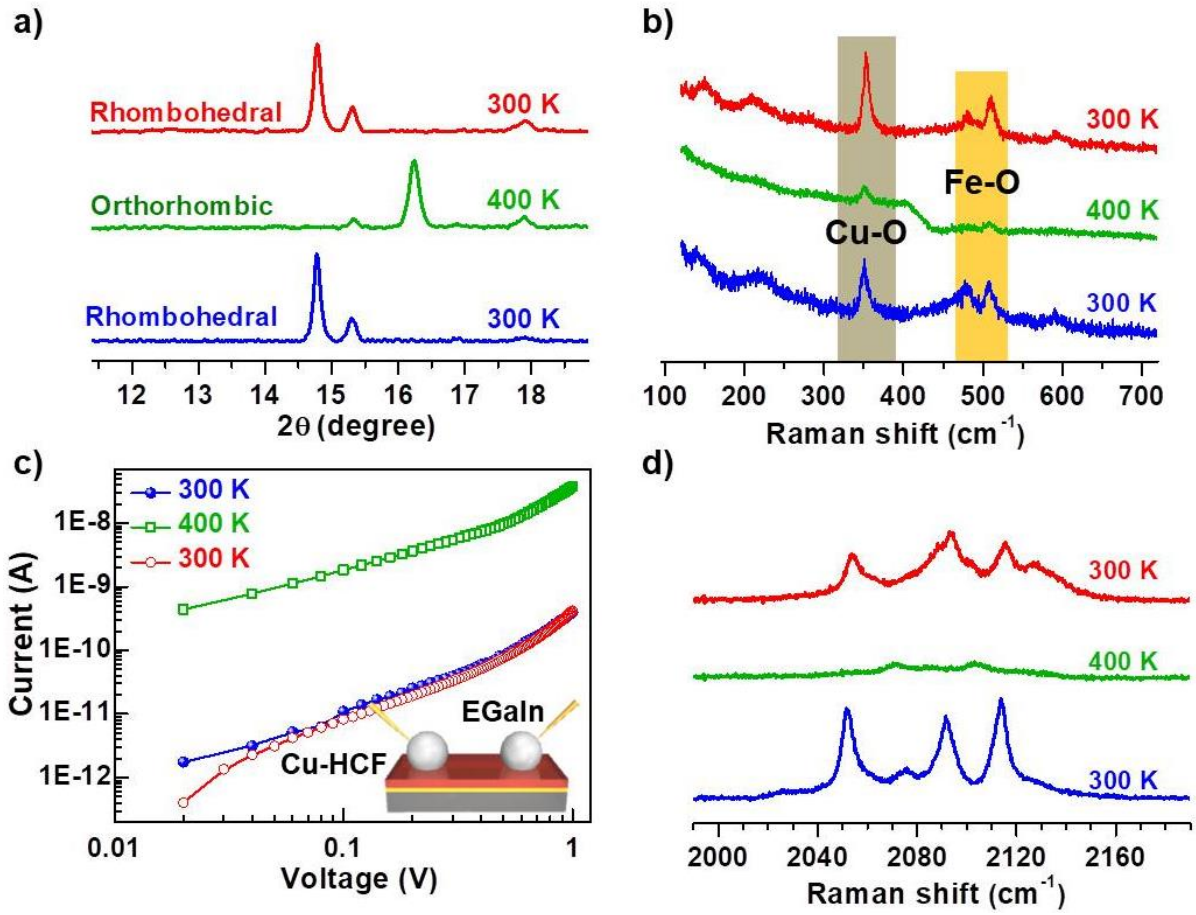

Figure 7: *XRD patterns (a), Raman spectra (b, d) and Current−voltage (I−V) characteristics of the thin film sample at room temperature 300 K (blue), at high temperature 400 K (green), and upon cooling down to room temperature 300 K (red). Inset image showed schematic of the I−V measurements on thin film (brown) by using EGaIn as the top-electrode.*

high temperature (400 K), which were characteristic of Fe(III)−CN bond and Cu(II)−CN bond, respectively (Figure 7d).[9] Thus, at room-temperature Cu(I) and Fe(II) were majorly present whereas at high temperature mixed-oxidation states Cu(I)/Cu(II) and Fe(II)/Fe(III) were observed. In principle, conversion of Fe(II) to Fe(III) at high temperature could take place at the cost of Cu(I) to Cu(0) which is apparently not an energetically feasible conversion so is the conversion of Fe(II) to Fe(I) at the cost of Cu(I) to Cu(II). Hence, it can be attributed that thermally activated charge-transfer to the antibonding π* orbital of CN bring about the sharp

metal-CN bands at 300 K which get smeared at 400 K, easily the electronic transport across the material.

4.4 Conclusions

In conclusion, we have discovered the spontaneous reduction of Cu(II) to Cu(I) at solid-liquid interface without using any reducing agent – unlike liquid-phase reaction where such reduction is found to be absent. This interfacial reduction reaction results in the fabrication of high-quality thin films of coordination network bearing Fe(II)−CN−Cu(I) link on functionalized Au substrate. Electron transfer from Fe(II), S of SAM (MUDA) and Au substrate was not found to be responsible for the interfacial reduction. A confinement effect of restricted coordination at interface is proposed to facilitate the reduction of Cu(II) to Cu(I). Thermally driven reversible structural phase transition was also observed in thin film which modulates the electron transport property.

References

(1) Zakaria, M. B.; Chikyow, T., *Coord. Chem. Rev.* **2017,** *352*, 328-345.

(2) Wessells, C. D.; Huggins, R. A.; Cui, Y., *Nat. Commun.* **2011,** *2*, 550-555.

(3) Hufner, S., *Springer* **2003**.

(4) Buschmann, W. E.; Ensling, J.; Gütlich, P.; Miller, J. S., *Chem. Eur. J.* **1999,** *5*, 3019-3028.

(5) Boyen, H.-G.; Kästle, G.; Weigl, F.; Koslowski, B.; Dietrich, C.; Ziemann, P.; Spatz, J. P.; Riethmüller, S.; Hartmann, C.; Möller, M.; Schmid, G.; Garnier, M. G.; Oelhafen, P., *Science* **2002,** *297*, 1533-1536.

(6) Moulder, J. F.; Chastain, J., Physical Electronics Division, Perkin-Elmer Corporation: **1992**.

(7) Brust, M.; Blass, P. M.; Bard, A. J., *Langmuir* **1997,** *13*, 5602-5607.

(8) Barsan, M. M.; Butler, I. S.; Fitzpatrick, J.; Gilson, D. F. R., *J. Raman Spectrosc.* **2011,** *42*, 1820-1824.

(9) Kettle, S. F. A.; Diana, E.; Marchese, E. M. C.; Boccaleri, E.; Stanghellini, P. L., *J. Raman Spectrosc.* **2011,** *42*, 2006-2014.

(10) Lim, B. S.; Holm, R. H., *Inorg. Chem.* **1998,** *37*, 4898-4908.

(11) Rogers, D. M.; Johansson, J. O., *Mater. Sci. Eng., B* **2018,** *227*, 28-38.

(12) Zhang, L.; Chen, L.; Zhou, X.; Liu, Z., *Sci. Rep.* **2015,** *5*, 18263-18274.

(13) You, Y.; Wu, X.-L.; Yin, Y.-X.; Guo, Y.-G., *Energy Environ. Sci.* **2014,** *7*, 1643-1647.

(14) Schneemann, A.; Bon, V.; Schwedler, I.; Senkovska, I.; Kaskel, S.; Fischer, R. A., *Chem. Soc. Rev.* **2014,** *43*, 6062-6096.

(15) Huang, Y.; Xie, M.; Zhang, J.; Wang, Z.; Jiang, Y.; Xiao, G.; Li, S.; Li, L.; Wu, F.; Chen, R., *Nano Energy* **2017,** *39*, 273-283.

(16) Wang, L.; Zhang, K.; Hu, Z.; Duan, W.; Cheng, F.; Chen, J., *Nano Res.* **2014,** *7*, 199-208.

Thank you for your order!

Dear Mr. Shammi Rana,

Thank you for placing your order through Copyright Clearance Center's RightsLink® service.

Order Summary

Licensee:	Mr. Shammi Rana
Order Date:	Feb 9, 2019
Order Number:	4524600766124
Publication:	Advanced Materials Interfaces
Title:	Highly Hydrophobic and Chemically Rectifiable Surface-Anchored Metal-Organic Framework Thin-Film Devices
Type of Use:	Dissertation/Thesis
Order Total:	0.00 USD

View or print complete details of your order and the publisher's terms and conditions.

Sincerely,

Copyright Clearance Center

Tel: +1-855-239-3415 / +1-978-646-2777
customercare@copyright.com
https://myaccount.copyright.com

Title:	Thermally Driven Resistive Switching in Solution-Processable Thin Films of Coordination Polymers
Author:	Shammi Rana, Anupam Prasoon, Plawan Kumar Jha, et al
Publication:	Journal of Physical Chemistry Letters
Publisher:	American Chemical Society
Date:	Oct 1, 2017

PERMISSION/LICENSE IS GRANTED FOR YOUR ORDER AT NO CHARGE

This type of permission/license, instead of the standard Terms & Conditions, is sent to you because no fee is being charged for your order. Please note the following:

- Permission is granted for your request in both print and electronic formats, and translations.
- If figures and/or tables were requested, they may be adapted or used in part.
- Please print this page for your records and send a copy of it to your publisher/graduate school.
- Appropriate credit for the requested material should be given as follows: "Reprinted (adapted) with permission from (COMPLETE REFERENCE CITATION). Copyright (YEAR) American Chemical Society." Insert appropriate information in place of the capitalized words.
- One-time permission is granted only for the use specified in your request. No additional uses are granted (such as derivative works or other editions). For any other uses, please submit a new request.

Thank you for your order!

Dear Mr. Shammi Rana,

Thank you for placing your order through Copyright Clearance Center's RightsLink® service.

Order Summary

Licensee:	Mr. Shammi Rana
Order Date:	Feb 9, 2019
Order Number:	4524610896545
Publication:	Acta Biomaterialia
Title:	Surface chemistry regulates valvular interstitial cell differentiation in vitro
Type of Use:	reuse in a thesis/dissertation
Order Total:	0.00 USD

View or print complete details of your order and the publisher's terms and conditions.

Sincerely,

Copyright Clearance Center

Tel: +1-855-239-3415 / +1-978-646-2777
customercare@copyright.com
https://myaccount.copyright.com

Journal of materials chemistry. A, Materials for energy and sustainability

ISSN:	2050-7496	**Language:**	English
Publication year(s):	2013 - present	**Country of publication:**	United Kingdom of Great Britain and Northern Ireland
Author/Editor:	Royal Society of Chemistry (Great Britain)		
Publication type:	e-Journal		
Publisher:	Royal Society of Chemistry		
Rightsholder:	ROYAL SOCIETY OF CHEMISTRY		

Permission type selected: Republish or display content

Type of use selected: Thesis/Dissertation

<< Select different permission

Total Price: $0.00

Terms and conditions apply to this permission type
View details

About Your Works

Please select from the works you are currently working on and click 'Continue'.

	Title	Institution Name	Date
◉	Chemical Reduction at Solid-Liquid Interface: Growth and Electrical Conductance of Thin Films of Cu/Ag-TCNQ and Cu-Hexacyanoferrate	IISER PUNE	Feb 2019 Edit

Total Price: $0.00

< Back New Work Continue >